TÉCNICO LISBOA

Characterization of Mozambique's Vulnerability to Coastal Erosion

Patrícia Filipa Barradas Domingos

Thesis to obtain the Master of Science Degree in

Environmental Engineering

Supervisor: Prof. Maria João Correia Colunas Pereira

Examination Committee

Chairperson: Prof. António Jorge Gonçalves de Sousa
Supervisor: Prof. Maria João Correia Colunas Pereira
Member of the Committee: Prof. Pedro Miguel Berardo Duarte Pina

September 2016

Acknowledgements

The completion of this thesis could not have been achieved without the support and orientation provided by my supervisor, Professor Maria João Pereira.

I would also like to thank phD student Alzira Gomes Ramos for the technical support provided during the execution of this project.

Abstract

Coastal erosion is identified as one of the most important processes affecting the Mozambican coast. With 44% of the country's population living in coastal areas, there is a serious need to better understand and quantify the changes imposed by this phenomenon. Moreover, is fundamental to infer about the vulnerability the coast is subject to. The main objective of this thesis is to make use of remote sensing and GIS techniques to study the evolution and vulnerability of the Mozambican coast throughout a period of 26 years (1989-2015), using Landsat satellite imagery. To achieve this objective an attempt was made to estimate coastline changes in terms of erosion and/or accretion in the country, more specifically along the Sofala Bay region, through the implementation of two different classification methods based on support vector machines (SVMs) and modified normalized difference water index (MNDWI), with posterior coastline extraction. Sites where changes deemed more significant were identified, change analysis was performed by the computation of erosion and accretion areas to have a better understanding of actual area lost or gained. Vulnerability was computed by the application of the coastal vulnerability index (CVI) in this sites. It was possible to conclude that extensive erosion and coastline retreat are occurring in this region even though CVI calculation revealed low to moderate vulnerability, with exception of sites located in the city of Beira, that obtained a high vulnerability value. Possible reasons that could explain the results obtained were also analysed in the process of this study.

Keywords: Mozambique, coastal erosion, remote sensing, Landsat, support vector machines, coastal vulnerability index.

Resumo

A erosão costeira é um dos processos mais importantes que afecta a costa de Moçambique. Uma vez que 44% da população vive em zonas costeiras, torna-se fundamental compreender de forma clara e quantificar as alteraçoes impostas por este fenómeno, e ainda inferir acerca da vulnerabilidade à qual a costa se encontra sujeita. O principal objectivo desta tese é a utilização de técnicas de detecção remota e sistemas de informação geográfica com o intuito de estudar a evolução e vulnerabilidade da costa Moçambicana num período de 26 anos (1989-2015), utilizando imagens de Landsat. Para alcançar este objectivo, foram estimadas as alterações da linha de costa em termos de erosão e/ou acreção no país, mais especificamente ao longo da Baía de Sofala. Isto foi feito através da implementação de dois métodos diferentes de classificação de imagens, SVMs e MNDWI, com posterior delimitação e extracção da linha de costa. Locais onde as alterações se mostraram mais significativas, foram identificados e a sua análise realizada através da estimativa de áreas de erosão e acreção, de modo a ter um melhor entendimento da real área perdida ou ganha. Vulnerabilidade foi estimada através do cálculo do índice de vulnerabilidade costeira. É possível concluir que extensa erosão e recuo da linha de costa estão a ocorrer na região estudada, apesar de o índice de vulnerabilidade ter revelado valores baixos a moderados, com excepção de locais situados na cidade da Beira, que obtiveram valores altos de vulnerabilidade. Possíveis razões que possam explicar os resultados obtidos são também analisadas.

Palavras-chave: Moçambique, erosão costeira, detecção remota, Landsat, SVMs, índice de vulnerabilidade costeira.

Contents

List of Figures

List of Tables

List of Acronyms

GIS	Geographical Information Systems
EO	Earth Observation
USGS	United States Geological Survey
RGB	Red - Green - Blue
TM	Thematic Mapper
ETM	Enhanced Thematic Mapper
MNDWI	Modified Normalized Difference Water Index
SVMs	Support Vector Machines
CVI	Coastal Vulnerability Index
DSAS	Digital Shoreline Analysis System
EPR	End Point Rate
EMI	Eolian Mapping Index

1 Introduction

All over the world, coastal zones are facing intensified natural and anthropogenic disturbances such as sea-level rise, coastal erosion, over exploitation of resources, among many others. According to Appeaning Addo et al. (2008), over 70% of the world's beaches are experiencing coastal erosion which represents a serious hazard to many coastal areas. Rapid coastline changes can lead to serious social and economic consequences, specially in highly populated areas (Addo and Kodzo, 2013). These facts have led, over the recent years, to an increase in awareness of the adverse impacts that the coastal environments are facing, which is translated in more coastline change and vulnerability studies being performed in several and very different regions of the world.

Coastal erosion is defined as the process of removal of material at the coastline, leading to loss of land and retreat of the coastline landward. Accretion is defined as the deposition of material at the coastline leading to gain in land and coastline advance seaward (Gibb, 1978; Ghosh et al., 2015). Monitoring temporal and spatial changes of coastal environments, can help understand these processes and predict their development (Addo and Kodzo, 2013). One way to identify changes in coastal ecosystems is by mapping changes in the coastlines, which makes it possible to observe how this ecosystems have changed over different time scales. Knowledge of coastline position is the basis for measuring and characterising land and coastal water resources (Liu and Jezek, 2004; Petropoulos et al., 2015).

An idealized definition of coastline can be characterized as the interface between land and water (Dolan et al., 1991; Li and Damen, 2010). However, a more realistic definition considers that the coastline position changes through time, due to sediment movement in the littoral zone and especially because of the dynamic nature of water levels at the coastal boundary (waves, tides, storm surge, etc.). When studying the coastline, one should take into account the temporal and spatial scale involved (Boak and Turner, 2005). Gens (2010) defines the coastline as the position of land-water interface at an instant in time, and with highly dynamic nature. In the wake of this study, Gens (2010) definition of coastline will be considered. It is also important to mention that the term 'shoreline' is used by the coastal research community, while the remote sensing community usually refers to 'coastline' (Gens, 2010). In this thesis, both terms will be considered synonyms and the term 'coastline' will be used in the remainder of this work.

Due to the importance of the processes that occur along the coast, rapid and reliable techniques are necessary to monitor the coastline and develop viable plans to protect the coast and reduce potential losses. Over the years, with increasing awareness to this problem, a series of techniques based on EO data have been employed to study coastline changes all over the world. (Ghosh et al., 2015)

Remote sensing techniques have been useful in the study of coastal processes, including erosion, due to satellites rapid, repetitive and multi-spectral coverage (Tirkey et al., 2005; Vinayaraj et al., 2011). This technology has since long been considered the most convenient way to evaluate coastline

changes and monitor coastal processes by making use of historical data. It is specially useful when ground data is not available (Maktav et al., 2002). One of its great advantages lies in the detection and expansion of information over vast remote regions at relatively low cost, or in the case of Landsat data at no cost at all and accessible to everyone (Donato and Klemas, 2001; Kuenzer et al., 2014).

In the last two decades various remote sensing techniques have become available for coastline delineation and extraction. Coastlines can be derived based on visually discernible features, digital image processing techniques, such as image classification methods, or specific tidal datum, through the use of digital terrain models and a number of data sources. This depends on the type of satellite from which the images are derived (Boak and Turner, 2005). Multispectral images provide detailed information over large areas, which makes them a great tool to study the coast (Boak and Turner, 2005). Moreover, this kind of imagery provides several spectral bands, including near and midle-infrared where the land/water boundary is well defined (Addo and Kodzo, 2013; Van and Binh, 2008). The major limitation of satellite images lies in their relatively low spatial resolution, when compared with aerial photographs (Appeaning Addo et al., 2008).

The main objective of this thesis is to make use of remote sensing and GIS techniques to study the evolution and vulnerability of the Mozambican coast throughout a period of 26 years, using Landsat satellite imagery. Coastal erosion in Mozambique has been identified as one of the most important processes affecting the coastal system, mainly due to natural processes. It is known that 44% of the country's population is living in coastal areas, mostly in coastal cities, and with the ever increasing trend for urbanization and tourism infrastructures, which exerts intensified pressure on coastal environments, it becomes so very important to perform this study specifically in this country (Palalane et al., 2015). To evaluate coastline change over the Mozambican coast, a study area was chosen, located within the Sofala province.

To achieve the objective proposed, coastline changes were estimated in terms of erosion and/or accretion in the country, more specifically along the Sofala Bay area, through the implementation of two different classification methods and posterior visual analysis. The two methods applied in order to extract the coastline were the Modified Normalized Difference Water Index (MNDWI) and a semi-automatic classification method based on Support Vector Machines (SVMs). After extraction and overlaying the coastlines of every image used, areas where changes occur were quantified in terms of area lost or gained. For these sites, a coastal vulnerability index (CVI) was developed based on three parameters (coastline change rate, landuse and population density). The CVI was used in order to map the relative vulnerability of these sites, characterizing the coastal processes and activities that may be affecting the coastal areas. Landuse is classified here according to its economic value and it is not a surprise that population density is considered when estimating vulnerability, since large concentrations of people near the coast can lead to increased pressure along this regions and consequently intensified risk to erosion processes (Jana and Bhattacharya, 2013; McLaughlin et al., 2002). Coastline change rate is used with the purpose to quantify and better understand the current rate of recession/accretion of the coast. In the

end, for each of the sites studied, risk and vulnerability maps were computed.

This thesis is divided in 6 main parts. The first part pertains to what has been already done in regards to remote sensing techniques throughout the world and in Mozambique for the study of coastal erosion and coastline change analysis. The second part deals with presentation and description of Mozambique coastal area and the specific area studied here. The third section is dedicated to the type of data used and methodology and techniques employed to obtain the results. The fourth section is precisely the description of the results obtained. Results are presented in a sequential manner, both intermediary and the final ones. In the fifth part, the results are discussed based on literature findings and own rational judgement. Finally, the sixth section is dedicated to final conclusions reached throughout the development of this thesis. It is also presented in this section an overlook over future work and techniques that could further deepen this study.

2 State of the Art

Coastal erosion is recognized as a global problem and increasing anthropogenic disturbances such as population and industrial developments near the coast have been raising attention to this so serious problem. (Appeaning Addo et al., 2008; Ge et al., 2013; Vinayaraj et al., 2011; Ghosh et al., 2015)

Remote sensing and GIS techniques allow coastline monitoring in a cost effective way. This is a good alternative to aerial photo and ground survey techniques, because conventional coastline monitoring techniques are expensive, time consuming and require trained staff (Ghosh et al., 2015). Various studies have been conducted employing several change detection techniques using different spatial and temporal resolutions of satellite imagery, in order to quantify erosion and/or accretion. Only with more accurate tools is possible to define better planning and management strategies for the coastal zones.

Guariglia et al. (2006) used a multi source approach to map the coastline and identify changes and observed that depending on their spatial resolution, satellite images are affected by tidal variations. However, in their study they concluded that the coastline can be extracted from Landsat TM images having a spatial resolution of 30 meters, without the interference of the tidal factor. However, in higher spatial resolution images, tidal effects must be considered when identifying the coastline.

Li and Damen (2010) explored the use of multi-temporal satellite Landsat TM/ETM+ and also SPOT images to study and map the coastline of the Pearl River Estuary in China. They tested different band false colour combinations to delineate the coastline.

Ge et al. (2013) focused on mapping coastal erosion by integrating multi-sensor satellite images from several years to estimate the change along the coastline of Gippsland basin in Victoria, Australia. They used a cost effective approach for mapping the eroded coastline, integrating Landsat multi-spectral (MS) imagery and synthetic aperture radar (SAR) imagery data, extracting the land-water interface at sub-pixel resolution.

Processing of satellite images is often necessary in order that water and land appear as contrasting features. For this, water indices are usually employed, where two bands are used for their computation, normally one from the visible portion of the spectrum and other from the near or midle-infrared portion (Ghosh et al., 2015). In particular, Liu (2011) made use of the MNDWI to extract the coastline using medium resolution Landsat TM and ETM+ images. By measuring the change of coastline along the Yellow river delta, this information was later used to calculate the coastal erosion area and the average rate of erosion through the application of GIS tools. This modified water index is seen as very effective in extracting the coastline since it can enhance open water features while efficiently removing and in some cases even suppressing the built-up land noise as well as vegetation and soil noise (Xu, 2006).

Ghosh et al. (2015) also used the MNDWI and on-screen digitization to identify and detect coastline changes and estimate the rate of this change on Hatiya island in Bangladesh.

An overview of the status use of EO techniques for detection, extraction and monitoring of coastlines, and also a reference to coastline indicators can be found in Gens (2010). It refers that, even though manual photo-interpretation has been regarded has one of the most commonly used techniques for delineating coastline when multi-spectral data is used, in recent years new approaches have been proposed for coastline extraction from EO data, more automated and with image classification being the most widely used.

Using multi-temporal satellite sensor data integrated with ground data during a period of 14 years, Maktav et al. (2002) examined the erosion at the Black Sea side coast of Lake Terkos in Turkey. They monitored the change in land barrier between the Black Sea and the Lake Terkos based on the comparison of land cover/land use classifications of the sequential data. This was done by allocating pixels to their most likely class based on an Iterative Self-Organizing data (ISODATA) algorithm, an unsupervised classification method.

Petropoulos et al. (2015) used Landsat TM imagery and GIS techniques to perform a semi-automatic classification method based on SVMs in order to map spatio-temporal changes of erosion and deposition of two Mediterranean river deltas. Huang et al. (2008), Otukei and Blaschke (2010), Petropoulos et al. (2012a),Petropoulos et al. (2012b) and Volpi et al. (2013), also computed this supervised classification method using different types of Earth Observation data, concluding that it was indeed a very robust method for coastline delineation. Mountrakis et al. (2011) presents an overview of support vector machines classification method.

When studying coastline change, quantifying rates of coastal retreat is also important, that is why several authors have been employing the Digital Shoreline Analysis System (DSAS), an ESRI Arc-GIS, extension developed by the USGS, that allows the users to calculate coastline change-rate statistics from a time series of multiple coastline positions, in combination with remote sensing techniques (Himmelstoss et al., 2009). This tool was also used in this thesis, for the calculation of coastline change rate.

Alhin and Niemeyer (2009) used medium resolution satellite imagery, Landsat ETM, Landsat TM-5 and SPOT 5 to monitor and analyse the coastline dynamics over two decades along Gaza coastline. They extracted the coastline employing four different methods, Band ratio, Tasseled Cap transformation, Principle Component Analysis (PCA) and Normalized vegetation Index (NVDI) and calculated the rate of change along Gaza coastal zone, making use of the DSAS tool.

Also making use of higher resolution satellite imagery, like SPOT, Quickbird and WorldView, Kuenzer et al. (2014) have employed manual digitization to extract the land-water boundary and derive rate of change statistics automatically from the DSAS system to study the coastal dynamics of the Yellow river Delta, China.

Addo and Kodzo (2013) analysed coastline change using medium resolution satellite imagery including Landsat TM, Landsat ETM+ and ASTER imagery, with implementation of the DSAS tool for change rate estimation of the Eastern coast of Ghana.

Allied to coastline change analysis, increasing attention has been directed to the development of vulnerability maps through the computation of the coastal vulnerability index (CVI) making use of remote sensing and GIS techniques. There has been an increase in the past years, in the number of vulnerability indices produced for specific coastal areas.

McLaughlin et al. (2002) investigated the incorporation of socio-economic variables (population density, cultural heritage, roads, railways, landuse and conservation status) into a GIS based CVI for wave induced erosion in Northern Ireland, and concluded that the inclusion of this variables is of extreme importance to assess coastal vulnerability. However, most studies still omit this variables in CVI calculation, mostly due to the difficulty of obtaining and ranking such data.

Most recently, Kumar et al. (2010) developed a CVI for the maritime state of Orissa using eight relative risk variables with the objective to develop a tool that can be used by coastal managers in order to better plan and mitigate losses due to hazards. The eight risk variables are, shoreline change rate, sea level change rate, coastal slope, mean significant wave height, mean tidal range, coastal regional elevation, coastal geomorphology and tsunami run-up.

Chandrasekar et al. (2013) mapped relative vulnerability of the Southern tip of India using coastline change analysis, with multi-temporal Landsat data, and calculated the coastal vulnerability index using six vulnerable parameters, shoreline change rate, coastal slope, relative sea level change, mean wave height and mean tide range.

Jana and Bhattacharya (2013) developed a coastal vulnerability index for Digha littoral, on the east coast of India, based on three parameters (coastline change rate, landuse cover and population density), in order to help in the development of management policies for sensitive coastal areas.

Studies to estimate vulnerability of the coast to sea level rise, due to global warming have also been increasing, with Mahapatra et al. (2015), Pendleton et al. (2004) and Rao et al. (2009) being among them.

Regarding studies of coastal erosion in Mozambique making use of remote sensing techniques, bibliographic research led to the conclusion that they are still few. Even so, some studies were found where erosion and coastal phenomenons have been analysed.

Moreira (2005) computed erosion change rates for some areas of Mozambique, specially focused on the country's south beaches. This study was mainly based on field work, observing the coastline between 1970 to 1975 and 1999 to 2004. Comparison of the results obtained was done making use of aerial photographs. Maansson (2011) presents a value for coastal recession for Beira region, however the period for which this was calculated and data sources used are not specified.

Langa (2007) has also studied the problems encountered along the Mozambican coast, but once again with some focus on the south part of the country, specially the city of Maputo.

Hoguane (2007) has performed a diagnosis of Mozambique coastal zone, where he pointed out the urgent need to adopt sustainable measures for the use and management of resources.

Attempting to understand how the most pressured areas in Mozambique respond to natural and anthropogenic action as well as to assess erosion rates, Palalane et al. (2015) developed a study that contributes to an increase in knowledge about coastal erosion in the country, its governing processes and what remedial measures are being adopted to deal with this problem. It also analyses the existing legal framework for coastal planning and management, and evaluates historical and existing practices in coastal protection.

Theron et al. (2012) performed a study on the response of Mozambique to climate change, in order to develop plans for adaptation and mitigation measures to the impacts on the coast. This study was the only one found that included coastal vulnerability analysis regarding erosion and accretion processes, for the period between 1991 and 2004, using remote sensing techniques for the major coastal cities of the country, including Beira, which will be analysed here.

Although Palalane et al. (2015) and Moreira (2005) also make some brief comments about the city of Beira and the area under study here, the governing processes in this region are still very ill explored and more insight on the actual change rate and vulnerability of this coast are needed.

Many more studies of coastal changes through out the world could have been presented here, however, the ones mentioned were the ones cited in several other sections of this thesis, and for that reason deemed to be of more immediate importance to be carefully described here than any others.

3 Case Study

Mozambique is located in the south-east corner of the African continent for which holds the title of the fourth longest coastline, with an estimated length of approximately 2800 km (MICOA, 2007). Figure 1 shows the country's location in southern Africa.

Figure 1: Geographical location of Mozambique in southern Africa. Image from Google Maps, 2016.

At present (2016), the country is estimated to have a population of 26.4 million inhabitants (INE, 2016) with the last population census, undergone in the year of 2007, estimating that 44% of the population resides in coastal districts (Palalane et al., 2015; INE, 2016). Five of the urban centres - Maputo, Matola, Beira, Nacala and Quelimane - which are located along the coast belong to the list of the seven most populated cities in Mozambique. The expected development in coastal areas will contribute to an increase in the number of people moving to these areas, implying an expansion of new urban infrastructural developments and tourist activities (Palalane et al., 2015). These factors are a precedent to the fact that these urban and suburban areas are experiencing the most critical levels of erosion (NAPA, 2007).

In terms of morphology, the coastal areas of Mozambique are divided in 3 regions. The northern region, characterized by small dunes alternating with cliffs and attached beaches, reefs and coral islands (Palalane et al., 2015). Due to this type of morphology this region, according to the literature, does not suffer much from the influence of erosion processes (NAPA, 2007). The central region, mainly represented by Sofala province, is characterized by fluvial-marine plain with sandy muddy soils and low beach ridges, while the southern region, which encompasses the areas of Inhambane city, Maputo and

Ponta do Ouro, is characterized for its sandy plain, system of dunes, inland lagoons, barrier islands, such as the Bazaruto Arquipelago, and platform barriers of sandstones (Palalane et al., 2015).

The coastal zones constitute a very important area since activities such as tourism and recreation, mining, oil and gas industry and also aquaculture, all occur in the coastal zone. These activities are clearly relevant to the economy of the country and being located in such high risk areas makes them vulnerable to a variety of disturbances that contribute significantly to erosion (NAPA, 2007). In fact, coastal erosion has been identified as one of the most important phenomena occurring in the Mozambican coastal system (Palalane et al., 2015). Coastal erosion in the country is driven by natural processes in combination with anthropogenic actions, which have an important role in accelerating this problem. It is estimated that 90% of erosion is caused by natural forces, and 10% by human factors (NAPA, 2007). Even though anthropogenic actions cause changes more evident in the coastal environment, natural processes are the main reason for the evolution of the Mozambican coast (Moreira, 2005). This conclusion was reached based on the observation that some stretches of the coast, not affected locally or regionally by human activity, were experiencing accelerating rates of erosion (Palalane et al., 2015).

Tides, waves and sea level fluctuation along with extreme climate events such as tropical cyclones and heavy rains, that occur frequently, are responsible for significant changes of the coastline as a consequence of their strong erosion action (NAPA, 2007; Moreira, 2005). Human action can be observed in the intensive occupation of areas adjacent to the coastline, with constructions on top of dunes, consequence of the proliferation of tourism, logging of vegetation and mangrove trees, or construction of houses in areas previously occupied by mangroves and wetlands, destabilization of coastal sand islands and placement and extension of coastal protection structures (Hoguane, 2007; Langa, 2007).

Regarding wave conditions, a variety of studies shows that larger significant wave heights are seen during the winter, which occurs between April and September. (Guiloviça, 2011; Martins, 2012; Theron et al., 2012)

Along the Mozambican coast, tides are observed to be semi diurnal with mean high water spring level varying between 1.4 and 3.7 meters above mean sea level (Theron et al., 2012). In the Mozambique Channel, encompassing the central region of the country, the mean spring tidal ranges can reach values above 6 meters, representing the maximum ranges observed along the entire African coast. As a consequence of such high tide heights, sea currents are also stronger, which leads to higher erosion on river banks and beaches (Hoguane, 2007).

These characteristics are what transforms the coastal zones in areas of great importance subject to many forces that make them dynamic areas where significant changes in the morphology occur over different scales in time and space (Palalane et al., 2015). This is why it becomes so important to study them in order to have a better understanding of the actual rate of recession and the activities or processes, either natural or anthropogenic, that contribute to this phenomenon. To do this, a specific area within the country was selected to be analysed throughout a considered period of time, from 1989

to 2015, making use of Landsat satellite images.

The region chosen is located within the Sofala province and between latitude 19°30 S and 21°10 S, approximately. This area is located in the central region of Mozambique and includes the city of Beira, which is referred in the literature as a very vulnerable city to erosion (MICOA, 2007; Palalane et al., 2015). It also includes part of the Sofala Bay extending from the Save river to the region of Tama. Figure 2 shows the coastal area under study within the Sofala Province and a representation of the city of Beira.

After extensive research on the vulnerability and high risk areas to erosion in the Mozambican coast, this specific region was chosen for the analysis of coastal erosion and rate of recession as the one which contains the areas with higher risk to erosion as it will be made clear in the following paragraphs.

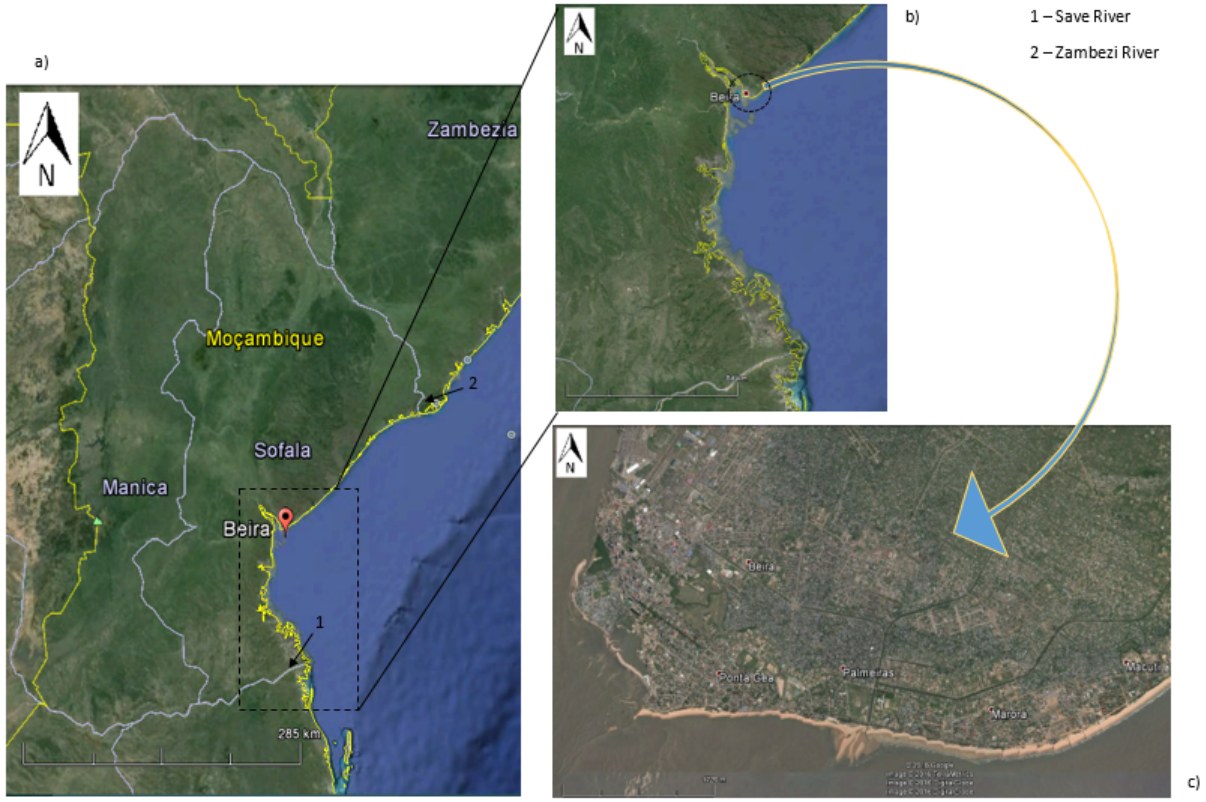

Figure 2: Coastal area under study. a) Representation of Sofala Province; b) Case study area under analysis within Sofala region; c) City of Beira. Images from Google Earth™.

According to NAPA (2007), the centre of high vulnerability to erosion in the Mozambican coast is around 20° latitude, which encompasses the Sofala Bay. This region is characterized by a delta and mangrove forest in the north and high vegetated dunes in the south. The interior is known for its plain area which is usually prone to floods during extreme climate events. There is also the fact that coastal dunes suffer from the increased pressure of tourism development and urban expansion.

In the area between the Save and Zambezi rivers (Figure 2a), it is known that erosion has been aggravated in the past years due to logging of the mangroves and reduction of water volumes from

the Zambezi river after the construction of the Cahora-Bassa hydro-electric dam (NAPA, 2007). Some authors have mentioned the link between the increased erosion along Beira and Sofala Bank coast and the construction of the Cahora-Bassa dam (finished in 1974) as well as the Kariba dam (finished in 1969) and the water extraction from Panque River (Davies et al., 2001; UNEP/Nairobi, 2009). The reduction of mangrove forest that has been observed along the Sofala Bank contributes to further erosion of the coast. This reduction has been recorded in the order of the 4.9% per year, due to destruction and overexploitation (Sitoe et al., 2014).

The city of Beira (Figure 2b and 2c) is located in the central region of Mozambique at the mouth of Pungué river and harbours one of the three major regional ports in the country. Several authors, such as Moreira (2005), Palalane et al. (2015) and Theron et al. (2012), consider that Beira is located in a very high risk region in terms of erosion.

Interference with natural sediment deposition and transport pattern is a reality in Beira Port, situated east of the Pungué River estuary and less than 10km from Buzi river mouth. Seawalls and groins from different materials are common structures that have been adopted in the city with the purpose to maintain the coastline and protect coastal infrastructures. However, these infrastructures induce changes in the dynamic of local sediments and lead to negative impacts on adjacent areas. (Hoguane, 2007)

As it is already known, high tides have also contributed to the increasing effects of erosion along the coast and in the case of Beira coastal areas, tidal amplitudes can reach and even exceed the 6 meters (Palalane et al., 2015). According to Hoguane (2007) this value is twice as high than the tides observed in northern and southern regions of Mozambique. It is also important to note that Beira is a flat area prone to flooding problems. As such it is not surprising that this city is cited as the most prone to coastal erosion of all the Mozambican cities with a high number of events reported indicating severe erosion hazards (Chemane et al., 1997; Orive and Cancelas, 2012; Theron et al., 2012). It has also been pointed as the most vulnerable city to sea level rise, in future climate change scenarios (Theron et al., 2012).

Another aspect to take into account is the frequency and intensity of cyclones along the Mozambican coast which have increased in the last 30 years, and future climate change scenarios suggest that this increasing trend will persist (INGC, 2009). Figure 3 shows the cyclone hazard over the Mozambican coast. It is possible to see that over the area of study the cyclone hazard is very high. The increasing intensity of cyclones and other storm events may result in more damages and losses in areas with infrastructures, more specifically in coastal cities where buildings are located close to the coast, like Beira. In fact, in August 2010 a destructive cyclone hit Beira coast leading to the destruction of the road along Ponta Gea Marginal (Palalane et al., 2015). During cyclones the sea level increase can induce a setback of the coastline and dune region leading to losses of land and flooding in flat and low-lying coastal plains, such as Beira (DNET, 2010).

After analysing these facts, it is possible to infer that the region chosen to perform this study is clearly considered a high risk area affected by direct and indirect anthropogenic pressure, such as tourism development and the construction of damns, and naturally induced erosion. As such, coastline change detection and vulnerability analysis will be performed over this area and results obtained discussed taking into account the facts presented here.

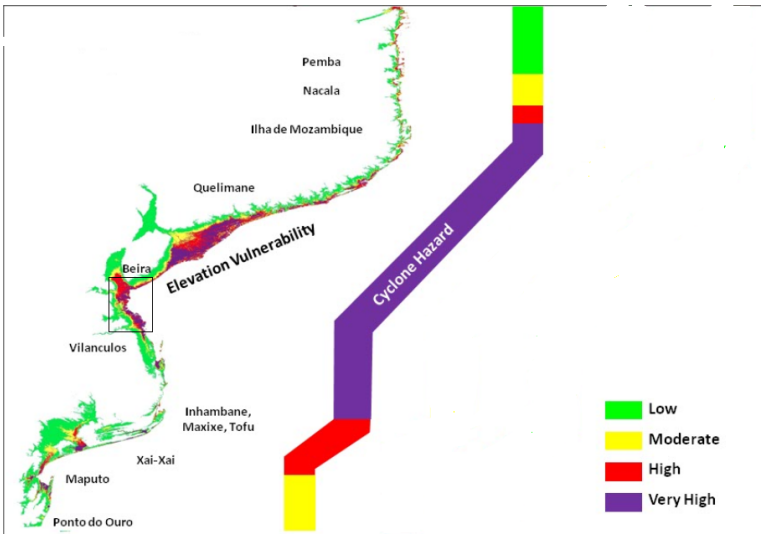

Figure 3: Cyclone vulnerability of the Mozambican coast, with case study area delimited (rectangle). Adapted from Theron et al. (2012).

4 Methodology

4.1 DataSets

In this study Landsat imagery from 6 different time periods, spanning approximately 26 years, was used. Landsat is the only multi-spectral satellite data available at no cost, providing coverage of the Earth that goes back to 1972 (Petropoulos et al., 2015). This is one of the reasons that it is so extensively used in many studies including coastline change evaluation, as seen in one of the previous sections.

The accuracy of coastline detection depends on the spatial resolution of the source data. With higher resolution, it is expected higher accuracy of the extracted coastline. However, sometimes using high resolution satellite images is not an option especially due to their cost. In these cases, medium-resolution optical imagery can be used to determine coastline in a cost-effective way. (Gens, 2010)

For the purpose of this study five images of Landsat Thematic Mapper (TM) and one from Landsat 8 were used (Figure 4-5).

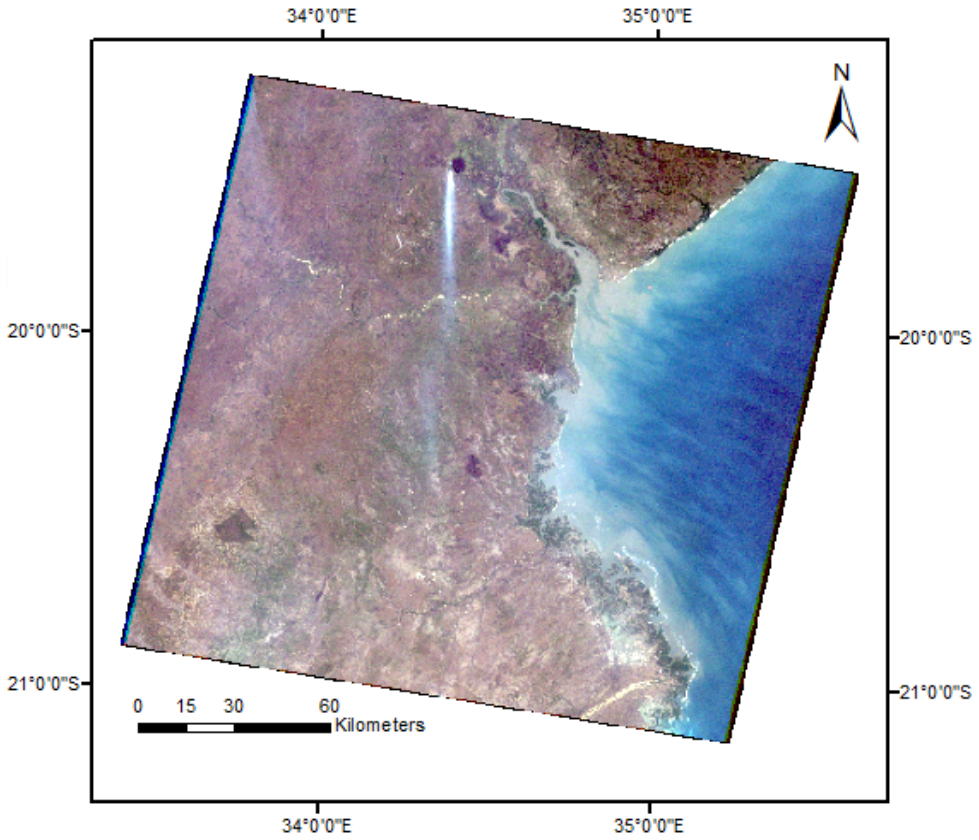

Figure 4: Landsat TM image from 1989 at 3-2-1 (RGB) band composition (path: 167; row: 74).

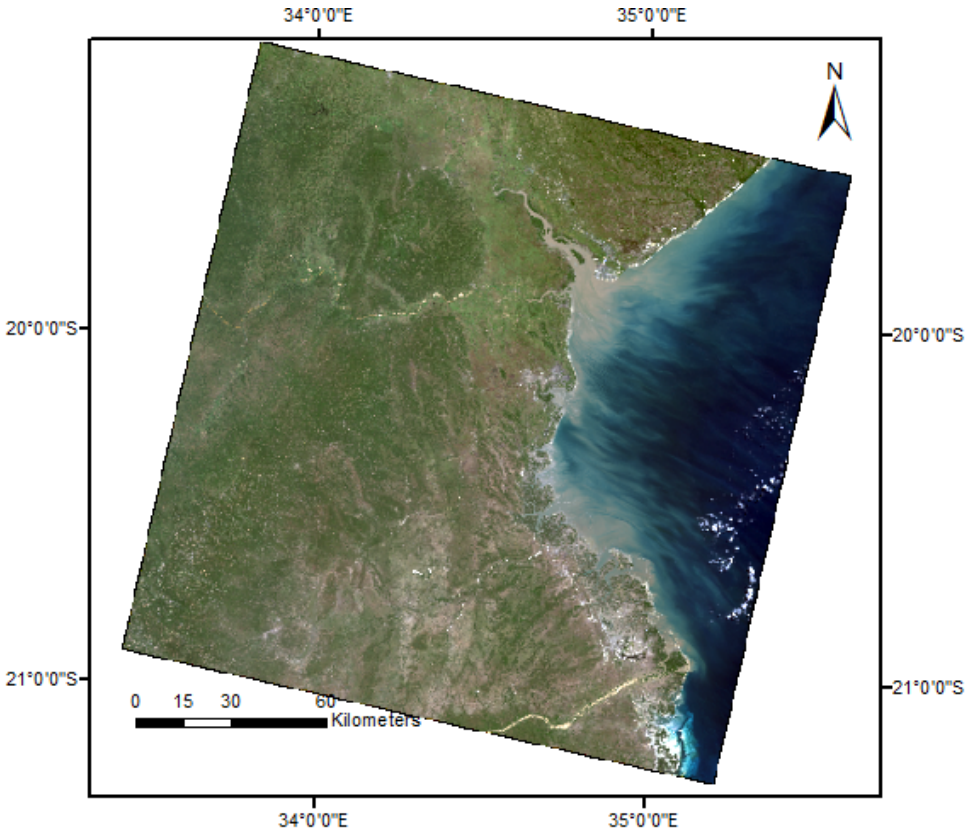

Figure 5: Landsat 8 image from 2015 at 4-3-2 (RGB) band composition (path: 167; row: 74).

The TM has seven spectral bands with a spatial resolution of 30 meters for Bands 1 to 5 and 7. Band 6, which corresponds to the thermal infrared band, has a spatial resolution of 120 meters, but is resampled to 30 meter pixels (Table 1). Landsat 8 images consist of nine spectral bands with a spatial resolution of 30 meters, bands 1 to 7 and band 9. There is a new band 1, useful for coastal and aerossol studies, and a new band 9 useful for cirrus cloud temperatures. Band 8, which corresponds to the panchromatic band, has a resolution of 15 meters. Thermal infrared bands, TIRS 1 and 2, are acquired at 100 meter resolution, but are resampled to 30 meter pixels (Table 2) (USGS, 2016a).

Table 1: Landsat TM Band designations.

Landsat 4 - 5	**Wavelenght (μm)**	**Resolution (meters)**
Band 1 (Blue)	0.45 - 0.52	30
Band 2 (Green)	0.52 - 0.60	30
Band 3 (Red)	0.63 - 0.69	30
Band 4 (NIR)	0.76 - 0.90	30
Band 5 (SWIR)	1.55 - 1.75	30
Band 6 (TIR)	10.40 - 12.50	120*(30)
Band 7 (SWIR)	2.08 - 2.35	30

Table 2: Landsat 8 Band designations.

Landsat 8	Wavelenght (μm)	Resolution (meters)
Band 1 (Coastal aerossol)	0.43 - 0.45	30
Band 2 (Blue)	0.45 - 0.51	30
Band 3 (Green)	0.53 - 0.59	30
Band 4 (Red)	0.64 - 0.67	30
Band 5 (NIR)	0.85 - 0.88	30
Band 6 (SWIR 1)	1.57 - 1.65	30
Band 7 (SWIR 2)	2.11 - 2.29	30
Band 8 (Panchromatic)	0.50 - 0.68	15
Band 9 (Cirrus)	1.36 - 1.38	30
Band 10 (TIR 1)	10.60 - 11.19	100*(30)
Band 11 (TIR 2)	11.50 - 12.51	100*(30)

For the purpose of this study, thermal bands, band 6 in TM and band 10 and 11 in Landsat 8, were not used for analysis of the coastline.

All images were obtained and downloaded from the United States Geological Survey (USGS) archive, (`http://earthexplorer.usgs.gov/`). The images were acquired at Level-1T processing which means they were already geometrically corrected, resampled and registered to a UTM 36 WGS84 ellipsoid with elevation correlation applied (USGS, 2016b). As reported by NASA, this product is georeferenced with a level of precision better than 0.44 pixels (meaning 13.4 m) (Petropoulos et al., 2015; Pardo-Pascual et al., 2012).

The characteristics of the images acquired can be found in the table 3.

Table 3: Landsat data used in this study and respective characteristics.

Satellite/Data	Path/Row	Date	Local Hour	Resolution	Level	Cloud Cover (%)
Landsat 5 TM	167/74	19/09/1989	07:07	30m	L1T	0
Landsat 5 TM	167/74	31/05/1995	06:48	30m	L1T	0.06
Landsat 5 TM	167/74	30/08/1999	07:19	30m	L1T	0
Landsat 5 TM	167/74	24/06/2004	07:23	30m	L1T	0
Landsat 5 TM	167/74	20/08/2007	07:35	30m	L1T	0.03
Landsat 8	167/74	06/05/2015	07:41	30m	L1T	0.02*

*This cloud cover value corresponds to the cloud cover on Land.

One can observe from this table that no images between 2007 and 2015 were used in this study. This was due to the fact that there were less images in this time period, and a lot of them had a considerable amount of clouds near the coast. Also, the fact that after 2003 all ETM+ acquisitions have an anomaly due to the failure of the Scan Line Corrector (SLC), on-board Landsat 7, and which resulted in data loss and stripped images, also decreased the amount of images available. Even though there are already some tools and software available to destripe these images, they can also lead to loss of information which could be critical for later processing of the images (Barsi et al., 2007). This being said, a choice was made not to use these images and work solely with the ones presented above.

The images were acquired between the months of May and September, as much as possible

cloud free and around the same date. This is important in order to decrease the effect of seasonal variations that affect specifically the coastal regions, like semi-diurnal tidal effect (Petropoulos et al., 2015; Savvidis et al., 2005).

It is also important to mention that it is difficult to compare two scenes that were taken at different times because of non-uniform tides. To minimize errors regarding this aspect, images during similar tidal phase were taken into account. (Petropoulos et al., 2015)

For this purpose tidal predictions have been acquired from SHOM, a French website that provides historic calculations of water level by hour for different Port locations around the world (`http://maree.shom.fr/`). This website allows the user to choose the Port to be analysed and input the date of choice. As a result a tide table and graph are computed, where one can observe at what time of the day low and high tide occurred and what were the minimum and maximum heights, respectively (Figure 6). It is also possible to choose a specific time of the day and compute water level height. Figure 7 shows the tide predictions obtained for the year of 1989 as an example. Time is possible to be chosen in 5 minute intervals, so approximate times to the ones at which the images were taken, have been considered.

Tuesday 19 September 1989			
	Hour	Height	Coefficient
LW	00:45	0.81	–
HW	06:36	6.45	–
LW	13:05	0.70	–
HW	18:51	6.32	–
–	–	–	–

Figure 6: Figure corresponding to the Tide Table for 19 September 1989, acquired from `http://maree.shom.fr/`.

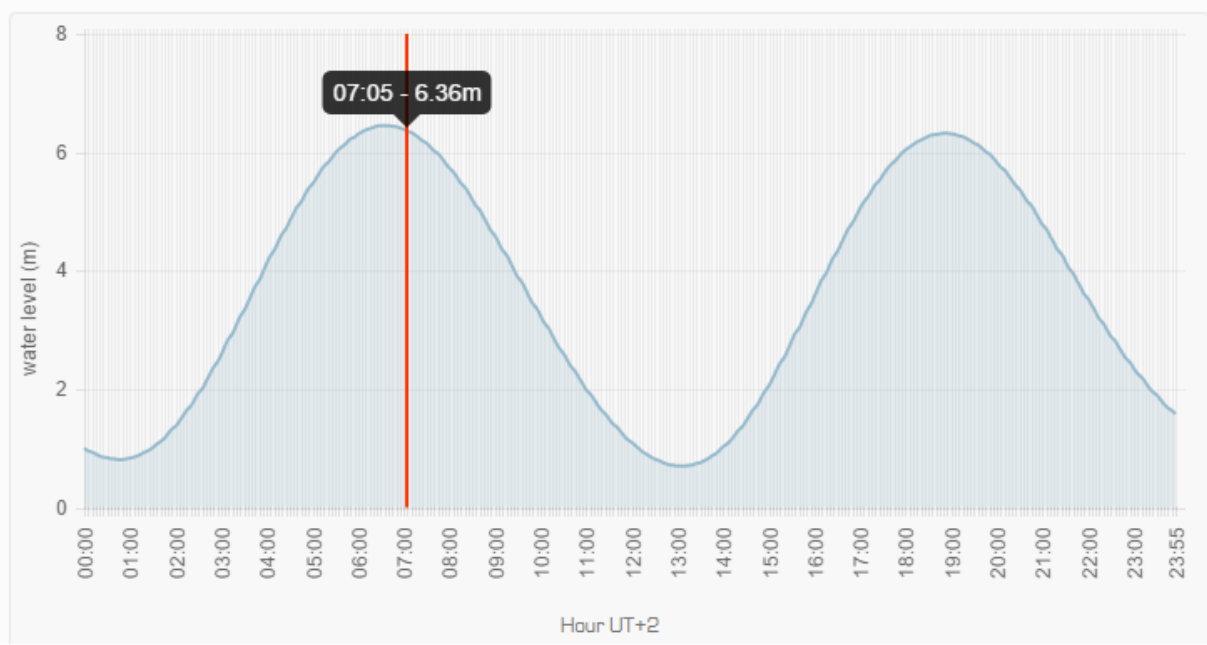

Figure 7: Water Level prediction for 19 September 1989, acquired from `http://maree.shom.fr/`.

Since the only Port in the area of study was the one present in Beira, this Port was used for the computation of tidal predictions for the entire area. It is recognized that generalizing tidal heights occurring in Beira Port region as the same as for the entire area of study comes with some error associated, which is considered in the discussion of the results.

Therefore, SHOM was used for computation of tide predictions for all the images acquired. Table 4 shows the occurring tides and their respective heights. It was possible to infer that at the time that all images were taken, high tide was occurring. When considering the images to use, tide height was also taken into consideration, since if there was a huge difference between tide heights from one year to the other, this would reflect in the results obtained when performing coastline change analysis, and erosion results would be either overestimated or underestimated.

Table 4: Occurring tide and wave heights, at approximate times, for all images under study.

Date	Occurring Tide	Height (m)	Local Hour
19/09/1989	High Tide	6.36 (07:05)	07:07
31/05/1995	High Tide	5.30 (06:50)	06:48
30/08/1999	High Tide	6.16 (07:20)	07:19
24/06/2004	High Tide	5.53 (07:25)	07:23
20/08/2007	High Tide	5.11 (07:35)	07:35
06/05/2015	High Tide	5.02 (07.40)	07:41

4.2 Pre-processing

Since the images were collected at Level-1T processing, it could be assumed that they where already geometrically corrected and georeferenced towards each other. However in order to make sure that this was indeed the fact, careful visual analysis was done using the swiping tool in ENVI and making sure that no easily changeable infrastructures, like the airport in Beira and some roads, were overlapping in all images used. This was done in order to avoid major errors in later evaluation of erosion areas and change rates. The images were already in the same spatial reference frame UTM projection and under a WGS84 ellipsoid, so there was also no need to register them towards each other. Even so, automatic co-registration of the images was tested, however some distortions would often occur, so this method was discarded.

During radiometric calibration of L1T data, TM and ETM+ sensors convert the reflected solar energy to radiance and rescale it into an 8-bit digital number (DN) with a fixed range between 0 and 255 (Table 5) (Chander et al., 2007; Barsi et al., 2007). These DN values can be converted into radiance values using bias and gain values specific for the scene under study (Chander et al., 2007). This information is contained within the metadata file of each image. Landsat 8 OLI sensor is more sensitive which translates in this data being rescaled into 16-bit DN values with a range between 0 and 65536. Also, this data has been converted to reflectance, instead of radiance (USGS, 2016c).

When performing Dark Object Subtraction (DOS) in ENVI, it was observed that no visible changes between the image obtained and the source image could be seen. DOS searches the image for the darkest pixel and subtracts its value from every pixel in the band bringing the minimum value down to 0. However, when computing statistics for both source and DOS images it was possible to see that no changes in minimum value occurred. This was due to the fact that L1T images already have this correction applied and the minimum value for each band was already 0. This allowed to reach the conclusion that no further radiometric correction would be performed.

Table 5: Statistics results representing DN values for Landsat image from 1989.

Basic Stats	**Min**	**Max**
Band 1	0	255
Band 2	0	232
Band 3	0	255
Band 4	0	255
Band 5	0	255
Band 7	0	255

In the end, it was decided that no further pre-processing would be done and the images would be used as acquired since the quality of their georeferencing and radiometric calibration was deemed satisfactory.

Before starting with the analysis, all images were clipped using the resize tool in ENVI (Figure 8), since there was a great part of the images which represented the interior and not the coastline area. With this done, the images were ready to proceed with coastline mapping by employing two different land/water classification approaches.

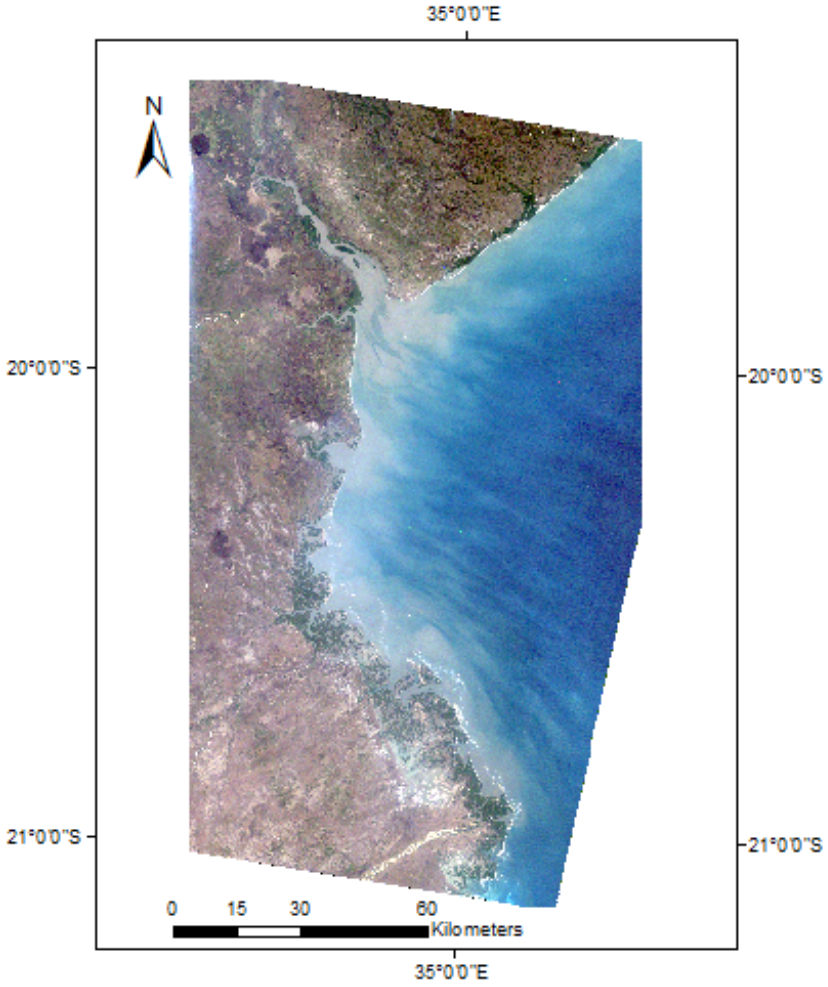

Figure 8: Image after resizing, corresponding to the year of 1989 at 3-2-1 (RGB) band composition.

4.3 Processing

4.3.1 Coastline mapping

Before proceeding with implementation of the classification methods in order to classify the images in two classes, "land" and "water", three aspects, for posterior coastline extraction, were taken into consideration:

- Class "Land" would include sand areas, beaches and sand dunes;

- Intertidal zone should be classified as "Water";

- Intertidal zone considered as land should be minimal or none at all.

The intertidal zone, often referred as littoral zone, is defined as the part of the coastline that is submerged during high tide and exposed at low tide (UNEP, 2001). As it was presented above, at the time the images were taken, high tide was occurring, which means, the intertidal zone is expected to be

submerged. As such, it should be considered as water class.

At 5-4-2 (RGB) band composition, the intertidal zone can clearly be seen, when compared with 3-2-1 (RGB) (Figure 9). How this zone is classified will greatly influence how the coastline is delimited and the following results obtained.

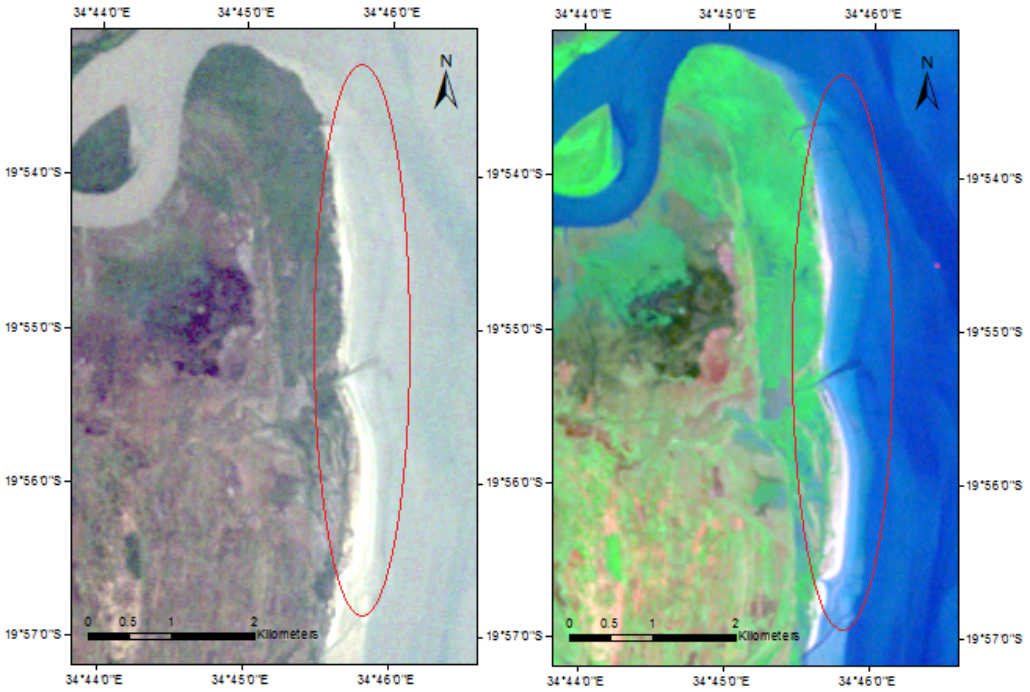

Figure 9: Intertidal zone difference at 3-2-1 (RGB) band composition, on the left, and at 5-4-2 (RGB), on the right, for 1989 image.

To classify the images and delineate the coastline, two different approaches were followed:

(1) Discrimination of land and water interface for coastline identification through the use of the Modified Normalized Difference Water Index (MNDWI) and

(2) a semi-automatic image classification method based on Support Vector Machines (SVMs).

After employing different methods this two were the ones that reproduced a more clear and accurate coastline for the region under study. Both methods were generated using ENVI 5.0.

The MNDWI water index is generated making use of the band math function in ENVI software by combining the green and mid-infrared bands. The green band is sensitive to water turbidity and it can be useful to discriminate broad classes of vegetation. The mid-infrared band exhibits a very strong contrast between land and water since there is a high degree of absorption by water and strong reflectance by vegetation and natural features in this range. This combination of bands makes this algorithm very useful for the discrimination between land and water. (Ghosh et al., 2015; Xu, 2006)

The MNDWI is estimated as,

$$MNDWI = \frac{Green - MIR}{Green + MIR} \quad (1)$$

where, green corresponds to band 2 and band 3 in TM and Landsat 8 images, respectively, and MIR (midle-infrared) corresponds to band 5 and band 6, in TM and Landsat 8, respectively.

This ratio of bands generates results between -1 and 1. Negative values represent land features while positive values represent water features (Xu, 2006). Afterwards, histogram thresholding was performed over the MNDWI images to create two classes, land and water, from which the coastline was extracted directly.

SVMs is a supervised classifier that has several advantages when compared with other classification approaches. "SVMs obtain their decision directly from the training data in a suitable space that is described by a kernel function" (Petropoulos et al., 2015). This method, contrary to others, is also easy to implement and has been implemented so far in different types of Earth observation data, at different scales, and generated reliable and promising results (Huang et al., 2008; Otukei and Blaschke, 2010; Petropoulos et al., 2012a,b; Volpi et al., 2013). However, compared to more traditional methods, the implementation of SVMs for coastline delineation is still very ill explored (Petropoulos et al., 2015).

Before starting with implementation of the SMVs, images were loaded into ENVI in a 5-4-2 (RGB) colour composite, in TM images, and 6-5-3 in the Landsat 8 image, which is relatively similar to true colour composite of the Earth surface and depicts the interface between land and water very well (Alesheikh et al., 2007). As seen in figure 9 this will also facilitate during validation of the results since it helps distinguishing between land, water and intertidal zone clearly.

SVMs was implemented in each of the images at their original spatial resolution. This was done in two steps. First, pixels were collected separately for each of the images on a random sampling strategy, through the selection of regions of interest (ROIs) representing each class, "land" and "water". Second, a multi-class pair wise classification was implemented where SVMs was applied using all the sensor reflective bands to define the feature space. This pair wise SVMs classification was performed using a non-linear kernel function, the **Radial Basis Function (RBF)** (Petropoulos et al., 2015). This kernel requires the definition of a small number of parameters in order to run and it has been shown to produce good results in a range of classification studies (Kavzoglu and Colkesen, 2009; Petropoulos et al., 2010; Yang, 2011).

In order to apply the SVMs, four parameters needed to be specified, the gama parameter, the penalty parameter, pyramid levels and the classification probability threshold. To do this parameterisation recommendations provided in ENVI On-line Software Users's Manual (ENVI, 2016) were taken into account as well as values used in previous studies (Petropoulos et al., 2015). The gama parameter is defined by the user and is normally equal to the inverse of the number of spectral bands of the image used each time. In this study this value is 0.167 for TM imagery, since 6 spectral bands were used, and

0.125 for Landsat 8 imagery, where 8 spectral bands were used. The penalty parameter is a floating point value greater than 0, that controls the trade-off between allowing training errors and forcing rigid margins. To ensure accuracy it was set to the maximum value, 100, which is also the default one. Pyramid levels parameter was set to 0, which means that each image was processed at full resolution. Classification probability threshold was set to 0, the default value, which forces all image pixels to be classified into one class label (ENVI, 2016; Petropoulos et al., 2015).

In the end, this method produced an image classified in two classes, land and water, from which it was possible to extract the coastline.

When analysing the results from both methods, MNDWI and SVMs, it was possible to observe that they delivered results slightly different in terms of where the interface between land and water was created. To better understand these results, validation was needed in order to be sure which of these methods was delivering a more accurate and correct coastline.

After validation, areas that reflected higher changes in terms of erosion and/or accretion, were identified and further analysis was performed for these regions, with coastline change detection, by creating erosion and accretion polygons, and afterwards with calculation of the coastal vulnerability index.

4.4 Coastal Vulnerability Index (CVI)

The CVI is determined by combining relative risk variables to create a single indicator (Jana and Bhattacharya, 2013). In this study and following the work done by Jana and Bhattacharya (2013), three risk variables were considered: coastline change rate, land-use and population density. The CVI is calculated based on the risk values assigned to each of the input parameters and is computed as the square root of the product of all ranked variables and divided by the total number of variables (n) (Jana and Bhattacharya, 2013; Chandrasekar et al., 2013; Kumar et al., 2010).

Equation 2 represents the CVI.

$$CVI = \sqrt{\frac{[a \cdot b \cdot c]}{3}} \tag{2}$$

Where a= risk rating assigned to coastline change rate; b= risk rating assigned to land-use cover and c= risk rating assigned to population density.

4.4.1 Coastline Change Rate ('a')

After compiling the coastline positions in ArcGIS 10.0, making use of the Append tool, the Digital Shoreline Analysis System (DSAS 4.3) developed by USGS in 2010 (Himmelstoss et al., 2009) was used to estimate the rate of coastline change. The DSAS has been successfully employed by various authors, which underlines the suitability of this tool for the analysis that is being undertaken here (Fletcher et al., 2012; Thieler and Danforth, 1994a,b; Himmelstoss et al., 2009). The DSAS is an ArcGIS extension that uses a measurement baseline method to calculate rate of change statistics for a time series of coastlines. The baseline is constructed by the user and serves as the starting point for all transects cast by the application (Addo and Kodzo, 2013). Inputs needed for this application consist in the constructed baseline, coastlines for several years, appended to each other and need to be dated, and transect distance (Kumar et al., 2010). The rate of change is calculated for the previous identified regions within the study area that suffered the most visible changes. 1900 transects were cast at 100 meter interval and historical rates of coastline change were then calculated for each transect using end point rate (EPR) statistics with 95% confidence interval. This method is calculated by dividing the distance of coastline change by the time elapse between the oldest and the most recent coastline, in this case approximately 26 years (Figure 10) (Himmelstoss et al., 2009).

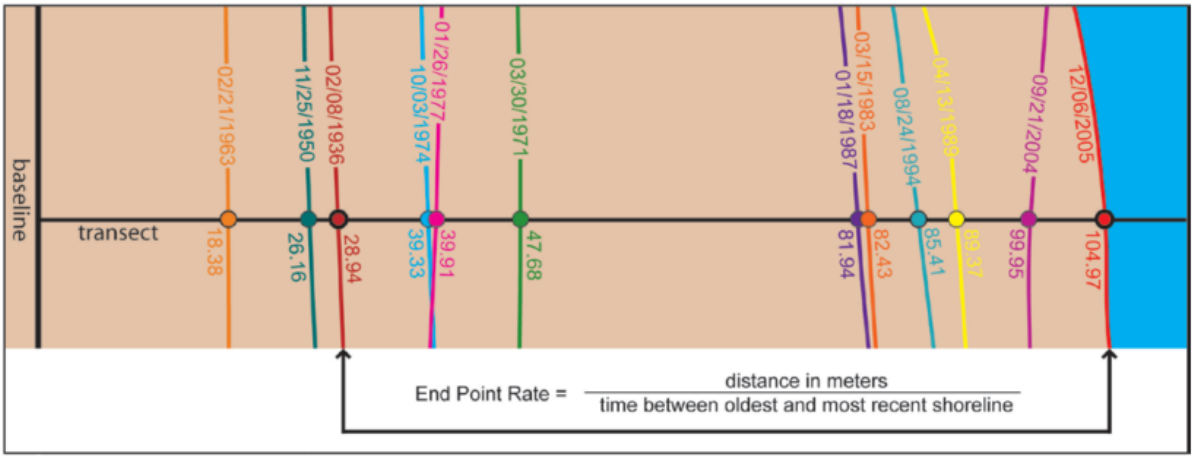

Figure 10: Example of how EPR statistics are calculated, acquired from Himmelstoss et al. (2009).

EPR statistics are easy to compute and have a minimal requirement of only two shorelines. The greatest disadvantage is that in cases where more data is available, like tidal data for example, the additional information is ignored (Himmelstoss et al., 2009). However, in this study it is not being considered any additional information besides the coastline positions for the calculation, and so this method was deemed to be a good choice.

After calculating the EPR and taking into account the risk categories employed by Jana and Bhattacharya (2013), coastline erosion and accretion rates were grouped in four risk classes (Table 6) and risk maps obtained.

In the table below, negative values represent erosion and positive values represent accretion.

Table 6: Risk classes assigned to coastline change rate parameter, adapted from Jana and Bhattacharya (2013).

Risk Classes	Change Rate (m/year)
Severe Erosion	< -10
Erosion	-10 - 0
Accretion	0 - 10
High Accretion	> 10

4.4.2 Landuse Cover ('b')

The protection of an area deemed vulnerable, will only be considered if the said area is recognized as sufficiently important in terms of economic, cultural and environmental aspects that justify its protection. This is why landuse type is of significant importance in determining vulnerability of an area (Jana and Bhattacharya, 2013; McLaughlin et al., 2002). There are many ways to assess the value of land, such as monetary terms, placement cost, in aesthetic terms or even in terms of conservation value. In this study, landuse types were grouped and ranked according to economic value. This was done based on a subjective assessment of which landuse types were more or less valuable, specially to humans (McLaughlin et al., 2002).

For the purposes of this present study, data from DINAGECA (Direcção Nacional de Geografia e Cadástro) of Mozambique, relative to the year of 2009, has been used to assess landuse. This Shapefile was loaded into ArcMap and a buffer of 1km, with landward direction from the coast, was computed. Landuse types occurring in this buffer zone were identified and ranked accordingly. Grouping and ranking were done based on the classifications performed by Jana and Bhattacharya (2013) and McLaughlin et al. (2002) (Table 7).

Industrialized areas, urbanized and semi urbanized dwelling areas are included in the "very high capital" category. Salt pans and agricultural areas are within the "high capital" landuse category. Mangroves and different types of vegetation have been mapped within the "moderate capital" category, while, bare soils and river banks were mapped within the "low capital" landuse category.

In the region of study it was possible to identify 11 different types of landuse areas. Industrialized areas, urbanized and semi-urbanized dwelling areas are found in the city of Beira, as one would expect. Rainfed cultivation is also found near the coast of the city. North of the city, salt pans, meadows and bare soil areas can be identified. The rest of the coastline is basically dominated by the existence of Mangroves, which have great importance in the Mozambican coast and their disappearance contributes to increased erosion hazard.

Mangroves provide several forest resources such as high-grade timber and non-timber products that support rural economies as well as eco-tourism. Mangroves are very important in coastal areas since they protect against natural disasters such as tsunamis, cyclones and erosion. In Mozam-

bique they are of great importance since they act as natural flood barriers, a very important function, since about 44% of the country's population live in coastal areas, many of them in floodplains (Palalane et al., 2015). Over the past decade, floods have become bigger and more frequent, which is predicted to further increase (Chevallier, 2013). However, densely populated zones have intensified the clearing of mangroves for coastal development, agriculture, aquaculture or for resource use, such as the case of Beira, which intensifies coastal vulnerability (Cohen et al., 1997; Chevallier, 2013). Beira has been identified as the Mozambican city most vulnerable to sea level rise and to the increase in frequency and intensity of cyclones (Palalane et al., 2015; Theron et al., 2012). Mangroves provide a natural defence against flooding and act as a barrier towards natural induced erosion. However, mangroves in the city are also seen as a great economic resource, not only in terms of fishing but charcoal burning is rapidly depleting mangrove forests that still remain in the city outskirts. Even though the sale of mangrove wood is prohibited, illegal activities still continue to take place decreasing even further this so precious resource. Not only that but urban growth is placing adittional pressure on mangrove areas, with growing demand for wood and non-timber products (Chevallier, 2013). Sofala Bay region is estimated to have the largest mangrove area and the second highest rate of deforestation of mangroves in Mozambique, with 4.9% per year (Sitoe et al., 2014). It is vital that traditional engineering interventions be accompanied by restoration of mangroves and with plantation of trees on dunes. This has been in fact recognized by the government and the National Institute of Disaster Management (INGC) has drawn a master plan for 2006-2016 which includes this interventions and mangroves are seen as an integral part of Mozambique's climate change adaptation and disaster risk reduction response (Chevallier, 2013).

Table 7: Risk classes assigned to Landuse parameter, adapted from Jana and Bhattacharya (2013).

Risk Classes	**Landuse areas**
Very High Capital	Urbanized dwellign area Semi-urbanized dwelling area Industrialized area
High Capital	Salt Pan Rainfed cultivation
Moderate Capital	Mangroves Meadow, Aquatic Meadow
Low Capital	Bare soils River banks

It is important to note once more, that landuse areas were identified for the buffer zone of 1km landward. Regions in the interior have other types of landuse, however, for the purposes of this study they are not considered.

4.4.3 Population density ('c')

There are two ways to look at the effects of population density over an area. Population can be looked as an 'economic' variable since people in highly populated areas will act to protect their properties from erosion. However, looking by this perspective, areas which have fewer people, will not suffer the same urge or willingness for protection as the ones in densely populated ones. On the other hand, heavy population in coastal areas can be interpreted as an "erosion-inducing" variable, since the presence of large numbers of people near the coast may produce damaging impacts on coastal areas. Both this views are complementary, since one affects the other in increasing or decreasing vulnerability (Jana and Bhattacharya, 2013; McLaughlin et al., 2002). This is why it becomes essential to study this parameter when assessing the vulnerability of the coast. As such, coastal areas with high population density are considered to be highly vulnerable and low population density areas are considered to have low vulnerability (Jana and Bhattacharya, 2013).

Census data from 2007, obtained from Mozambique Instituto Nacional de Estatística, was used to evaluate and estimate this parameter. For each province, census data available was divided by the respective area and population density obtained. Data relative to the area of each province, was obtained from DINAGECA (Direcção Nacional de Geografia e Cadástro) of Mozambique, last updated in 2009. Following the categories assigned by Jana and Bhattacharya (2013), population density over the area of study was then grouped in four risk classes (Table 8).

Table 8: Risk classes assigned to Population Density parameter, adapted from Jana and Bhattacharya (2013).

Categories	**Population density (people/km^2)**
Very High Density	> 1500
High Density	1001 - 1500
Moderate Density	501 - 1000
Low Density	< 500

4.4.4 Computation of the CVI

Table 9 presents an overview of the overall variables and their rankings. Each of the three variables was loaded into ArcMap software environment and a "Fishnet" was created over the coastline, with a cell size of 500x500 meter (Figure 11). After a few cell sizes were tested, this was considered to be enough in order to proceed with the classification.

This Fishnet was intersected with the 1km buffer created in regards to 1989 coastline as baseline. From this intersection resulted the area between the 1km buffer line and the baseline to be divided into polygons. Each of the polygons were then ranked for each parameter, according with the classification displayed in table 9, with a value between 1 and 4, by manipulating the attribute table. After

Table 9: Vulnerability classification, adapted from Jana and Bhattacharya (2013).

	Risk Rating			
Variables	**Low (1)**	**Moderate (2)**	**High (3)**	**Very High (4)**
Coastline Change Rate (m/year)	>10	0 - 10	-10 - 0	<-10
Landuse	Bare soils River banks	Mangroves Meadows	Salt Pans Irrigated cultivation Rainfed cultivation	Urbanized dwelling area Semi-urbanized dwelling area Industrialized area
Population density (people/km^2)	< 500	501 - 1000	1001 - 1500	>1500

having this ranking performed, CVI was calculated, as represented in equation 2, by making use of "Field calculator" option. In the end, vulnerability maps for every parameter and for the CVI were obtained and visual analysis of the results was then performed.

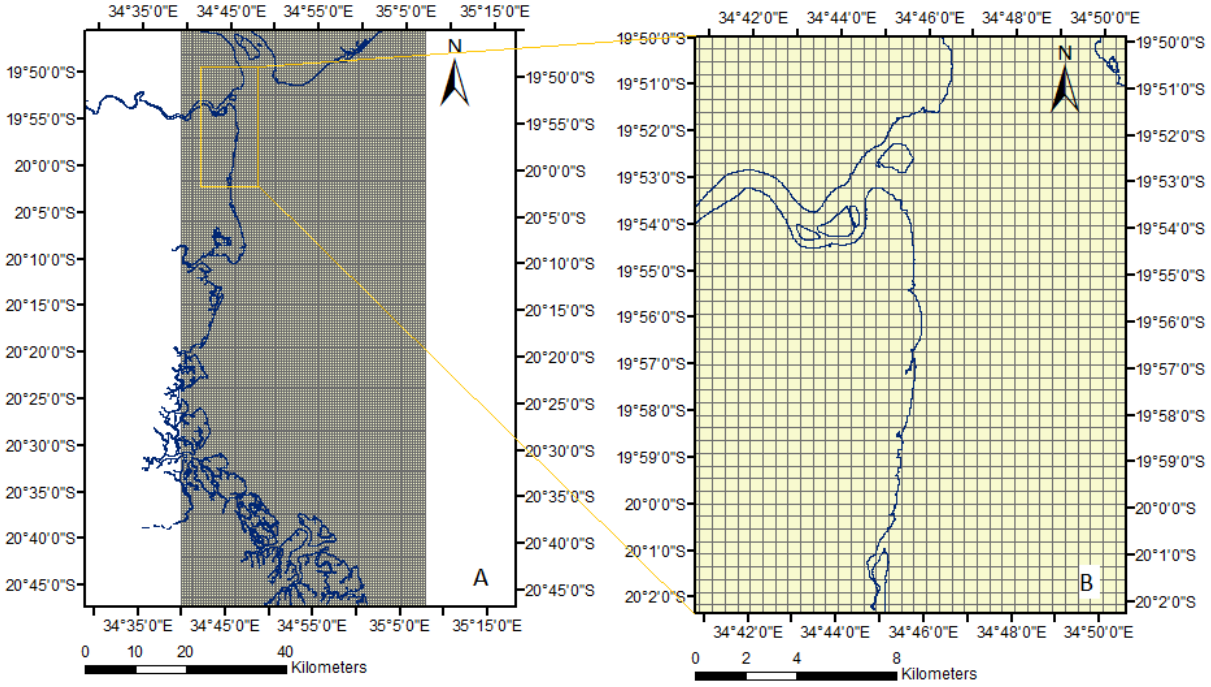

Figure 11: A - Exemplification of how the Fishnet was created over the coastline; B - Zoom over a specific region of the coastline.

4.5 Methods used for validating the results

For the validation of the results, **Google Earth™** images as well as the **Eolian Mapping Index (EMI)**, were used. For the images in recent years (2004, 2007 and 2015) this could be observed by comparing the MNDWI and SVMs images with high spatial resolution images from Google Earth™ and with the EMI index. For older images (1989, 1995, 1999) the validation could only be done via EMI index due to the unavailability of images this old in Google Earth™ to allow comparison (Table 10). Google Earth™ images were very useful to identify intertidal zones, when these cannot be clearly seen in the images acquired or from the indexes employed.

EMI is an index that uses the red and near-infrared spectral bands to generate an image that emphasizes areas with low vegetation density and high soil reflectance. The near-infrared (NIR) and red (R) spectral bands combined with the ratio of red to near-infrared (R/NIR) were used, respectively, as RGB components to make a color composite (NIR - R - (R/NIR)). In the results obtained it is expected that the brighter tone of yellow represents sand areas, while bright red regions represent areas with high vegetation density (Khiry, 2007). Figure 12 shows the example of 2007 image after implementation of the EMI. This index was used with the objective to validate the classification obtained through MNDWI and SVMs application, acquire a better delimitation of the coastline and identification of erosion and accretion areas. It was generated using ENVI and ArcGis environment.

It is possible to infer from the table below that for the years of 2004 and 2007 the images acquired from Google Earth™ are relatively close in date to the ones under study here. However, for the validation of 2015 image, it was not possible to acquire a single image to validate the entire area, and so several images had to be used, being one very close in date with the one acquired from Earth Explorer.

Table 10: Data used for validation of the scenes under study.

Aquisition Date	Data Used for Validation
19/09/1989	EMI
31/05/1995	EMI
30/08/1999	EMI
24/06/2004	Google Earth image acquired on 26/10/2004; EMI
20/08/2007	Google Earth images acquired on 09/08/2006 and 11/07/2007; EMI
06/05/2015	Google Earth images acquired on 30/04/2013, 09/08/2013 and 20/05/2015; EMI

To assess for the accuracy of the land/water classification done by the implementation of SVMs, kappa coefficient (κ) and overall accuracy were calculated by computing confusion matrices in ENVI for each classified Landsat image. The overall accuracy is calculated by summing the number of correctly classified pixels and dividing them by the total number of pixels, the sum of the pixels in all the ground truth classes. The true class of pixels is defined by the ground truth regions of interest (ROIs). The kappa coefficient is another measure of the accuracy of the classification and measures the agreement between classification and ground truth pixels. A value of 1 represents perfect agreement while a value of 0 represents no agreement. (ENVI, 2016)

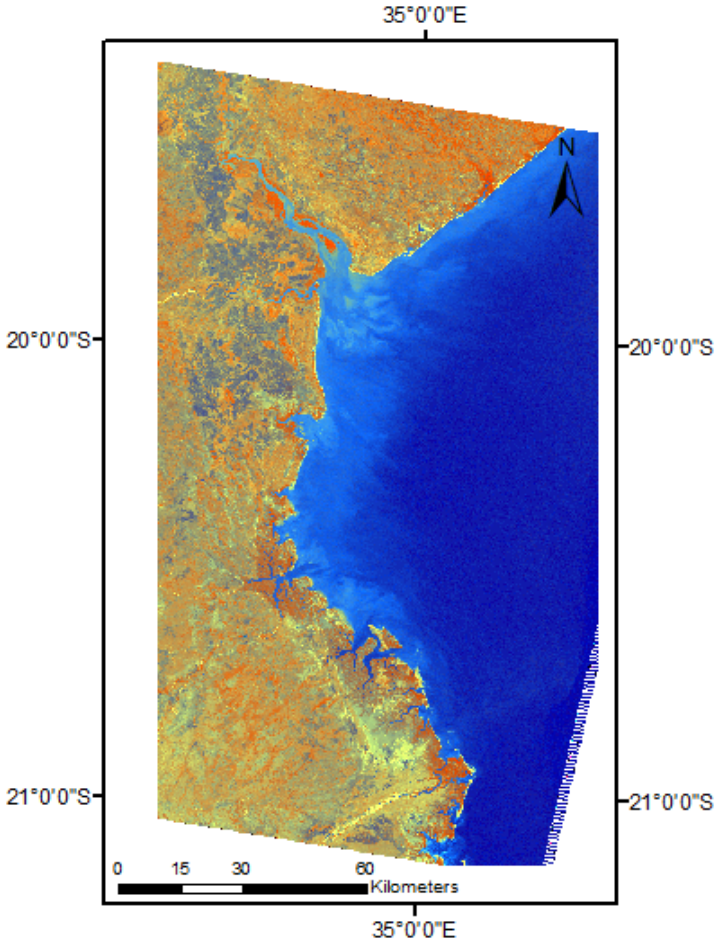

Figure 12: Image obtained after computation of the EMI for the year of 2007. Color Composite (NIR - R - R/NIR).

Accuracy assessment for MNDWI images was done exclusively through visual analysis of the obtained images with Google Earth ^{TM} and EMI index. No statistics were calculated since the approach for extraction of the coastline through these images is very direct.

Validation of change detection areas, erosion and accretion polygons, was performed once again by visual analysis of source images and EMI index which allowed to have a clearer understanding if recession and accretion were due to movements in land or due to movements in dynamic regions, like sand. Theron et al. (2012) presents results for erosion and accretion areas in the city of Beira between 1991 and 2004, which will be taken into consideration in the discussion of the results.

It was not found during the bibliographic research, CVI studies that had been performed in this region. As such, no results are available to compare and validate the ones obtained in this thesis. Maansson (2011) presents a value of 1 m/year for change rate along Beira city, which will also be taken into consideration during the discussion of the results.

5 Results

After obtaining the **MNDWI images**, histogram thresholding was performed. Figure 13 shows the images obtained after the computation of the MNDWI for the years of 1995 and 2015 as an example.

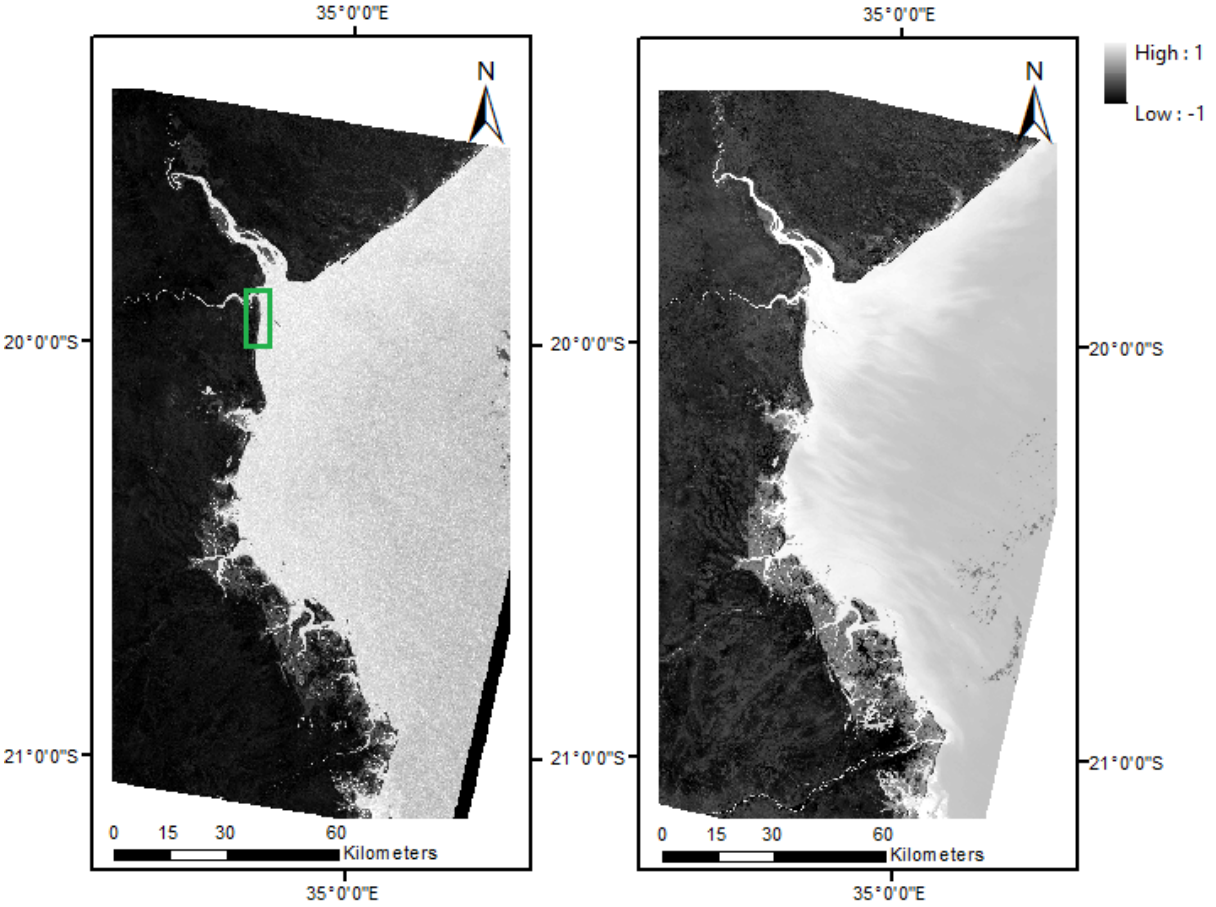

Figure 13: MNDWI images for the years of 1995, on the left, and 2015, on the right.

It is possible to observe from these images that the computation of the MNDWI generates an image where there is a great contrast between land and water features. This is a result of water being enhanced, and so represented with a lighter colour, while land is suppressed, with a darker tone, by the application of this index (Xu, 2006). The green square in the 1995 MNDWI image, delimits a region where deeper analysis regarding the classification employed will be performed further in this study.

The image generated is characterized by values between -1 and 1, where negative values represent land features while positive values water features (Xu, 2006). However, sometimes this relation is not so direct and land values can be found above 0, which has to be carefully analysed and taken into consideration when performing the classification into these 2 classes. Table 11 gives the thresholds applied to the different images in order to obtain an acceptable classification into water and land. Figure 14 shows the result of this classification for the image of 1995 as an example. Here, one can see that there seems to be a good classification of land and water features in regard to the coastline, but some other elements in the image are also being classified as land, when in fact they are not. Even though they are not shown here, this situation also occurs in the classified images of 1989, 1999, 2004, 2007

and 2015. Although this is true, for this study it poses no immediate problem since the objective of this classification is later extraction of the coastline and so it will not interfere with the results obtained for coastline change analysis.

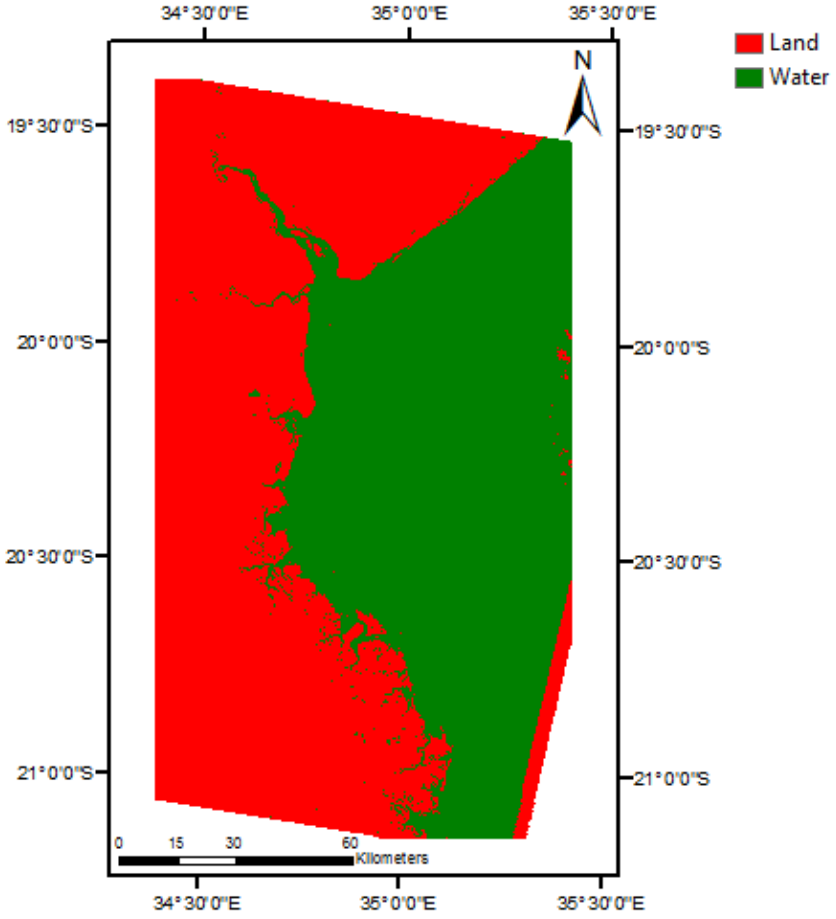

Figure 14: MNDWI Classified (land and water) image from 1995.

Table 11: Thresholds considered for classification of the MNDWI images into land and water when performing histogram thresholding.

Classified Map (Year)	Land	Water
1989	(-)1 - 0.15	0.15 - 1
1995	(-)1 - 0.05	0.05 - 1
1999	(-)1 - 0	0 - 1
2004	(-)1 - 0	0 - 1
2007	(-)1 - 0	0 - 1
2015	(-)1 - 0.05	0.05 - 1

Classification after employing **Support vector machines** also generated images with 2 classes, land and water (Figure 15).

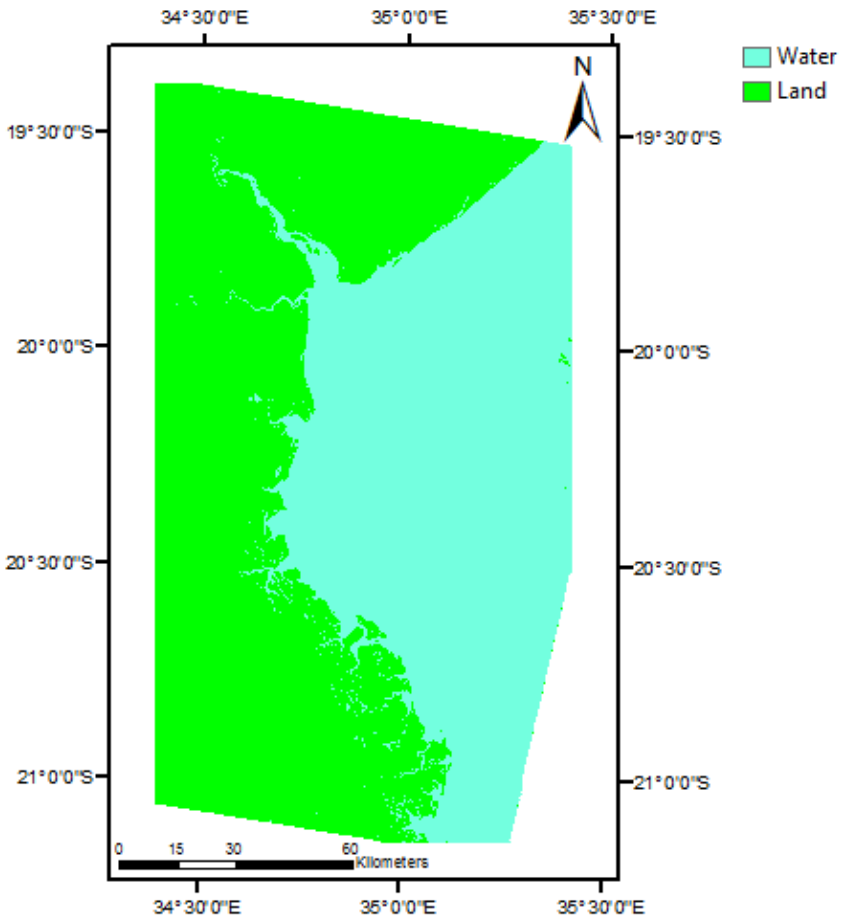

Figure 15: SVMs Classified (land and water) image from 1995.

As mentioned in the previous section, to assess the accuracy of land/water classification, from SVMs, kappa index and overall accuracy were computed for all the images under study, which can be found in table 12.

Table 12: Kappa Coefficient and Overall classification accuracy for Landsat images under study.

Classified Map (Year)	Kappa Coefficient	Overall Classification Accuracy (%)
1989	0.9991	99.96
1995	0.9943	99.73
1999	0.9909	99.57
2004	0.99	99.58
2007	0.9965	99.84
2015	0.9964	99.84

It is possible to conclude from table 12 that the overall accuracy of this classification is very high, with all classified images presenting a value close to 100%. Regarding the kappa coefficient, the value obtained is also very high, close to 1 in all images. This suggests that this technique is indeed very robust. It is important to note that the pixels considered for the regions of interest, in order to perform SVM's classification, were selected along the coast, respectively as Land and Water class. This contributed to obtain accurate classification results as it is possible to conclude from the data in the table

above.

After all images were classified, using both methods, extraction of the coastline was performed. For MNDWI classified images, coastlines were extracted directly from ENVI software and loaded into ArcMap for overlaying of all six coastlines. SVMs classified images were loaded into ArcMap and coastlines extracted making use of the "contour" tool, found in Spatial Analyst toolbox. However, it is not enough to simply extract the coastlines and proceed with further analysis and manipulation of the results. Careful validation is needed to observe if both methods employed are in agreement and if not, which of them produces more accurate and less error prone results.

5.1 Extracted Coastlines

When proceeding with validation of the extracted coastlines, it was possible to observe that there were clear differences between the coastlines obtained by the two methods, MNDWI and SVMs.

While performing histogram thresholding, parts that were classified as "land" had values above 0, which meant that some adjustments to the thresholds used for classification had to be done, as mentioned above. It was possible to notice that doing this procedure would affect the amount of intertidal zone considered as land, and which induced an overestimation of erosion, when later performing coastline change analysis. This was very clear during validation using Google Earth imagery, for the images of 2004, 2007 and 2015 and using the EMI index, for all images.

One of the greatest problems with the implementation of the MNDWI, found here, lies in the fact that one cannot distinguish clearly the intertidal zone from the rest of the land, and some parts of it end up being considered as land, overestimating the area of erosion. A region was chosen as an example of this problem since one of the major issues in delineating the coastline without including the intertidal zone was precisely in this region. The area chosen is delimited with a green rectangle, seen in figure 13. Although only the example of the extracted coastlines for 1995 is presented here, this situation happened in this area for almost every image in the entirety of the study period. Other areas were also affected by this problem but with less relevance. Figure 16 shows an extract of the MNDWI image for the selected region with the coastline obtained through histogram thresholding.

Another problem occurred in some cases where a few parts that were surely land were not delimited until higher positive values were reached. With this, the intertidal zone delimited, as land class, in other areas further increased, and with it the error associated with later estimation of erosion. When overlapping the extracted coastline from the MNDWI image with the EMI image, one can clearly observe that some of the intertidal zone was being considered as land (Figure 17).

In the EMI image the brightest tone of yellow corresponds to sand areas, and since it was decided this regions would also be considered as land in the limitation of the coastline, it was expected that the land/water boundary is precisely at the end of this sand regions. However, analysing figure 17,

one can see clearly that the coastline obtained via MNDWI image, blue line, was considering much more than just until this bright yellow regions.

On the other hand, the coastline obtained from SVMs supervised classification was delimited right at the end of these sand areas and basically no intertidal zone was considered in almost the entirety of the region of study and for all the images classified. An example of this is presented in figure 18, where the intertidal zone can be clearly seen (very pale tone of yellow after the coastline) with the coastline delimiting the land very accurately and in this specific example none of the intertidal zone was included in this delimitation.

Finally, when overlapping the coastlines extracted from both methods with the EMI (Figure 19), the difference in coastline positions was clear. While the coastline obtain through SVMs supervised classification delimited very accurately the land/water boundary, the MNDWI derived coastline did not, since it considered a considerable part of the intertidal zone as land. For this reason, conclusion was reached that for more accurate analysis of the results in subsequent sections of this thesis, the coastline obtained through SVMs supervised classification would be used, since it was expected to reproduce a more accurate and exact results with decreased error associated.

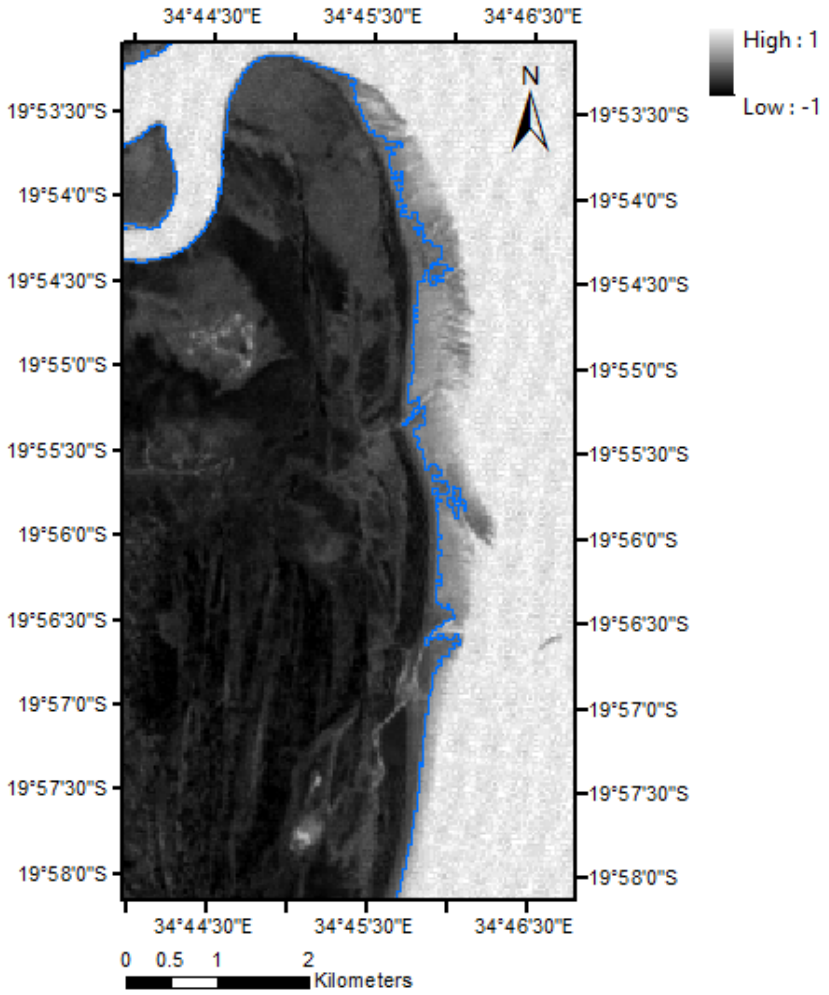

Figure 16: Extract of the MNDWI image with coastline delineated using histogram thresholding, in blue, from 1995.

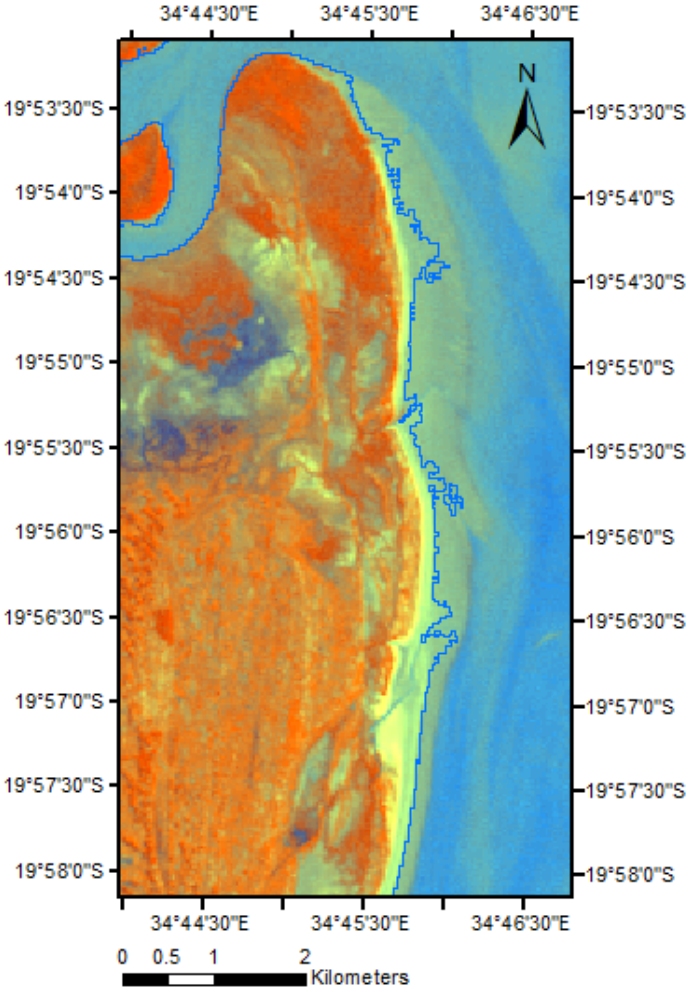

Figure 17: Extract of the EMI image with coastline delineated using histogram thresholding, in blue, from 1995.

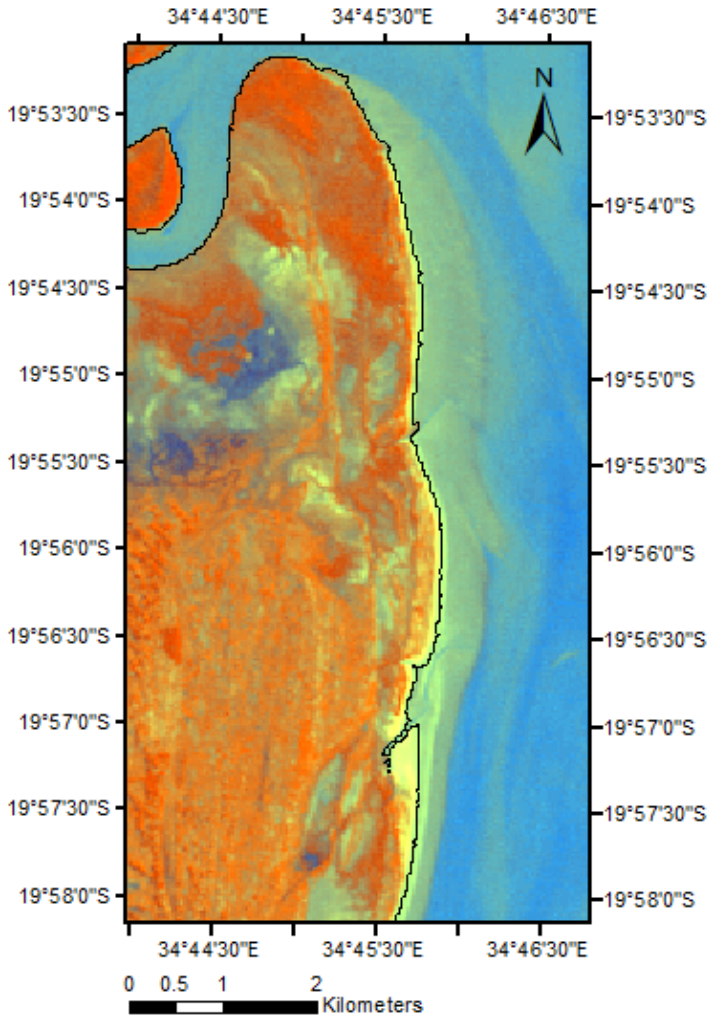

Figure 18: Extract of the EMI image with coastline obtained through SVMs, in black, from 1995.

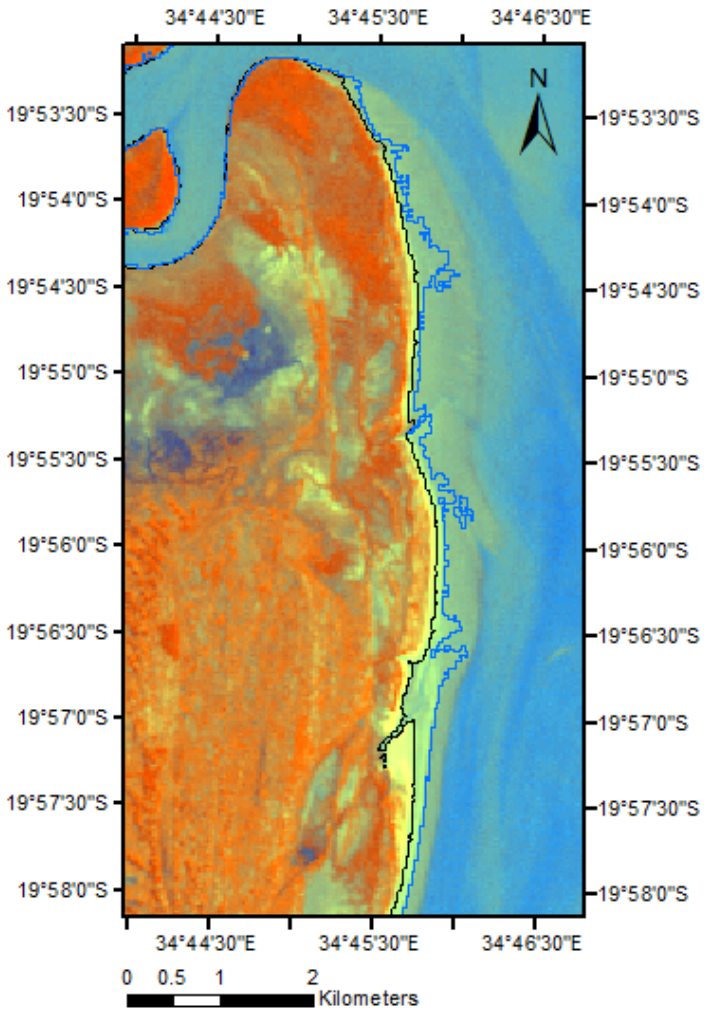

Figure 19: Extract of the EMI image with coastlines obtained through histogram thresholding, blue, and SVMs, black, from 1995.

5.2 Change Detection

After reaching the conclusion that coastlines extracted through the implementation of SVMs were more accurate, they were used for further analysis of erosion along the coastline. To detect changes, the resulting coastlines from the classified images were overlaid in ArcGIS 10.0 and coastline positions could be seen for each date (1989, 1995, 1999, 2004, 2007 and 2015). Different colours were given to the coastline of each year in order to make it easier to see the differences between them.

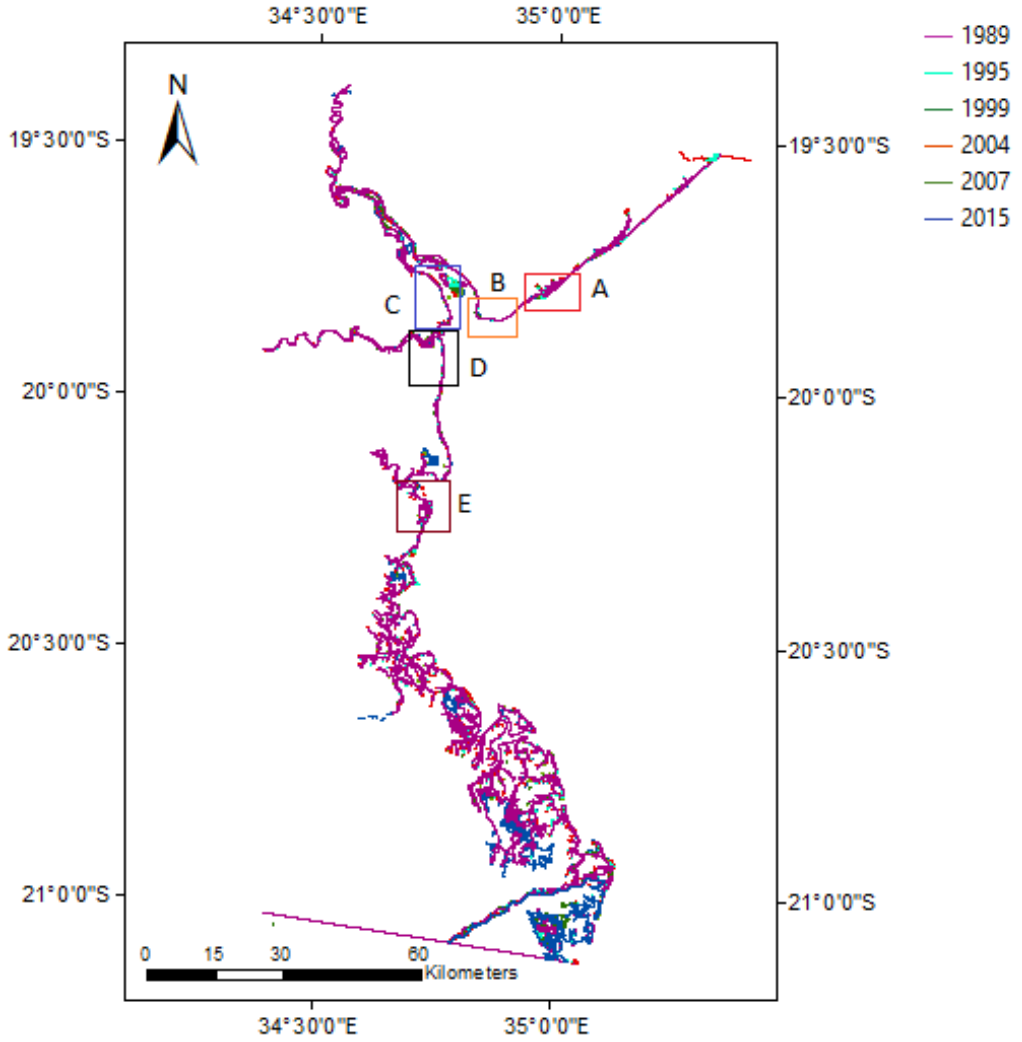

Figure 20: Coastline positions (1989-2015), with sites delimited from A to E.

The obtained coastlines were studied carefully through visual analysis, in order to identify erosion and accretion dominant locations. This was performed while comparing and validating coastline changes with the Landsat source images and EMI index. From this analysis 5 sites (A-E) were identified as the ones where erosion and accretion changes were greater when compared to others. These sites are identified in the image where all coastlines are overlaid (Figure 20).

It was possible to notice a specific trend through out the years. In case of erosion, the coastline

positions would shift landward from one year to the following. This means that from 1989 to 2015 there was constant recession of the coastline almost through out the entire area of study. It was also observed, in very few cases, that from one year to the other, in regards to each image, the coastline shifted landward, but in the following year it would shift seaward again. When these changes happened they were seen in sand regions, which have a dynamic nature and so, not surprising that this might happen since it depends from the sediments brought by the sea water and from sea currents.

Where accretion was concerned, the same trend was observed but in this case, from 1989 to 2015 a constant increase of coastline position, with seaward direction. There were identified regions where this increase was due to sand movement and others where land seemed to be increasing over the years. Deeper analysis of this situation is done further in this section and in later discussion of the results.

Some of these situations are present and can be clearly observed in the figures of the sites (A-E) chosen to perform deeper evaluation of coastline changes.

Since this trend was noticed, the conclusion was reached that there was no need to represent coastline changes for all the coastlines delineated but instead, a global analysis of the areas lost or gained between the oldest (1989) and the most recent coastline (2015) was performed. For every site chosen, polygons were created between these two coastlines in order to create erosion and accretion areas. Red areas represent erosion while green areas accretion.

Table 13 presents an overview of accretion and erosion areas and overall change in hectares and hectares per kilometre.

Site A

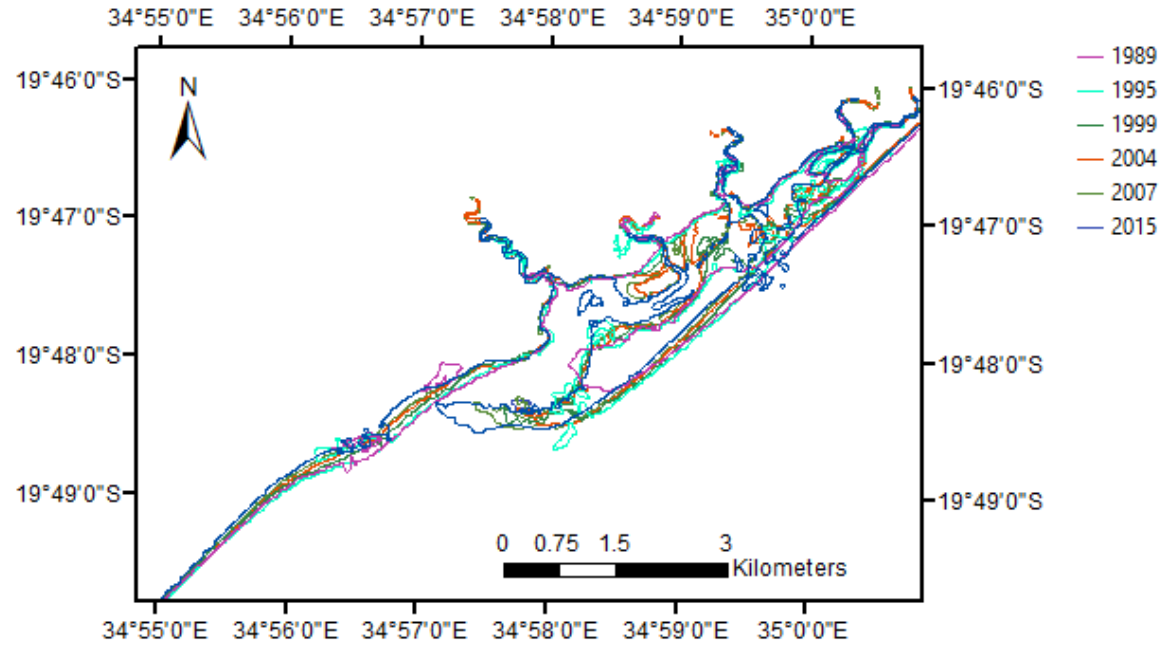

Figure 21: Coastline positions (1989-2015), for Zone A.

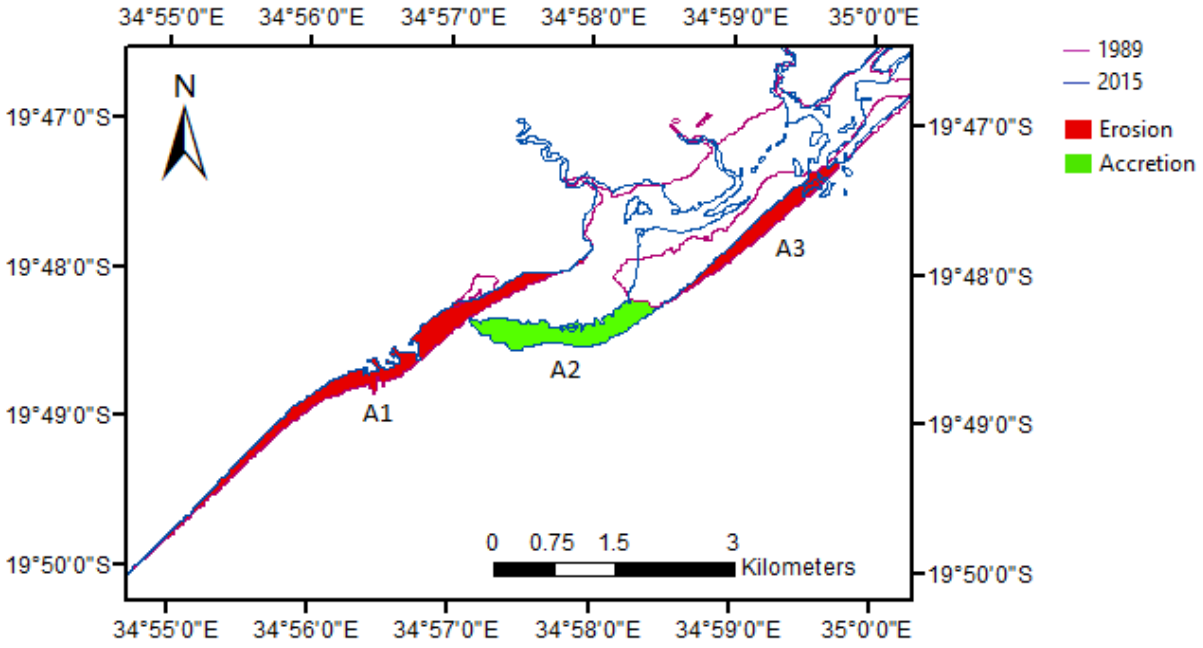

Figure 22: Difference between 1989 and 2015 coastline, for Zone A.

In this site, two erosion areas and one accretion area can be identified. One can observe that when erosion occurs, continuous recession of the coastline through out the years can be seen (Figure 21). Where accretion occurs, the area increased through out the period of study. Figure 22 shows this regions highlighted with respective colours, red for erosion (A1 and A3) and green for accretion (A2).

While performing validation of these changes it was possible to identify that all three of them represented changes due to sand movement. This could be clearly confirmed by analysing EMI images from 1989 and 2015 where changes in sand can be identified easily, since this feature had a bright tone of yellow. Figures 23 and 24 show these changes with EMI images from 1989 and 2015 respectively. Landsat source images also confirmed this fact.

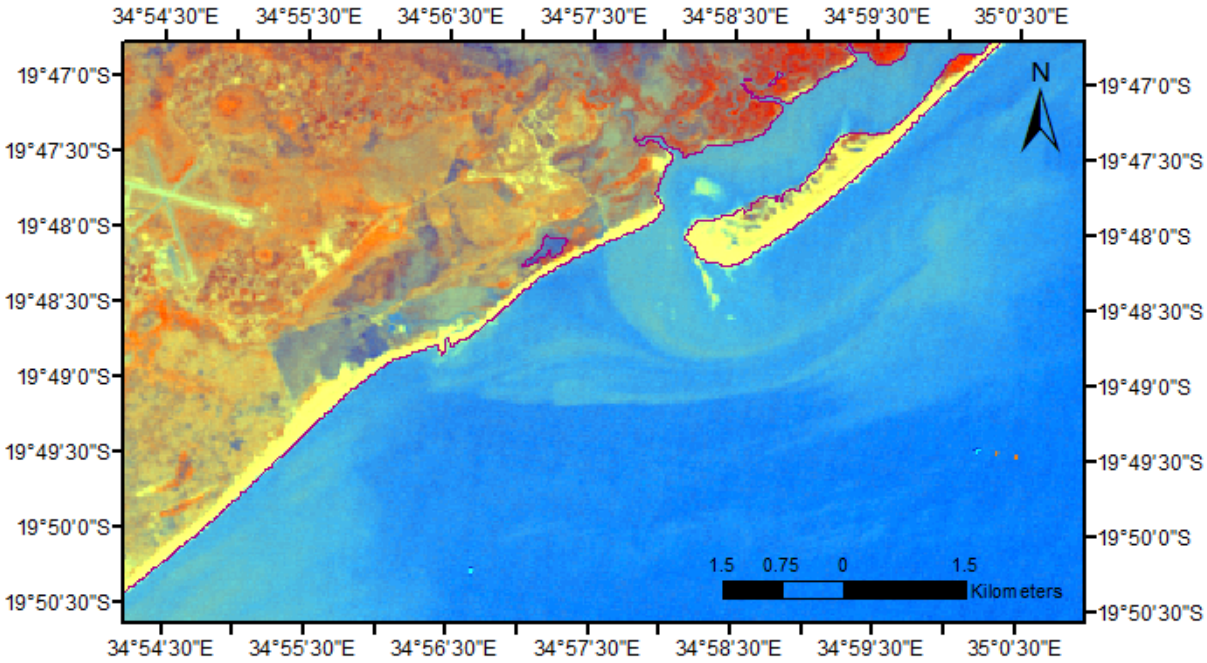

Figure 23: 1989 EMI image with respective coastline delineated.

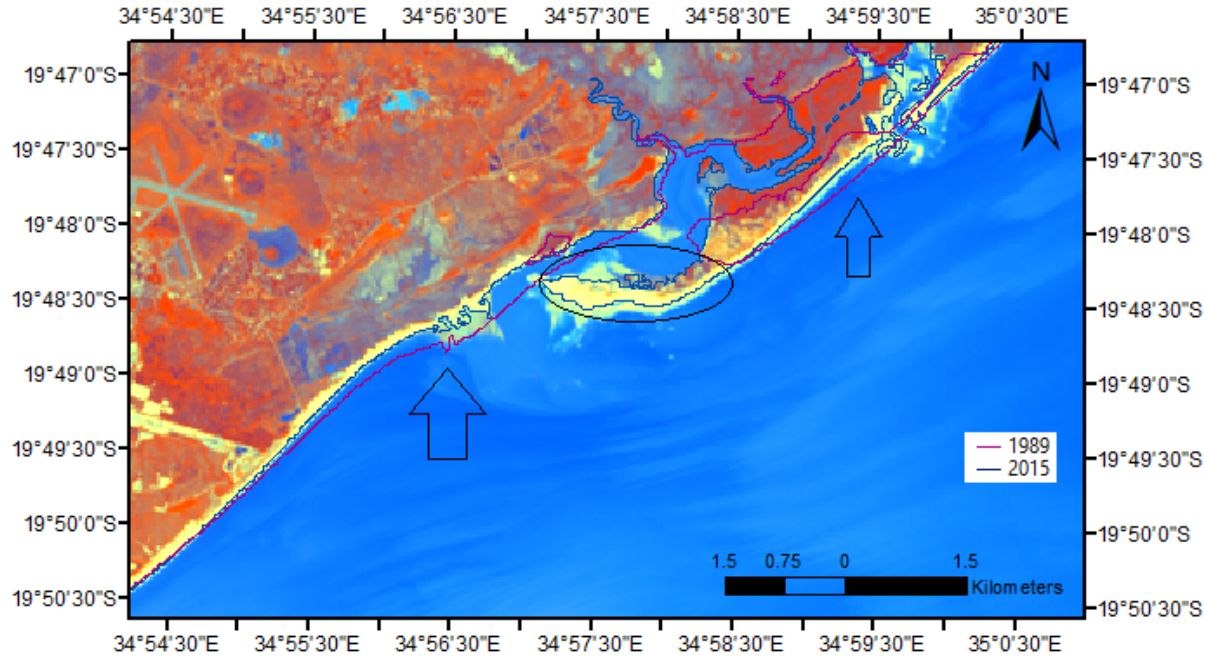

Figure 24: 2015 EMI image with 1989 (purple) and 2015 (blue) coastlines overlapped.

The arrows in figure 24 are pointing to the losses in sand between 1989 and 2015, and the circle the gain in sand in the same period.

Site B

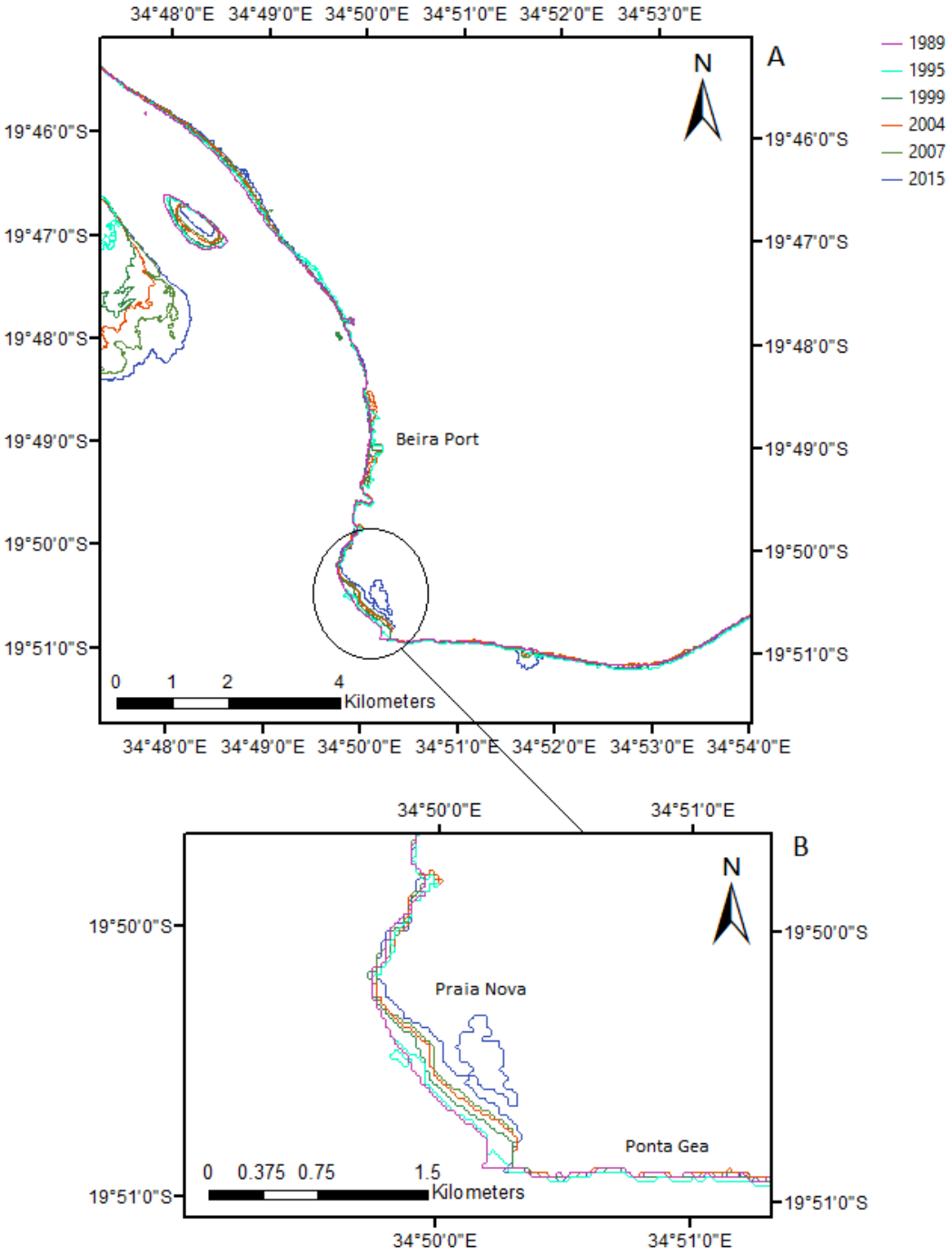

Figure 25: A - Coastline positions (1989-2015), for Zone B; B - Close up of coastline positions for Ponta Gea and Praia Nova regions.

In the region zoomed (Figure 25B), one can see the regression of the coastline throughout the years in study. There was no increase of coastline from one year to the other, there was always

regression. Validating this results with source images and EMI index it was possible to observe that in both regions where erosion occurred this represented an overall loss in land area. This is very warring specially in B2, because it represents a serious retreat of land in a very populated region, such as the city of Beira.

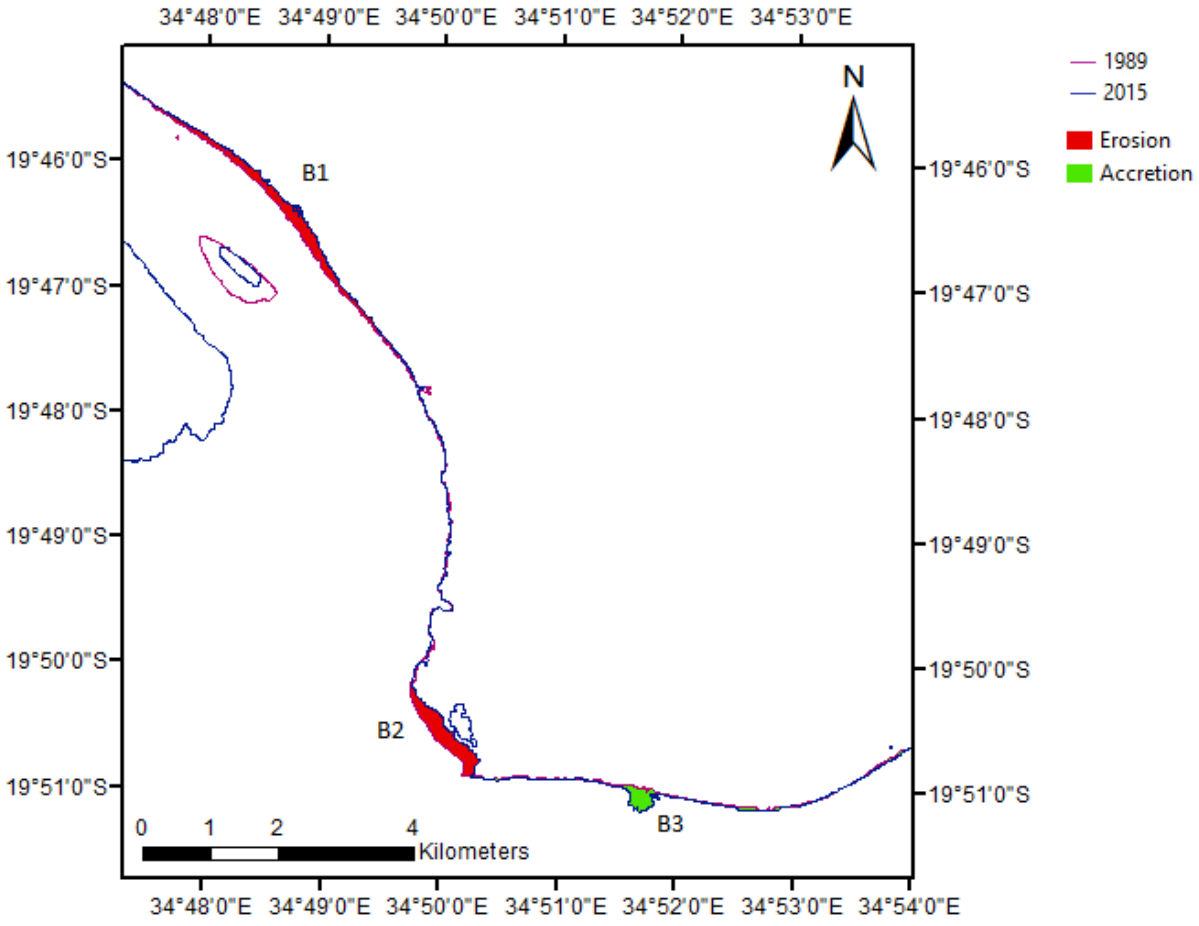

Figure 26: Difference between 1989 and 2015 coastlines, for Zone B.

Where accretion occurred (B3), after validation, it was possible to conclude that this illustrated a movement in sand. This was clearly visible in the EMI image since the evolution of this region through out the years was represented with a bright tone of yellow (Figure 27). Landsat source images at RGB band composition also proved this point. The observed accumulation of sand was a result of the construction of seawalls in the region immediately East of B3.

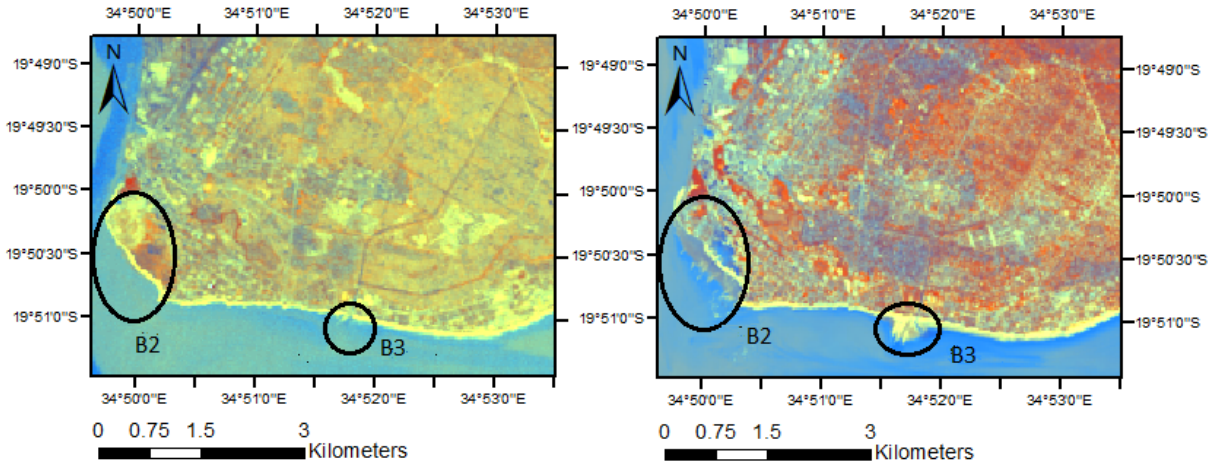

Figure 27: Validation of erosion and accretion for B2 and B3 in the city of Beira with 1989 EMI image, on the left, and 2015 EMI image, on the right.

Site C

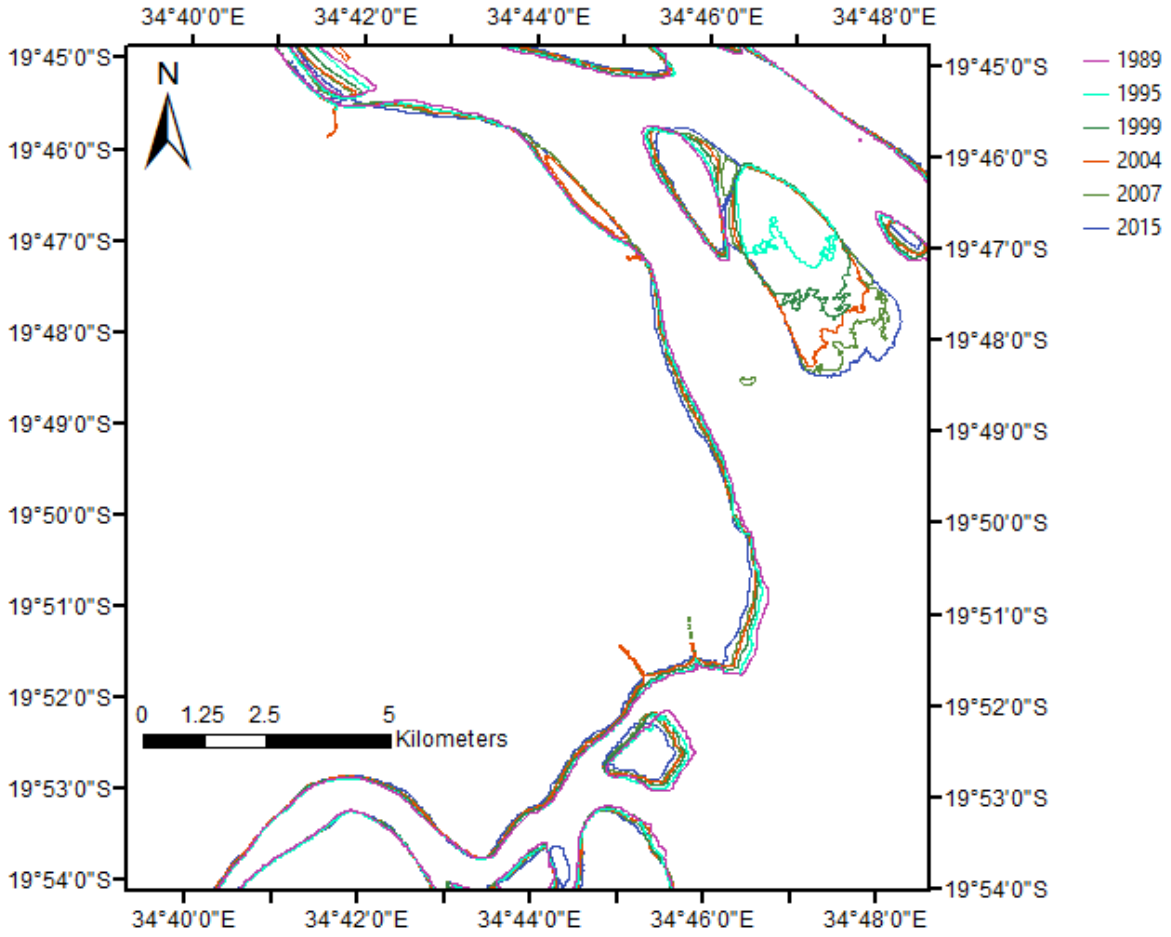

Figure 28: Coastline positions (1989-2015), for Zone C.

For this site, it was observed that through the years, there was recession of the coastline in C1 and C3, meaning that from 1989 to 2015 eroded area continued to increase (Figure 28-29). This areas concern to losses in mangrove area, since this region is dominated by the existence of mangrove forests.

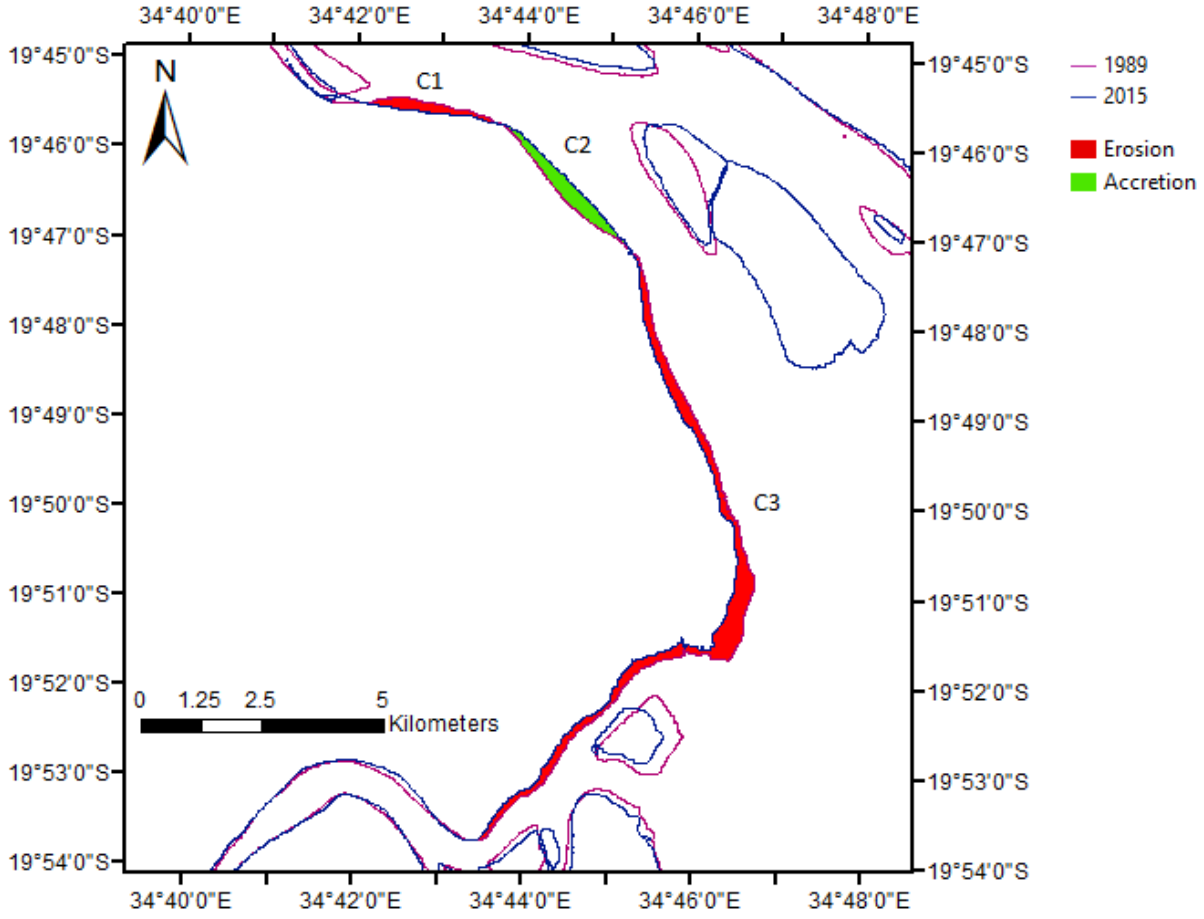

Figure 29: Difference between 1989 and 2015 coastlines, for Zone C.

Accretion in this case seemed to be due to an increase in land area, and not sand movement. This is clearly observed in figure 30. This increase is most likely to be in vegetation establishment. EMI index was also employed to validate this fact and it was observed that this region is characterized by a strong tone of red, which indicates high levels of vegetation density, contrary to yellow tones which indicate low vegetation density and high soil reflectance (Figure 31). This means that the probability of this increase in area, being due to vegetation establishment is quite high. In fact, this entire site is characterized by vast mangrove forests, and C2 accretion area is most likely due to mangrove establishment in this region. For why only in C2 this seems to occur, an attempt will be made to reach an explanation in the section of this thesis concerned with discussion of the results.

It is also possible to identify in the figures 28-31 some islands where accretion or erosion occurred. Although this changes were quite visible and in some cases major, they were not considered

for the estimation of overall change in area of coastline. Precisely because they were not considered to be part of the coastline in the wake of this study. However, it has to be recognized, especially in the cases where the size of these islands is decreasing, that recession can contribute to increased erosion pressure over some areas of the coast, once this islands are gone.

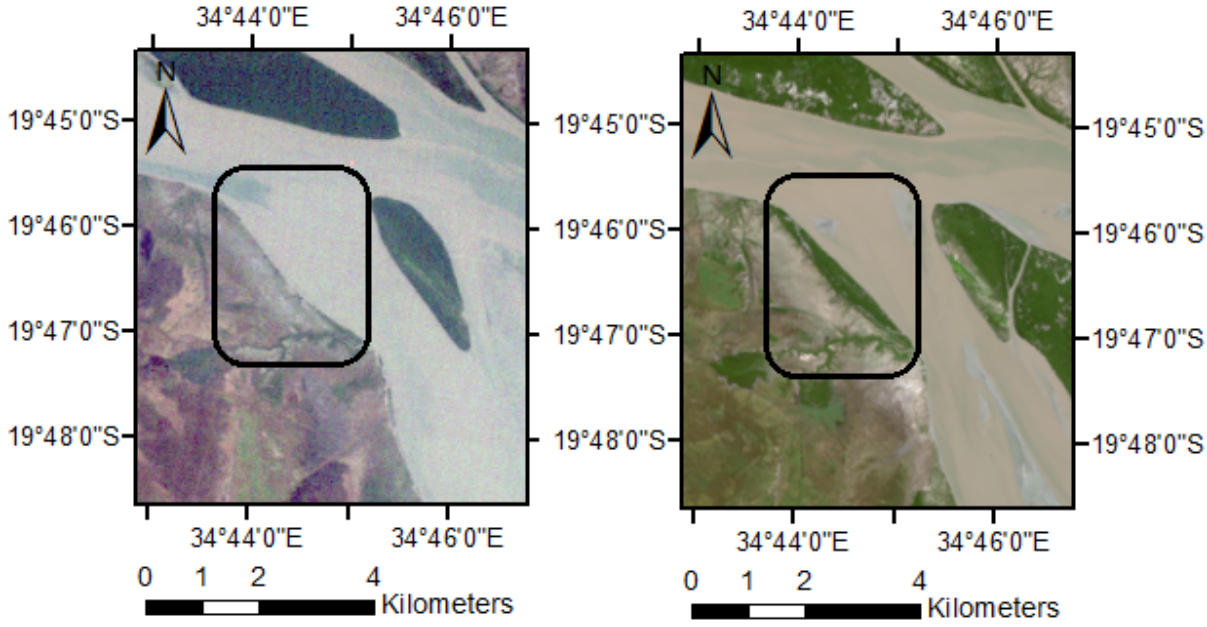

Figure 30: Source image from 1989, on the left, and 2015, on the right, delimited for C2 accretion area.

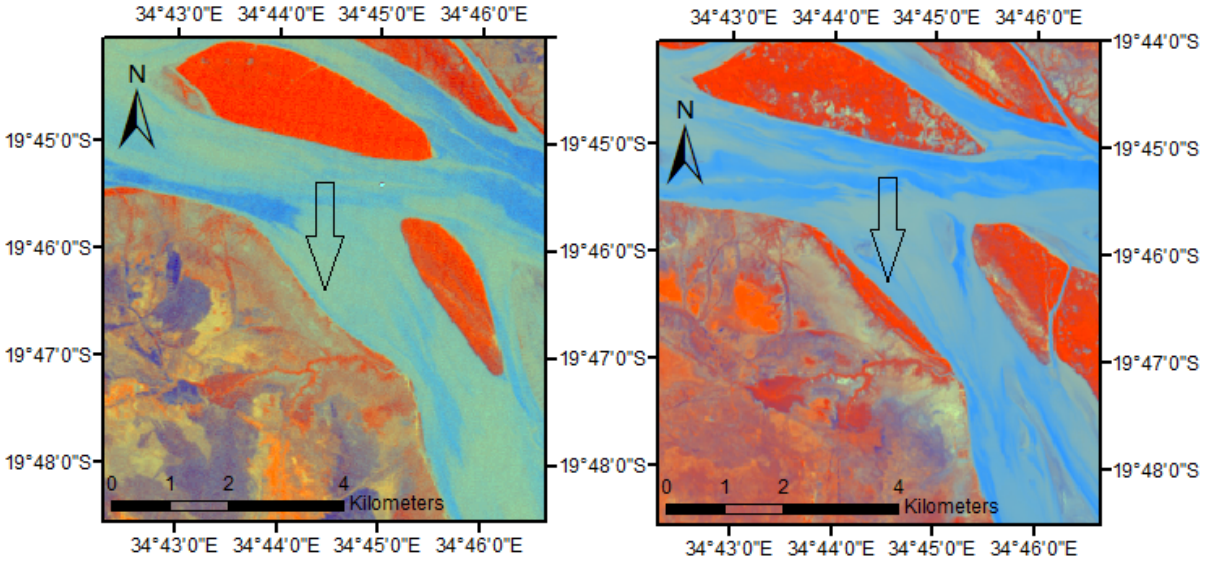

Figure 31: EMI images from 1989, on the left, and 2015, on the right, delimited for C2 accretion area.

Site D

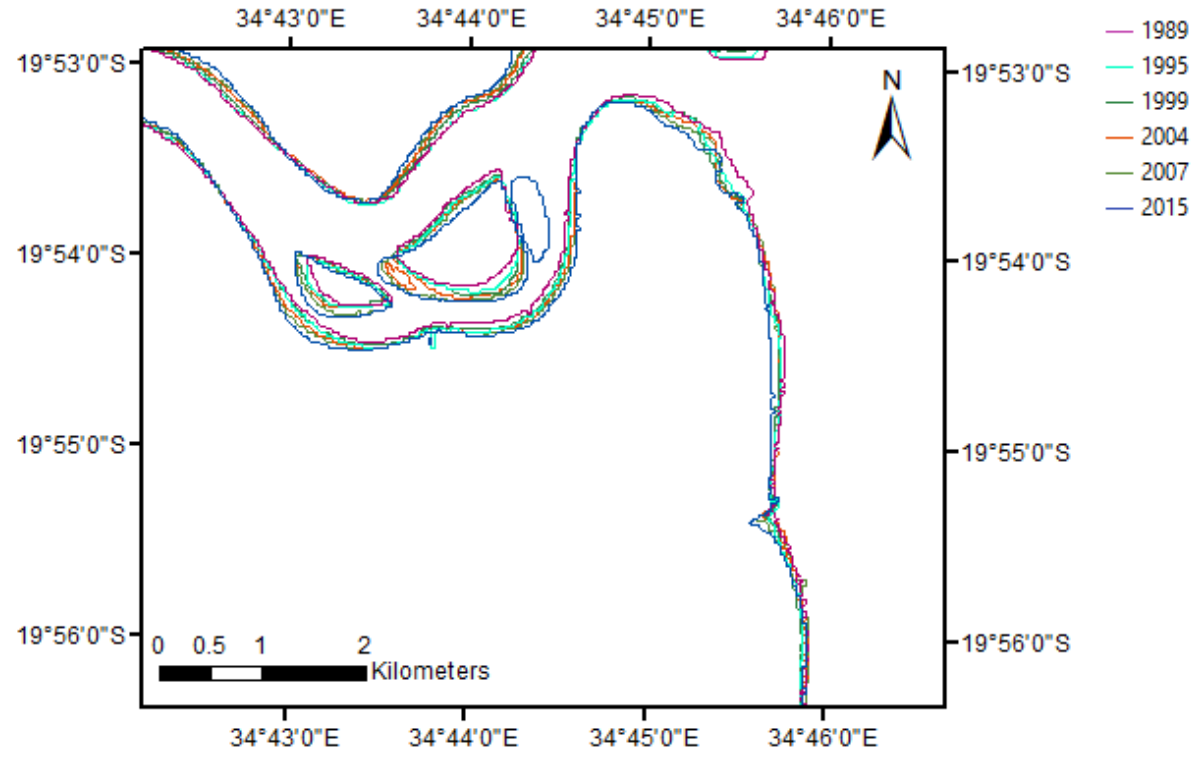

Figure 32: Coastline positions (1989-2015), for Zone D.

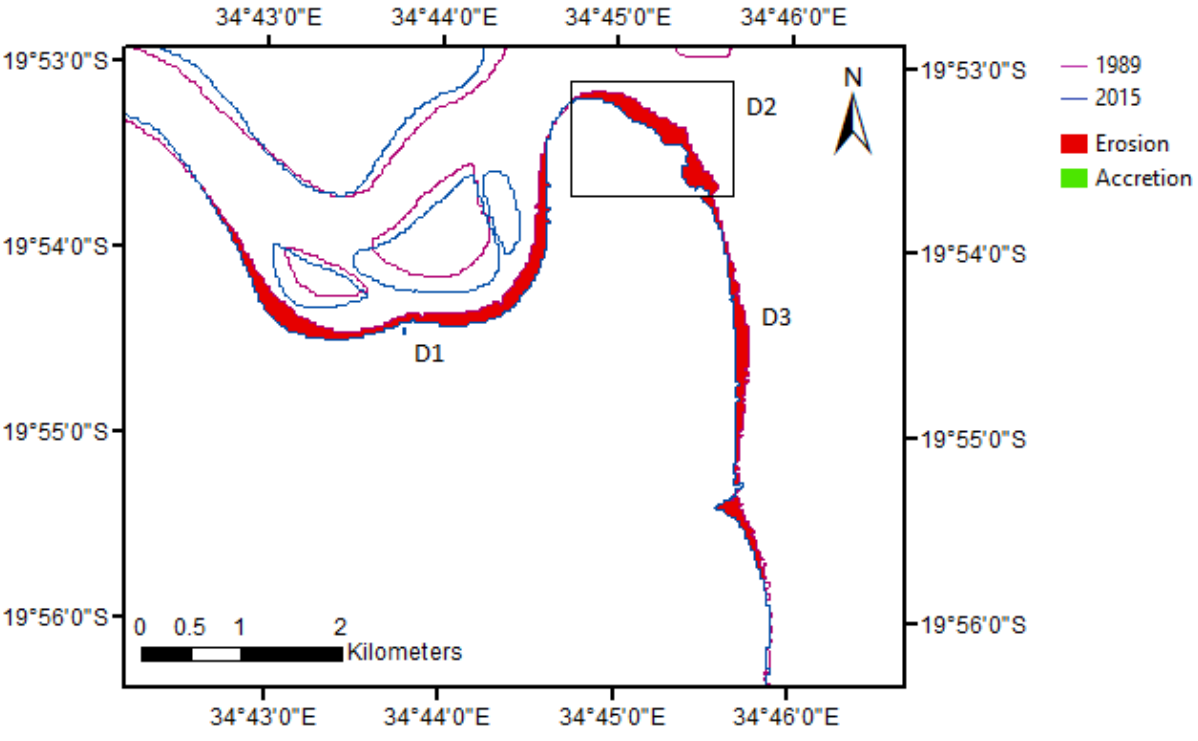

Figure 33: Difference between 1989 and 2015 coastline, for Zone D.

In this site, only erosion was observed and once again through out the years only recession occurred, as seen by the images above. However, there were two situations here. D1 and D2 represented areas where there was loss of land whilst D3 illustrates erosion relative to sand movement. Figure 34 shows the difference in land eroded from 1989 to 2015 for D1 and D2.

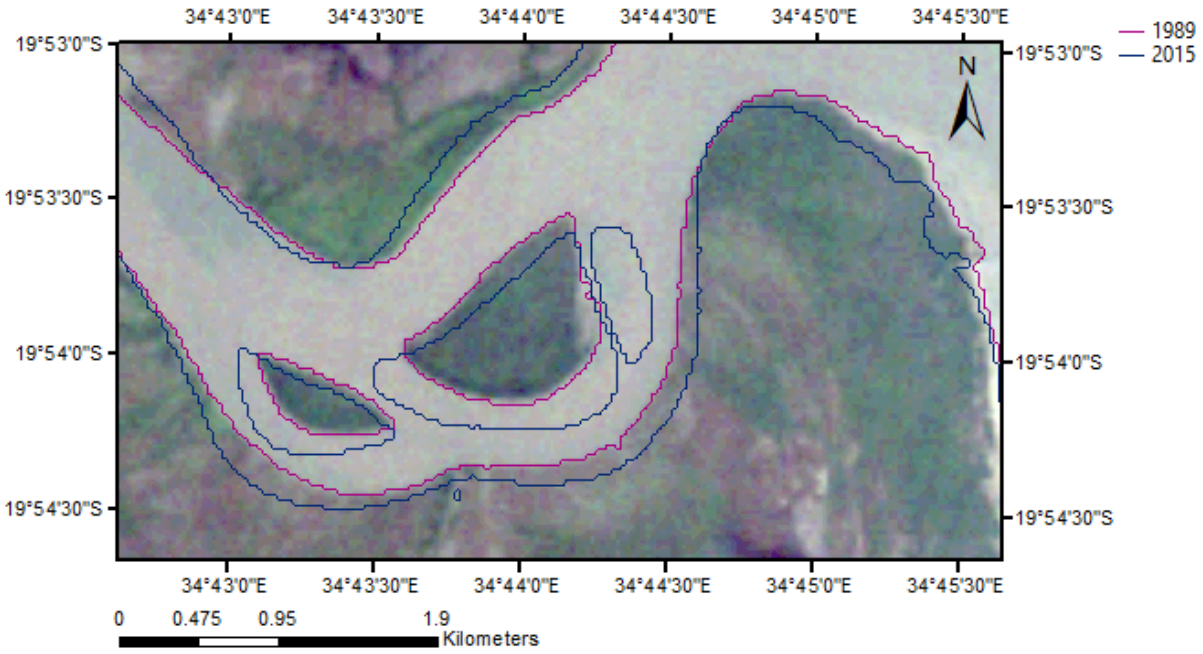

Figure 34: Source image from 1989 overlaid with 1989 and 2015 coastlines.

Source images as well as EMI images have also been employed for D3 erosion area validation. However, when doing so, it was possible to observe that 1989 coastline was being delineated a little over the real water/land boundary. Figure 35 illustrates the 1989 EMI image overlaid with 1989 and 2015 coastlines. One would expect that the land water boundary for 1989 would be delineated right at the end of the bright yellow area, representing sand. However, this does not happen and some of the intertidal zone is being considered as land, which results in an overestimation of erosion area. Actually, one can see from figure 35 that except for the part delimited with a rectangle, 2015 coastline is a much better representation of the real coastline in 1989 than the one actually derived.

This was one of the very few regions in the entire area of study where this situation actually happened in a coastline derived from SVMs approach. In fact, only in 1989 coastline this problem was found. It is important to notice that this overestimation of the coastline in this region was not even close to the one happening on coastlines derived from MNDWI images, reason for which they were discarded. Validation of the coastlines from 1995, 1999, 2004 and 2007, revealed that they were delineated correctly. In fact, if 1989 coastline had been correctly delineated, it would be approximately at 2015 coastline level, as mentioned above. It was observed that from 1989 to 2007 there was accretion, which means that sand accumulated in this region. However, from 2007 to 2015 the coastline went back, approximately, to its original position of 1989. This means that the overall balance of change through out the entire period of study, 1989-2015, is basically null. This can be observed in figure 36.

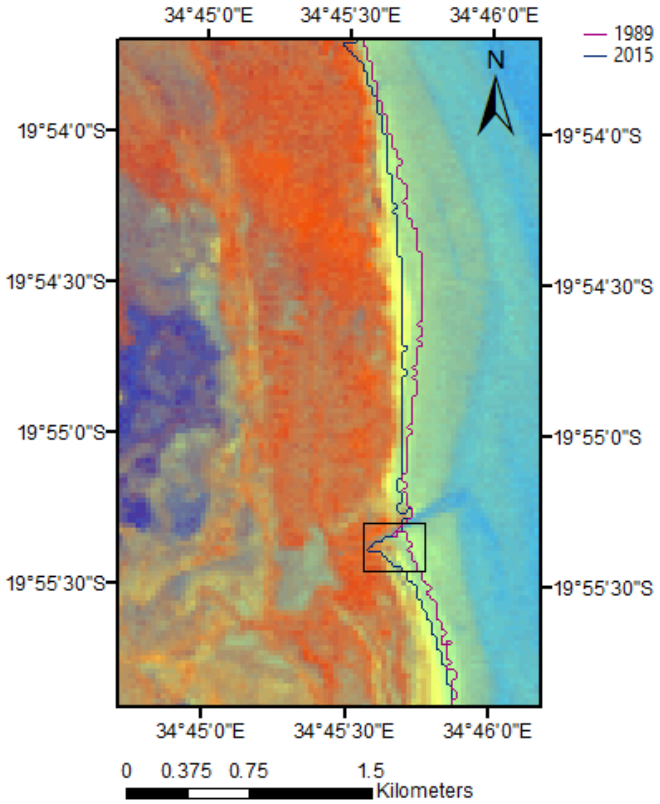

Figure 35: 1989 EMI image overlaid with 1989 and 2015 coastlines.

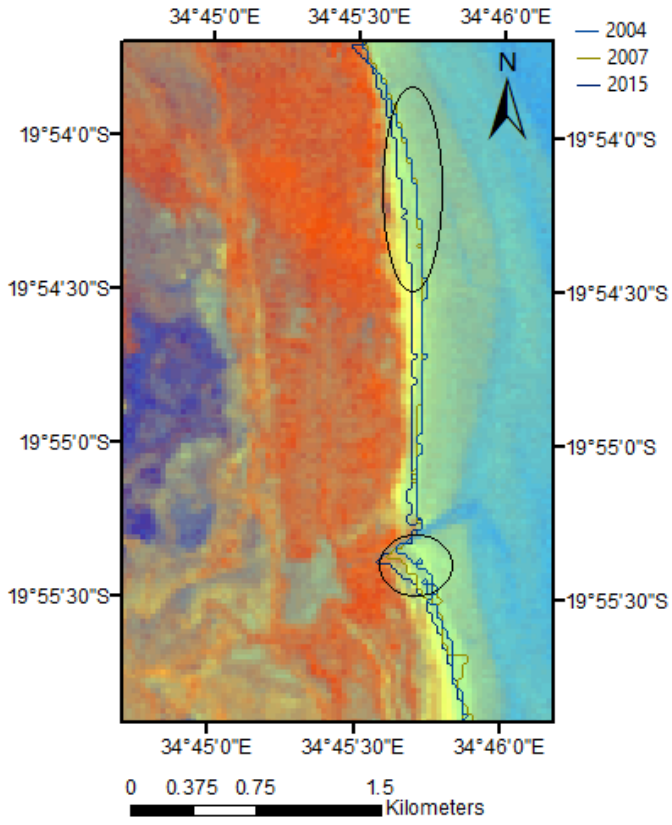

Figure 36: 1989 EMI image overlaid with 2004, 2007 and 2015 coastlines.

Since estimation of erosion area was done for the overall time elapsed, conclusion was reached that D3 erosion area seen in figure 33, would not be considered for the estimation of overall change area.

Figure 33 also shows two islands where erosion and/or accretion can be seen, however as for the same reason specified in the previous site, these areas were not considered for estimation of overall change area.

Site E

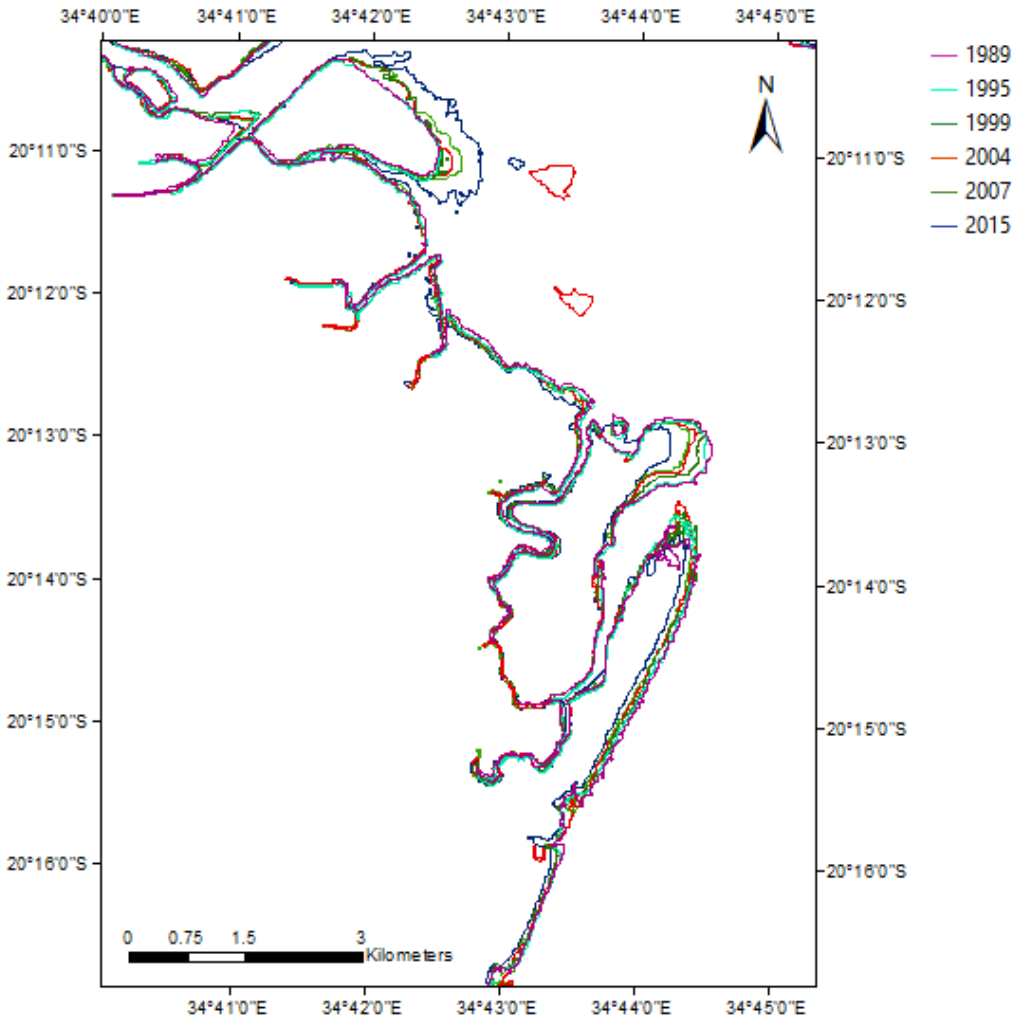

Figure 37: Shoreline positions (1989-2015), for Zone E.

In this site it was observed that from 1989 to 2015, accretion areas always corresponded to an increase in area, whilst for erosion areas only recession occurred, eroded area continuously increased (Figure 37). From Figure 38 one can observe that E1 represents an accretion process and E2 to E5 erosion processes.

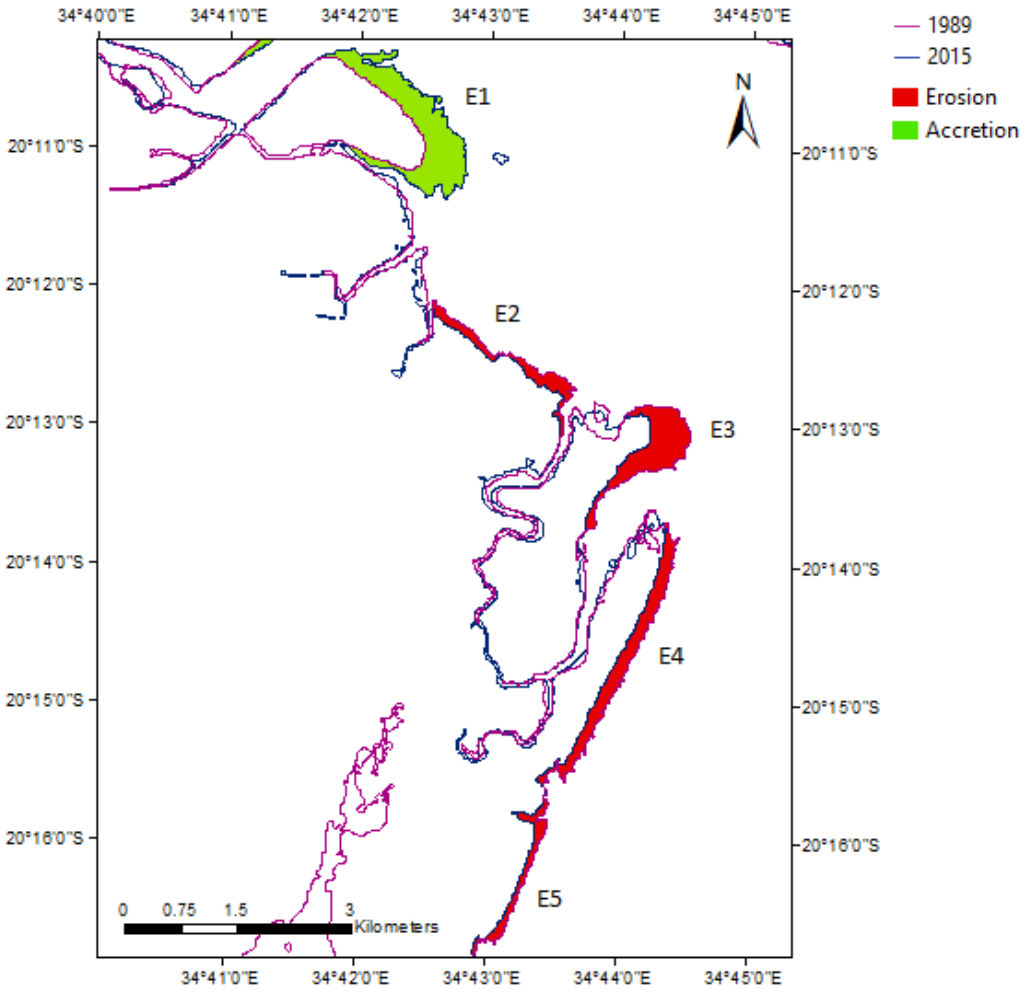

Figure 38: Difference between 1989 and 2015 coastline, for Zone E.

Accretion in E1 involved an increase in land area which is illustrated in figure 39, where one can see that the largest increase occurred between 2007 and 2015. This increase seems to be related to vegetation establishment. The EMI image for E1 also clearly shows the area increased with a strong tone of red, characteristic of high vegetation density. This region is also characterized by the existence of mangrove forests, which probably means that this increase in area was most likely due to mangrove establishment.

Erosion in E2, E3 and E5 represent loss in overall land area while erosion in E4 relates to sand movement. This can be seen in Figure 40, where in E4 the bright tone of yellow, representative of sand, is clearly visible. The other regions do not seem to be high density vegetation areas and so there is a high probability that this erosion represented an overall loss in land area.

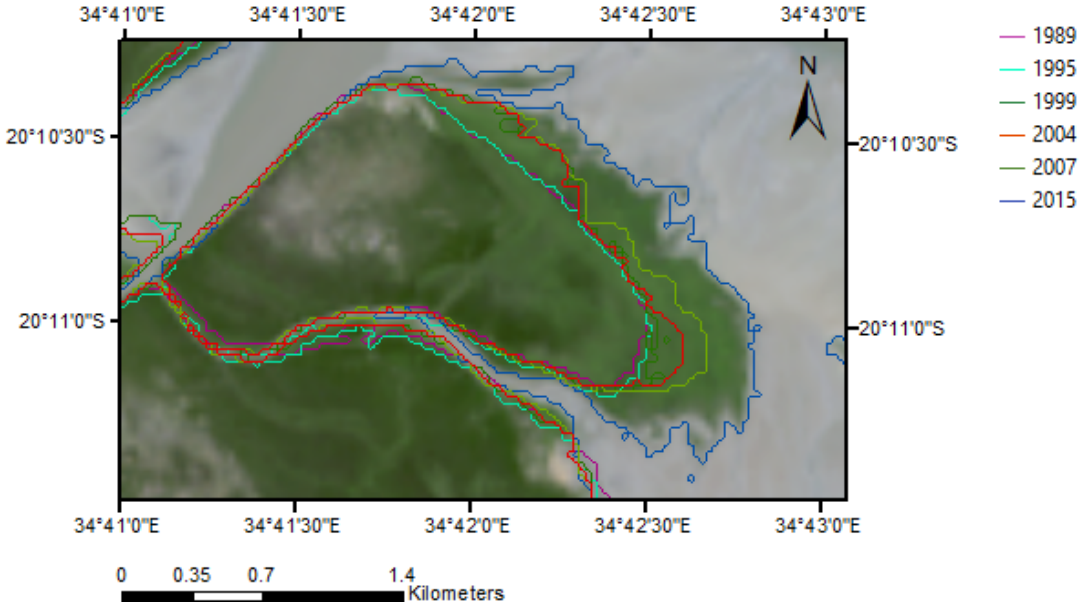

Figure 39: 2015 source image overlaid with all the coastlines under study for region E1.

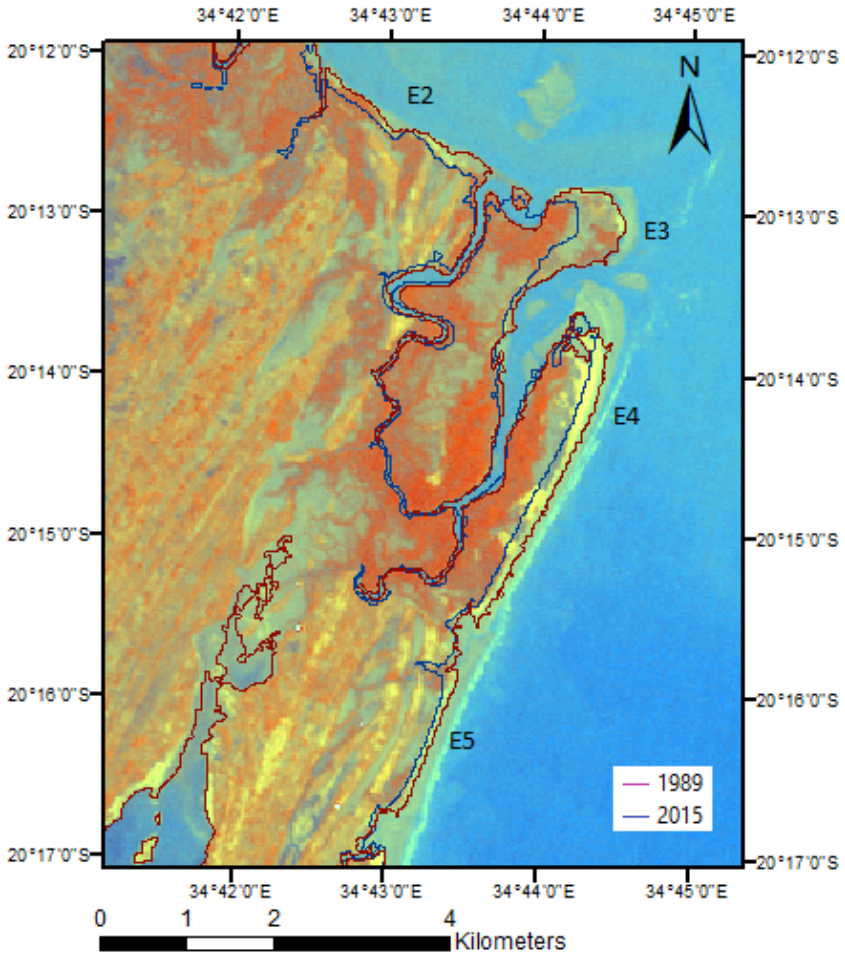

Figure 40: 1989 EMI image overlaid with 1989 and 2015 coastlines, for region E2-E5.

The following table shows the overall change observed, in hectares, for each of the sites studied here.

Table 13: Overall change area between 1989 and 2015 for sites A to E.

Site	Approximate coastline stretch size (km)	Erosion (hectares)	Accretion (hectares)	Overall change (hectares)	Overall change (ha/km)
A	29.77	123	60	(-) 63	(-) 2.12
B	21.09	79	17	(-) 62	(-) 2.94
C	25.27	324	76	(-) 248	(-) 9.81
D	9.45	83	0	(-) 83	(-) 8.78
E	53.26	169	111	(-) 58	(-) 1.09

From this table, one can conclude that site C was where erosion was by far the greatest and accretion was more significant in site E. For all sites, erosion areas were always higher than accretion, from where it can be inferred that these regions have higher predisposition for erosion than accretion.

Approximate change in coastline presented in table 13 refers to the studied areas and considering 1989 coastline as baseline.

It is possible to observe that site C was where overall change in ha/km was higher, followed by site D. It is interesting to note that even though site D has to the lowest coastline size, it has the second highest overall changed area. This means that these two sites are subject to greater forces that contribute to erosion than the others. Site E was where overall change was lower with only (-) 1.09 ha/km. This result can be due to the fact that accretion was considerably high.

Although more sites that suffered changes could have been presented here, during validation it was concluded that the changes occurred in other areas were not so relevant. Also, some areas appeared to have suffered a significant change, however during validation this supposition was discarded as changes were due to a bad delimitation of 1989 coastline position which resulted in overestimation of actual erosion area.

5.3 Coastal Vulnerability Index (CVI)

For the three parameters, risk classes where employed and risk maps obtained. Figures 41-43 show a general overview of the risk classes over the entire region of study.

5.3.1 Coastline Change Rate

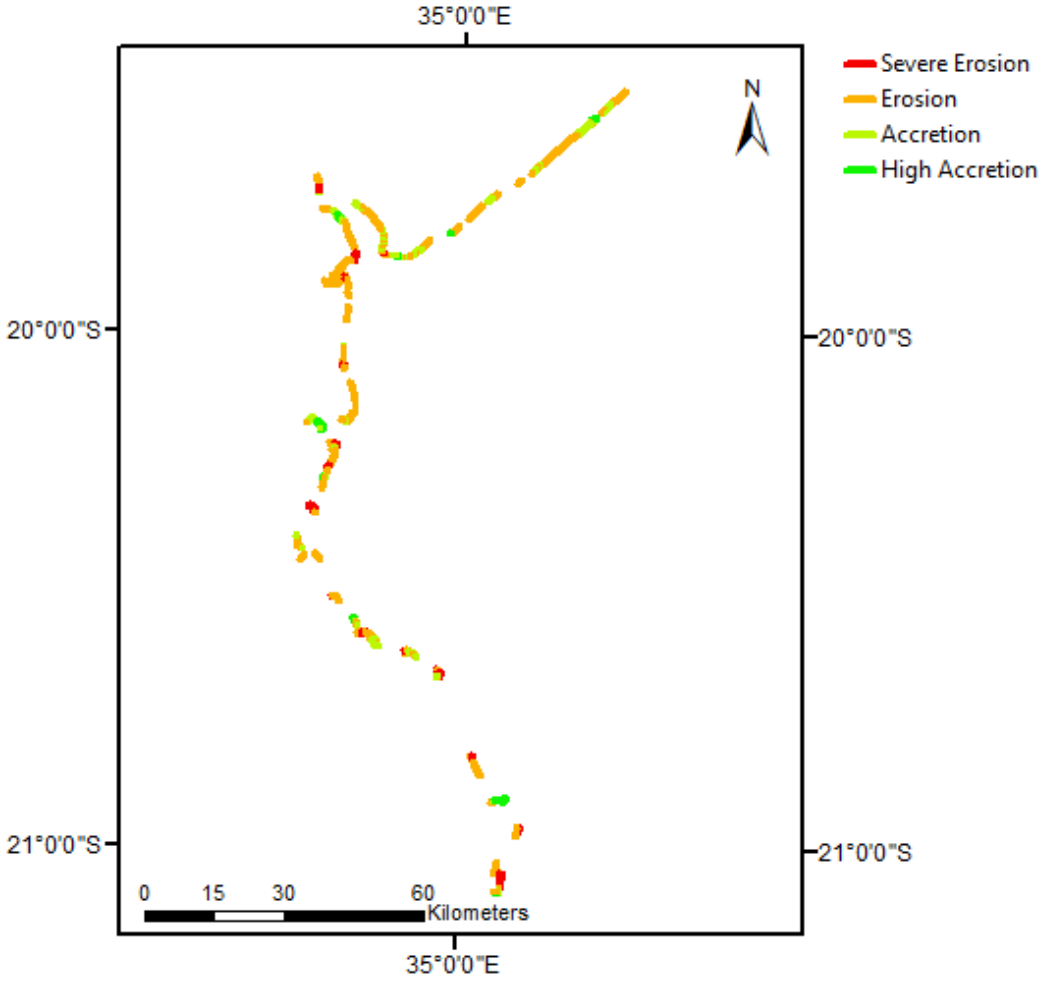

Figure 41: Risk classes for Coastline Change Rate.

This map was obtained after EPR statistics were computed for the transects cast by the DSAS extension for ArcMap.

In general, coastline change rate varies between -33.91 m/year and 29.47m/year, with the average value being -2.64m/year.

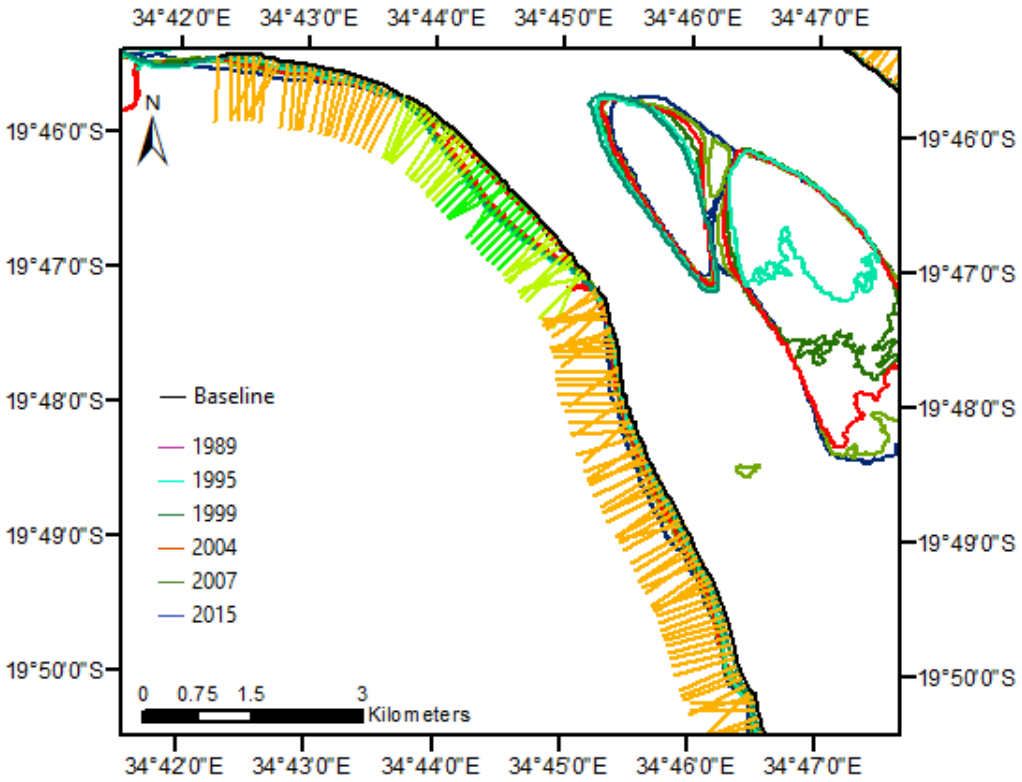

Figure 42: How transects were cast for a region within Site C, as an example.

Figure 42 shows an example of how transects were cast for a specific region within site C. From the baseline, in black, transects were cast intersecting the coastlines for every year in study. It is from this intersection and distance between coastlines that statistics can than be computed, in this case with EPR. Transect length is determined by the user and in this case 900 meters.

5.3.2 Landuse Cover

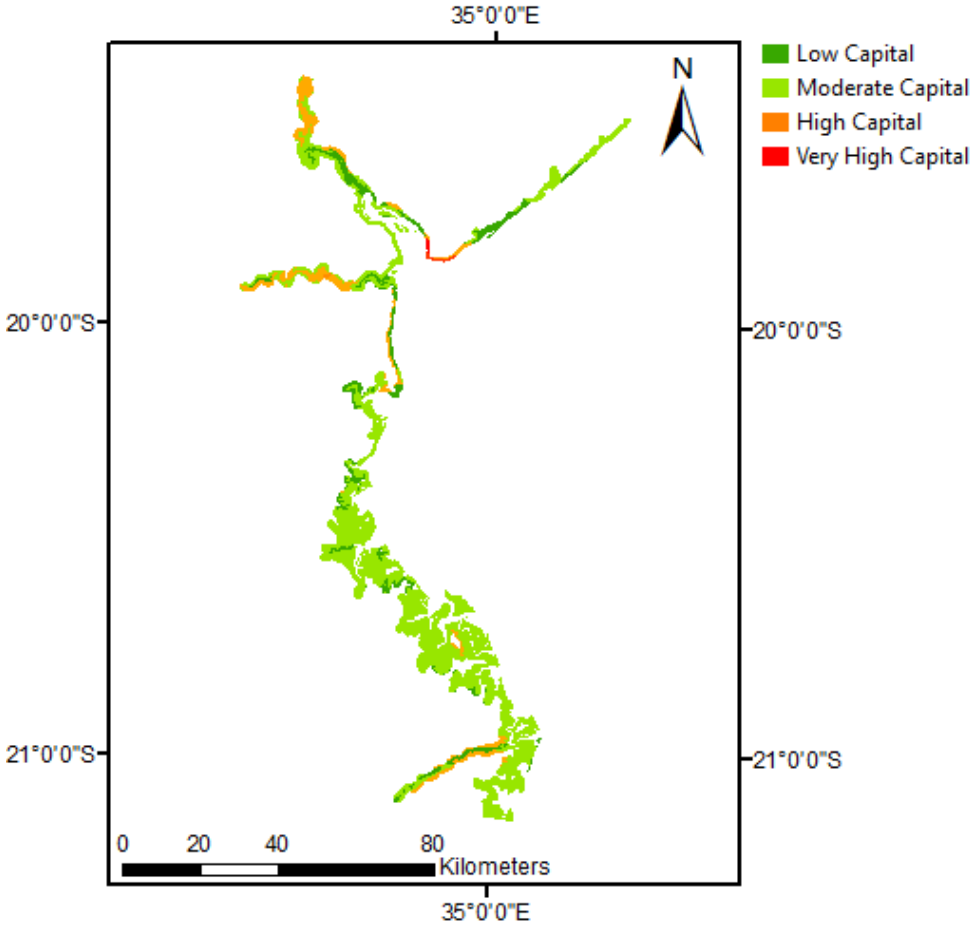

Figure 43: Risk classes for Land-use.

It is possible to observe from this map that more than 50% of the area of study is within the Moderate capital, with mangrove forests being the landuse type more frequent inside this class. Very High capital occurs in Beira city, as one would expect, with urbanized and semi-urbanized dwelling areas dominating this class.

5.3.3 Population Density

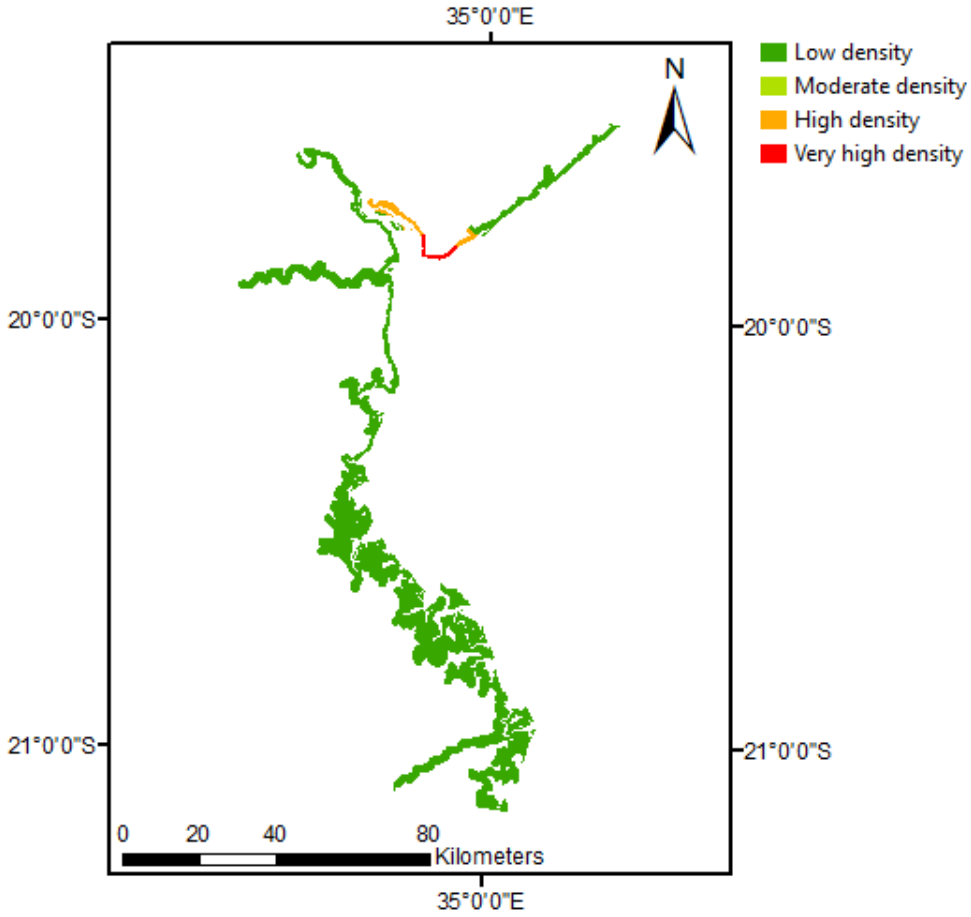

Figure 44: Risk classes for Population density.

This map shows that more than 60% of the area is within the low population density class, which means that very few people, less than 500 people/km^2, occupy these regions. As it would be expected, very high density and high population density occur in the city of Beira, where the number of people per square kilometre is either between 1000 and 1500 or higher than 1500.

5.3.4 Site Specific CVI calculation

After obtaining the previous risk maps, it was deemed that it would be more interesting to study in more depth coastal vulnerability for the previous identified sites (A-E), than for the entire study area.

In order to do this, a 1km buffer, using the 1989 coastline as baseline, was created. The resulting buffer was then intersected with a Fishnet, which resulted in the area between the buffer and the baseline, being subdivided into polygons. Figure 45 shows this intersection result for site C as an example.

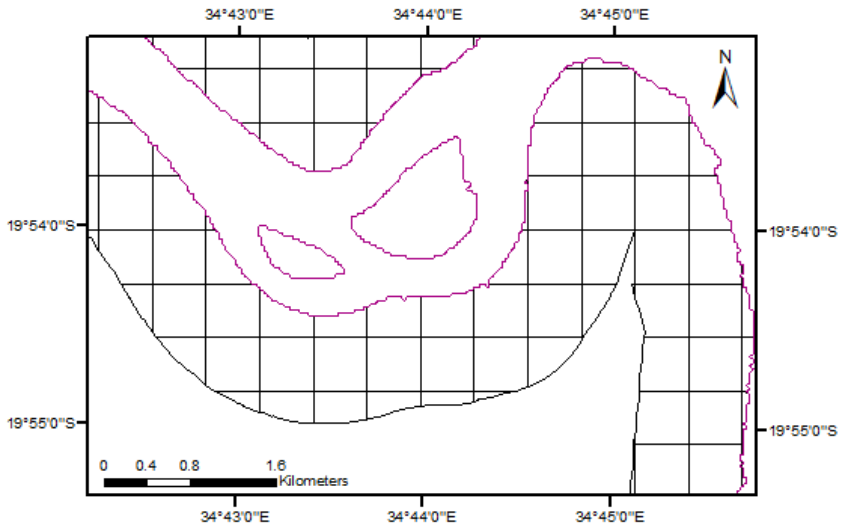

Figure 45: Result of Fishnet intersection with the 1km buffer.

After analysis of the parameters and respective risk classes for each one of these sites, making use of the general risk maps obtained, these polygons where classified accordingly with a value between 1 and 4, translating the risk associated with each parameter. This meant that 3 columns were added to the attribute table, one for each parameter. After this, another column was added for calculation of the CVI, and vulnerability maps were computed.

For each site, risk maps for the three parameters and a final vulnerability map were obtained and are presented below (Figures 46-65). Each risk map shows the 1km buffer classified for each parameter and the 1989 coastline. For the stretch of coast of each site, the coastline was classified according to the vulnerability values obtained.

Site A

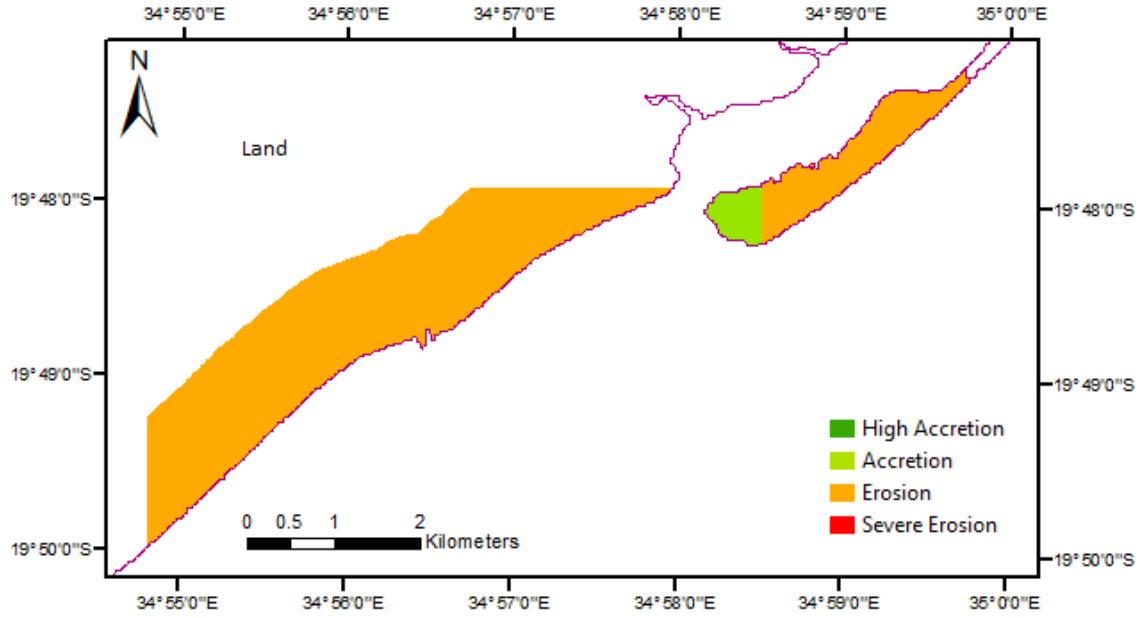

Figure 46: Risk classes for Change Rate, site A.

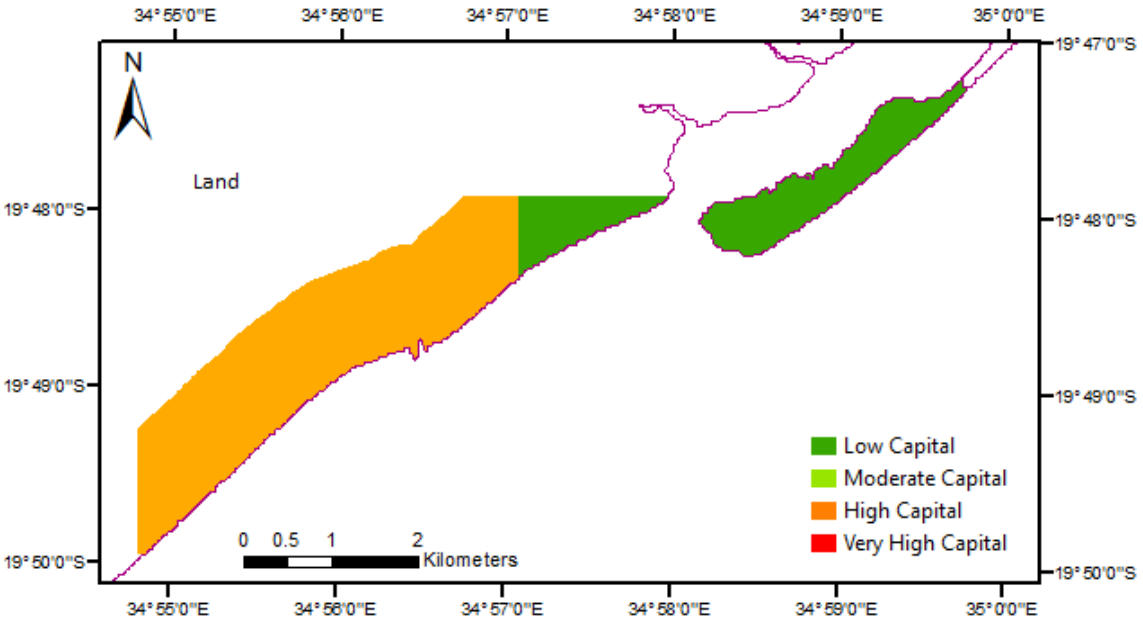

Figure 47: Risk classes for Landuse, site A.

In this site, for the 15.37 km of classified coastline, approximately 90% of the coastline recorded erosion, and 10% recorded accretion. Regarding landuse, approximately 38% was within the high capital class, composed by salt pans and rainfed cultivation, while 62% was within the low capital, composed mainly by sand.

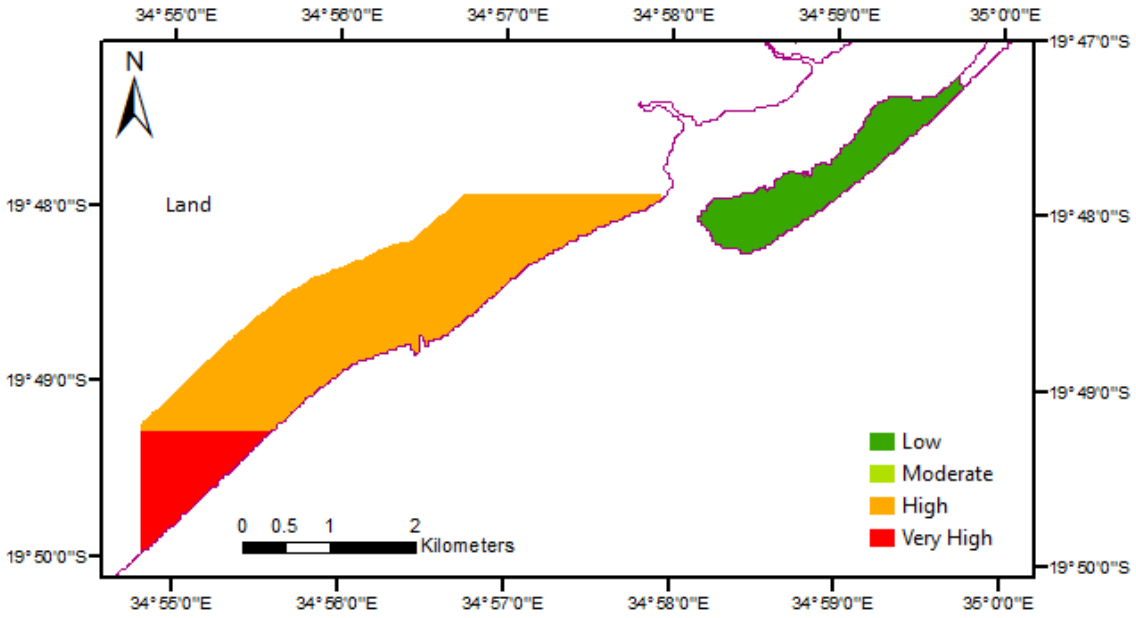

Figure 48: Risk classes for Population density, site A.

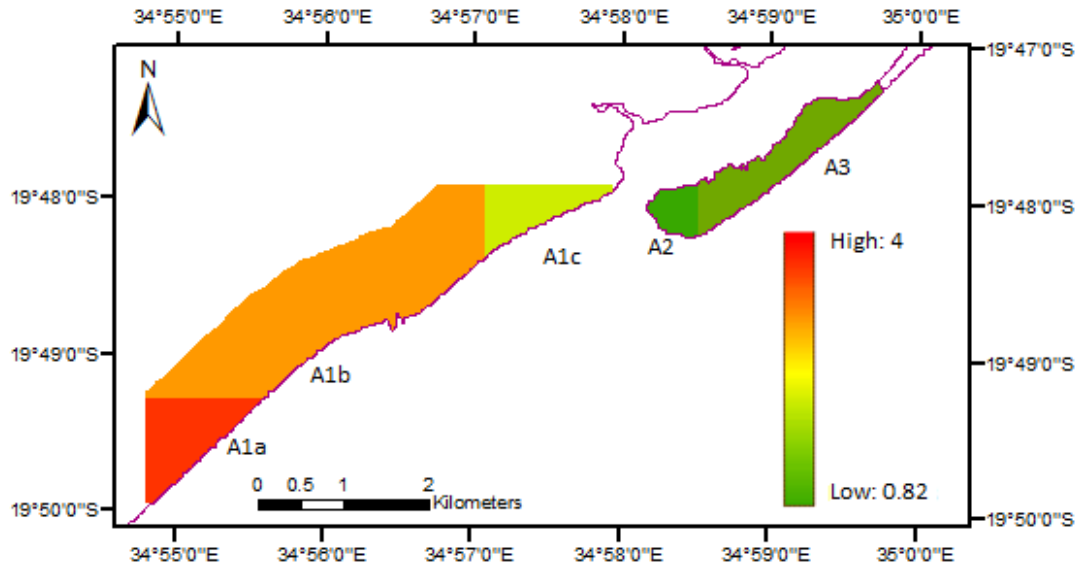

Figure 49: Vulnerability Map, site A.

Relative to population density, approximately 13% of the area within the 1km buffer recorded very high population density, 38% high population density and the remaining 49%, low.

In the end, the CVI was computed and the vulnerability map presented in figure 49, where 12.8% of the coastline presented a vulnerability index of approximately 3.46 (A1a), 25.1% with a value of 3 (A1b), 12.7% with 1.73 (A1c), 39% with 1 (A3) and 10.4% with 0.82 (A2). The higher the value of CVI the higher the vulnerability of a region.

Site B

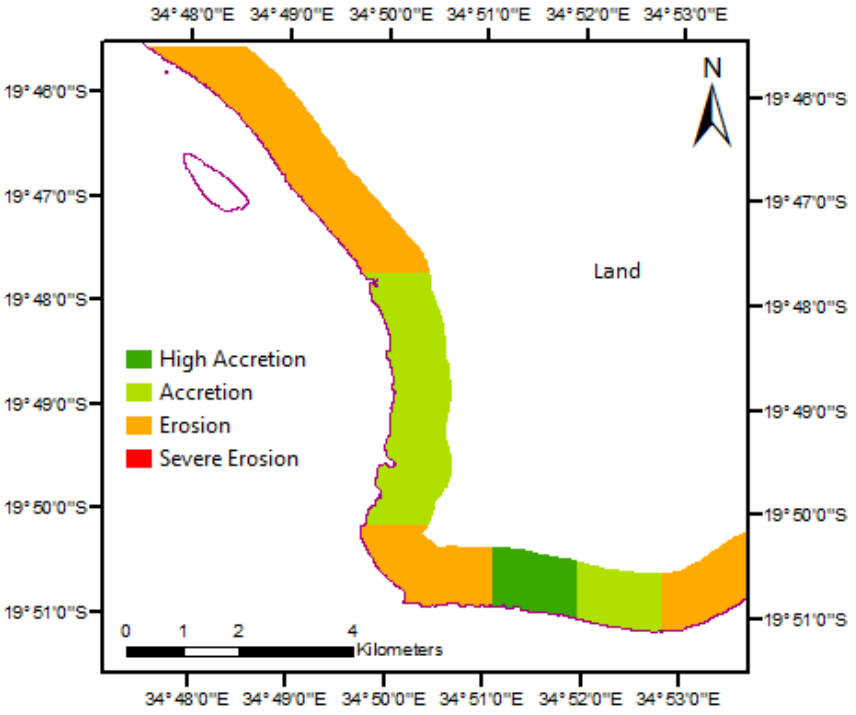

Figure 50: Risk classes for Change Rate, site B.

In figure 50, from a total of 21.09km of coastline classified, approximately 54.9% represented erosion, 36.8% accretion and 8.3% high accretion.

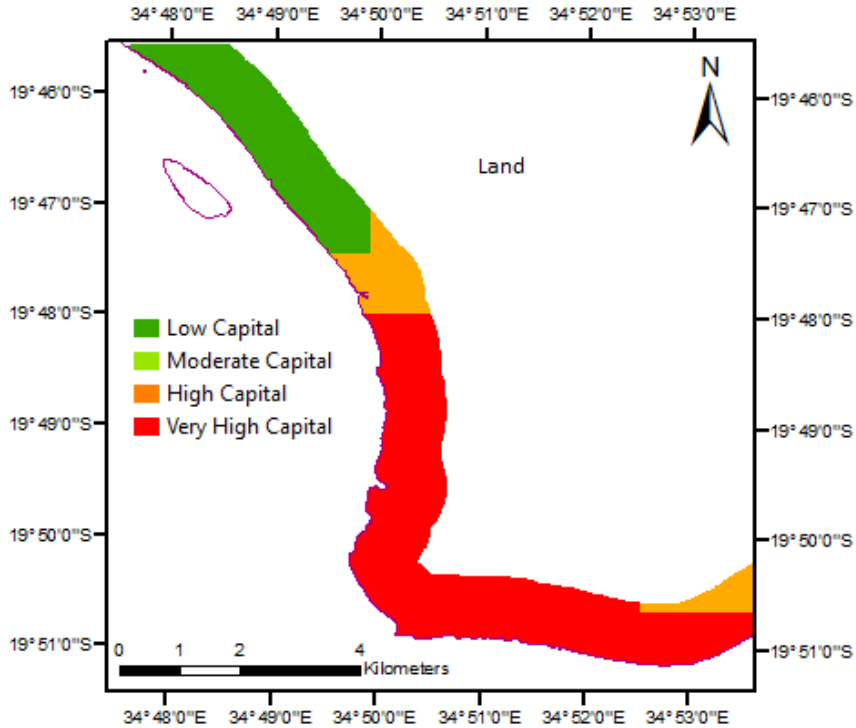

Figure 51: Risk classes for Landuse, site B.

Very high capital regions represent urbanized and semi-urbanized dwelling areas with more than 1500 people per square kilometre, corresponding to approximately 66.6% of coastline. Low capital areas are found in 25.9% of coastline stretch, with bare soil as the main landuse type present, and the remaining 7.5% correspond to rainfed cultivation, high capital (Figure 51).

Figure 52, gives the risk classes for population density. It can be observed that approximately 71% of the coastline was within the very high population density, as it would be expected since this area represents the city of Beira, highly populated. The remaining 29% correspond to high population density, with 1001 to 1500 people per square kilometre.

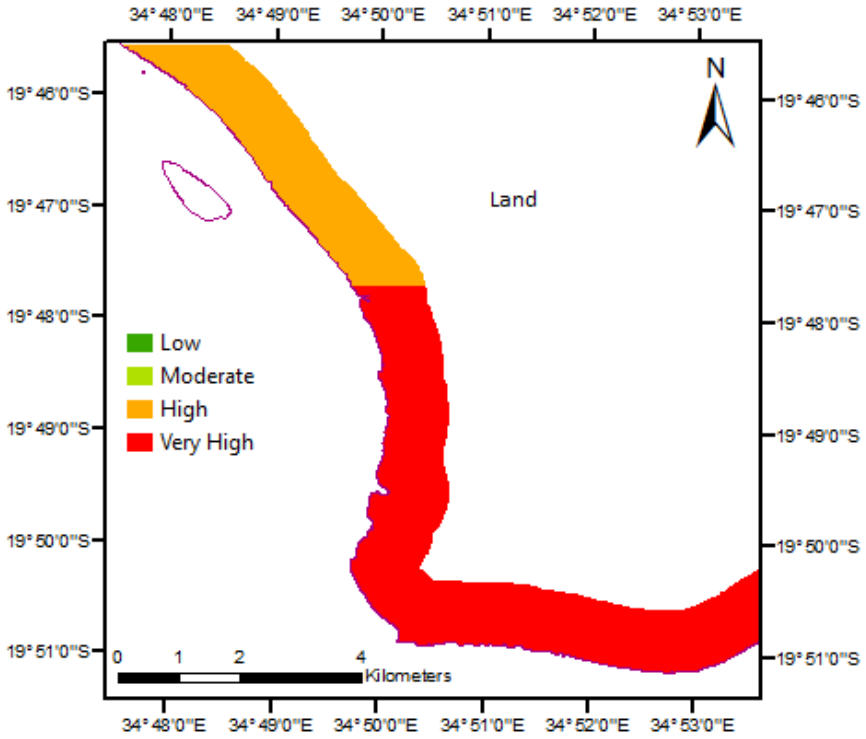

Figure 52: Risk classes for Population density, site B.

From the vulnerability map (Figure 53), it is possible to infer that 25.6% of coastline had a vulnerability index of 4, the maximum value, 32.7% a vulnerability of 3.26, 3.4% a vulnerability of 3, 4.1% a vulnerability of 2.83, 8.3% a vulnerability of 2.31 and finally, 25.9% a vulnerability of 1.73. Classification in this site in general very high.

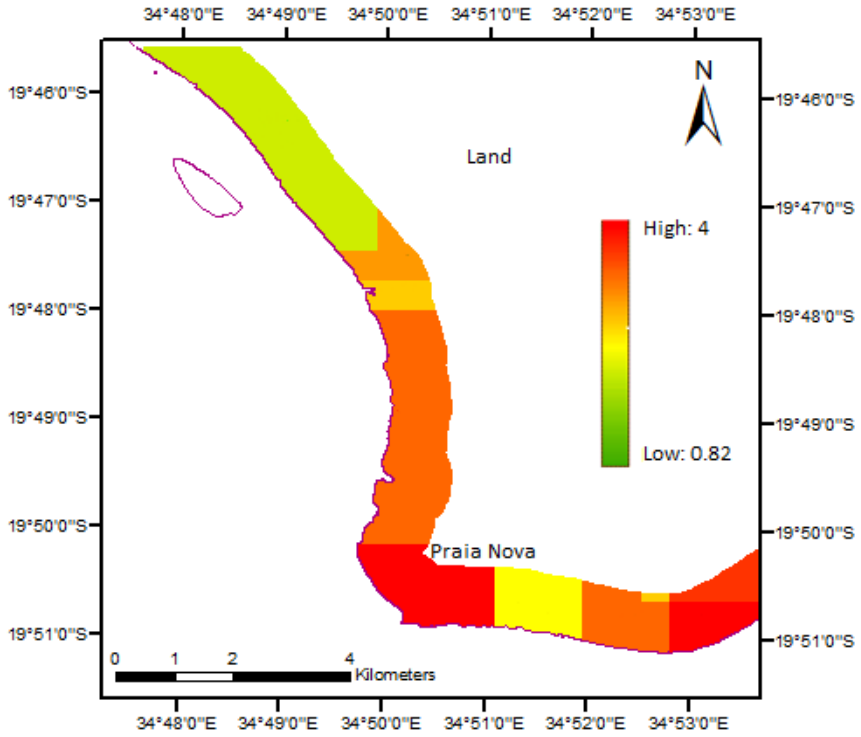

Figure 53: Vulnerability Map, site B.

Site C

In this site, approximately 25.27km of coastline were studied in regards to vulnerability. Figure 54 shows the risk map for change rate, where it can be seen that all classes occurred within this site. Severe erosion occurred in approximately 11.9% of the coastline, erosion class in 69.5%, accretion in 12.3% and high accretion occurred in 6.3% of the coastline.

Regarding landuse, this site is characterized entirely by the existence of mangroves and in the central region by some open woodland, corresponding to the moderate capital class (Figure 55).

Low population density occurred in this site, with less than 500 people per square kilometre (Figure 56).

These rankings led to a vulnerability map where 11.9% of the coastline presented a vulnerability of 1.63 (C3b), 69.5% a vulnerability of 1.41 (C1, C3a and C3c), 12.3% a vulnerability of 1.15 (C2 lighter green), and finally, 6.3% a vulnerability value of 0.82 (C2 darker green) (Figure 57). Vulnerability in this site revealed to be in general quite low, even though erosion was quite severe. This was mainly due to the low population density observed and moderate landuse type, that brought the CVI to a lower value.

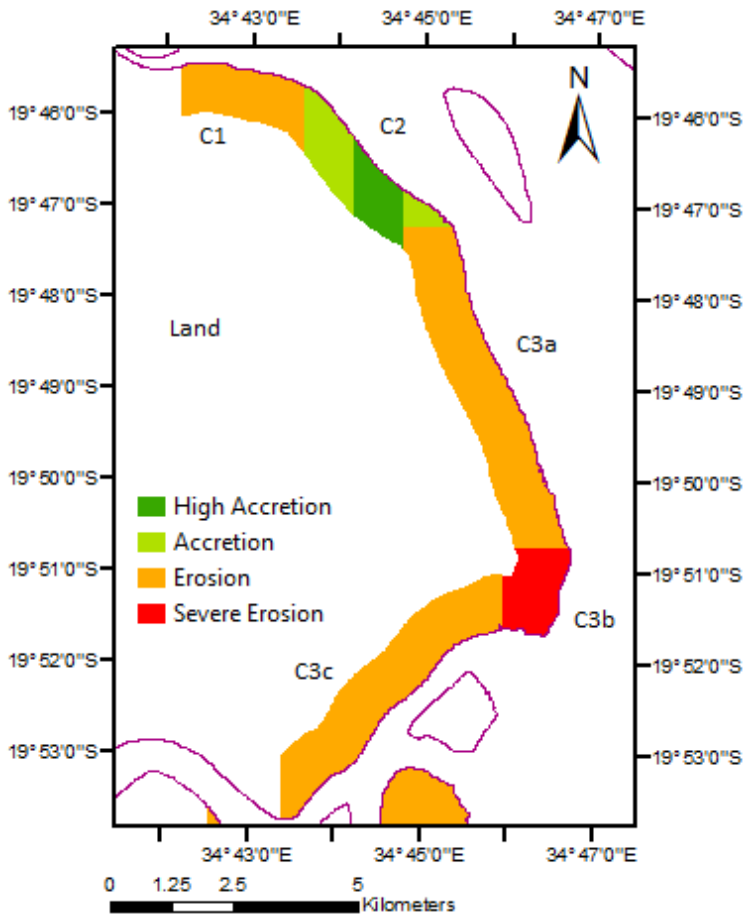

Figure 54: Risk classes for Change Rate, site C.

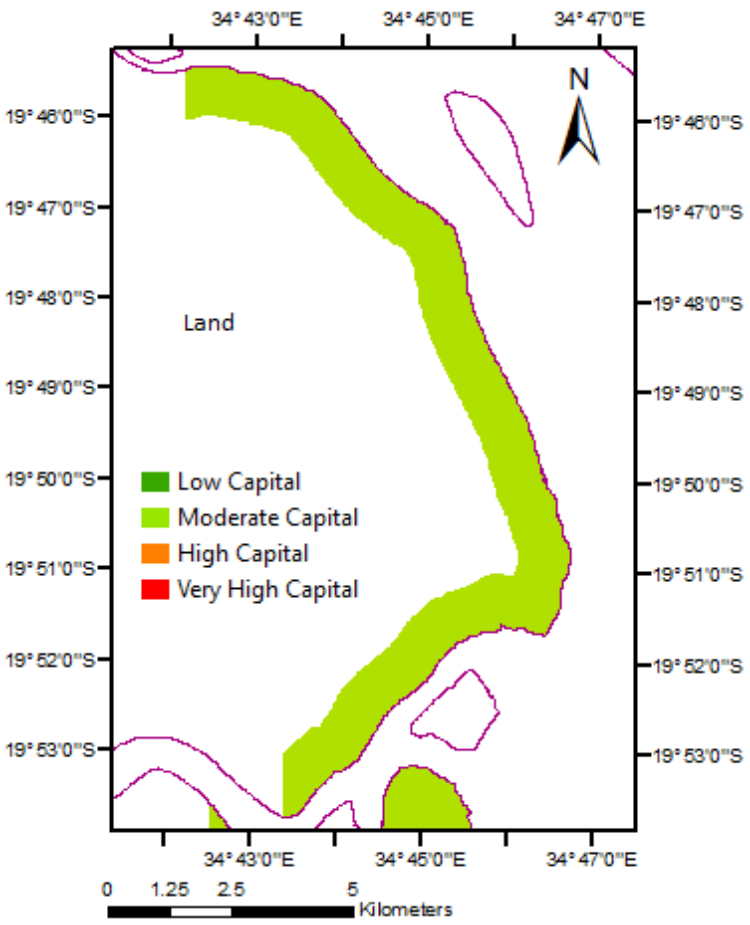

Figure 55: Risk classes for Landuse, site C.

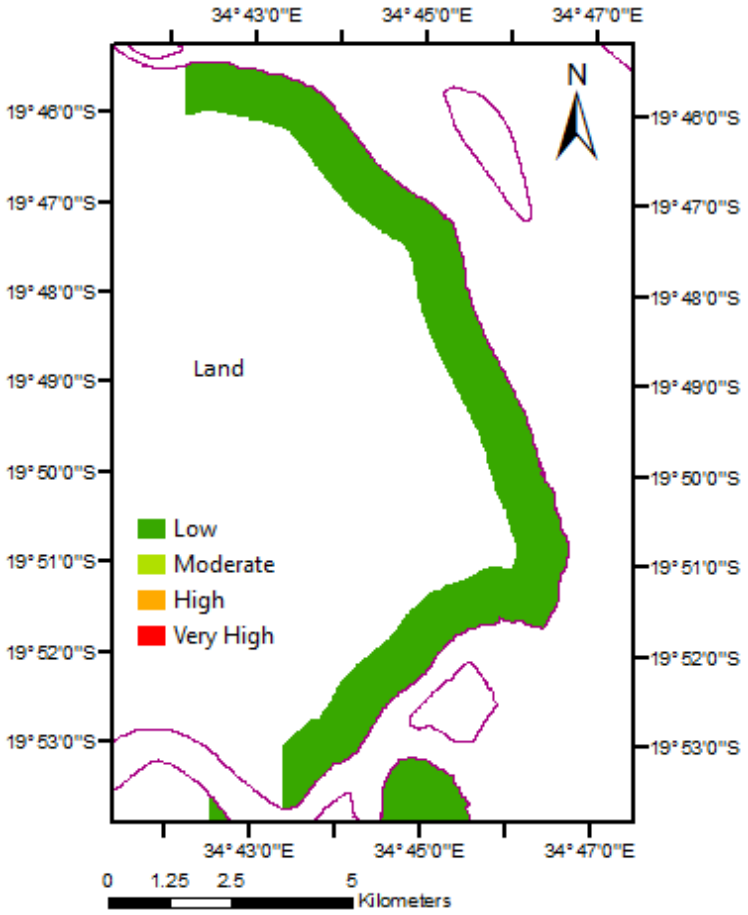

Figure 56: Risk classes for Population density, site C.

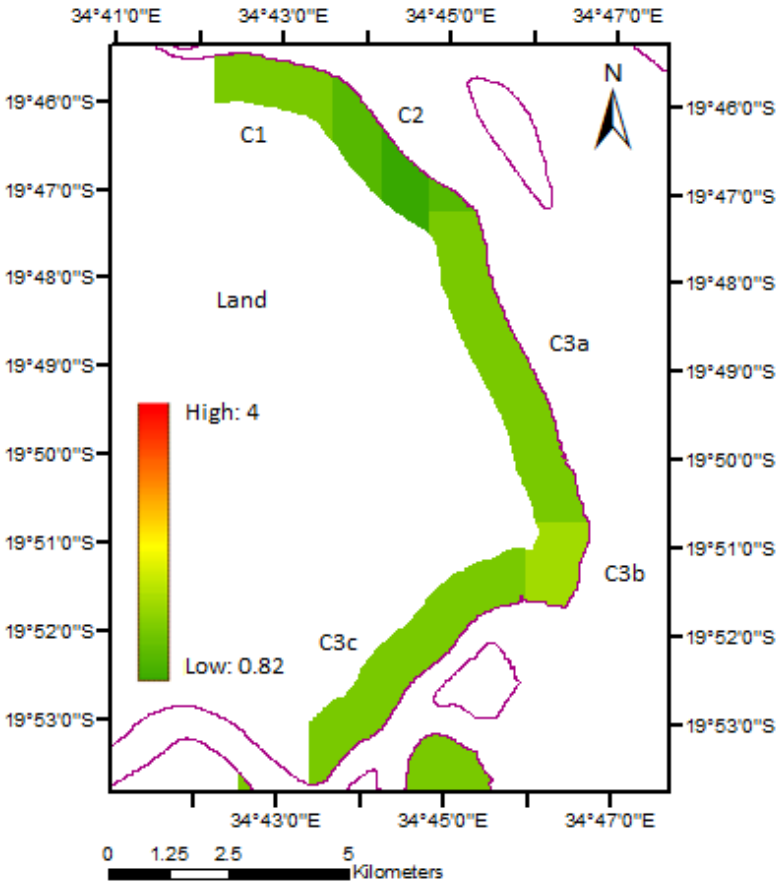

Figure 57: Vulnerability Map, site C.

Site D

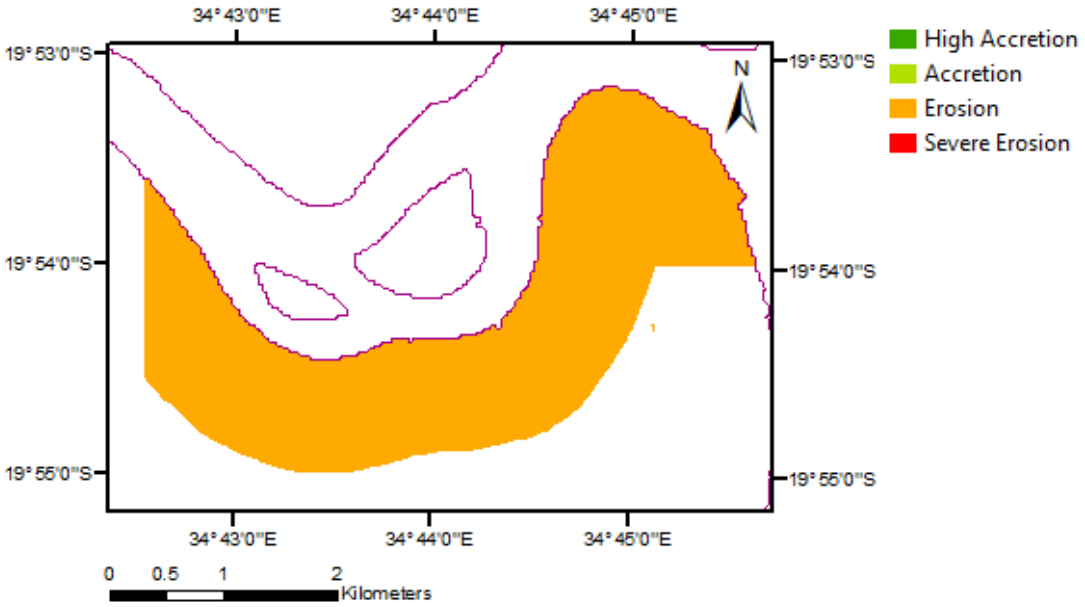

Figure 58: Risk classes for Change Rate, site D.

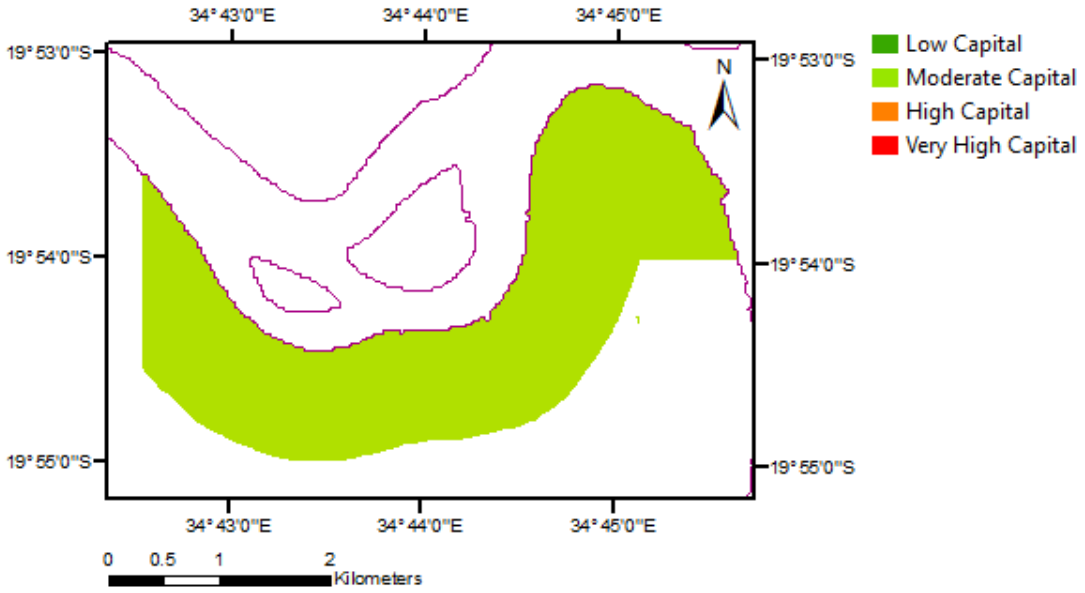

Figure 59: Risk classes for Landuse, site D.

It is possible to observe from figure 58 that site D was completely dominated by erosion, with a change rate varying between -10 and 0. This site is within a region that is mainly characterized by the existence of mangroves, belonging to the moderate capital class (Figure 59). Population wise, it was within the low density class with a population of less than 500 people per square kilometre (Figure 60).

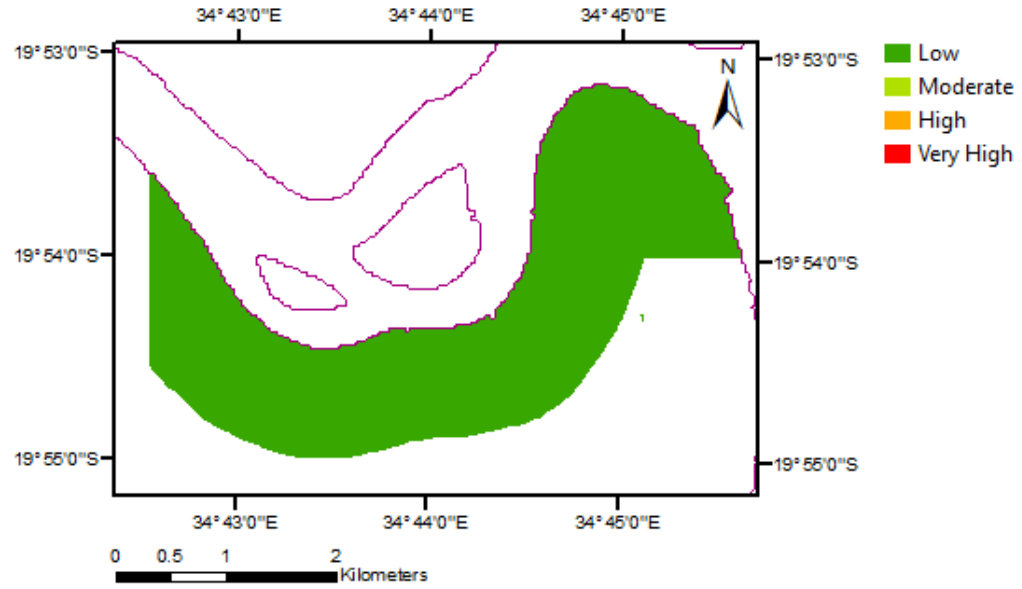

Figure 60: Risk classes for Population density, site D.

This resulted in an overall vulnerability index of approximately 1.41, quite low when compared with the maximum value of 4 (Figure 61).

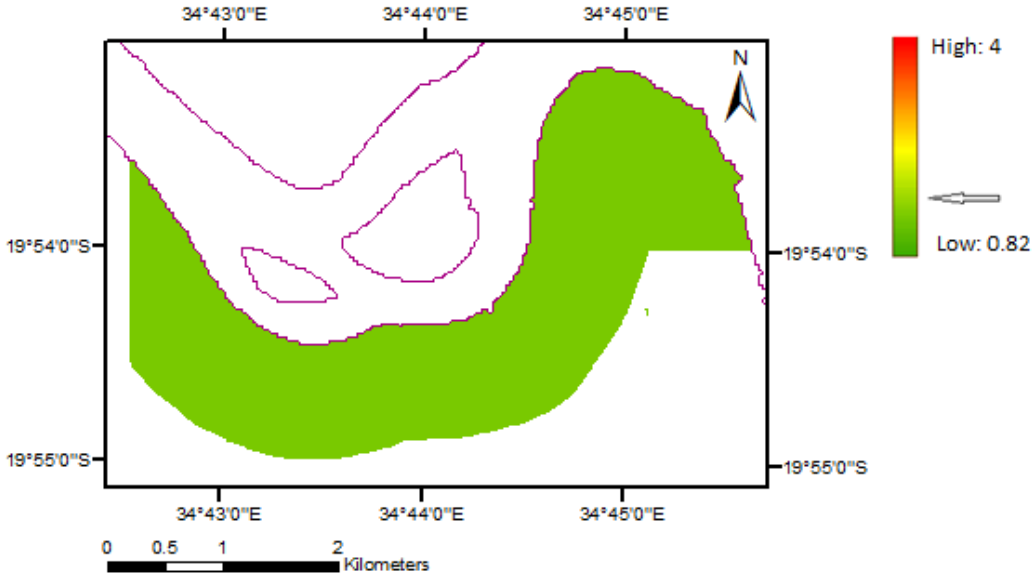

Figure 61: Vulnerability Map, site D.

Site E

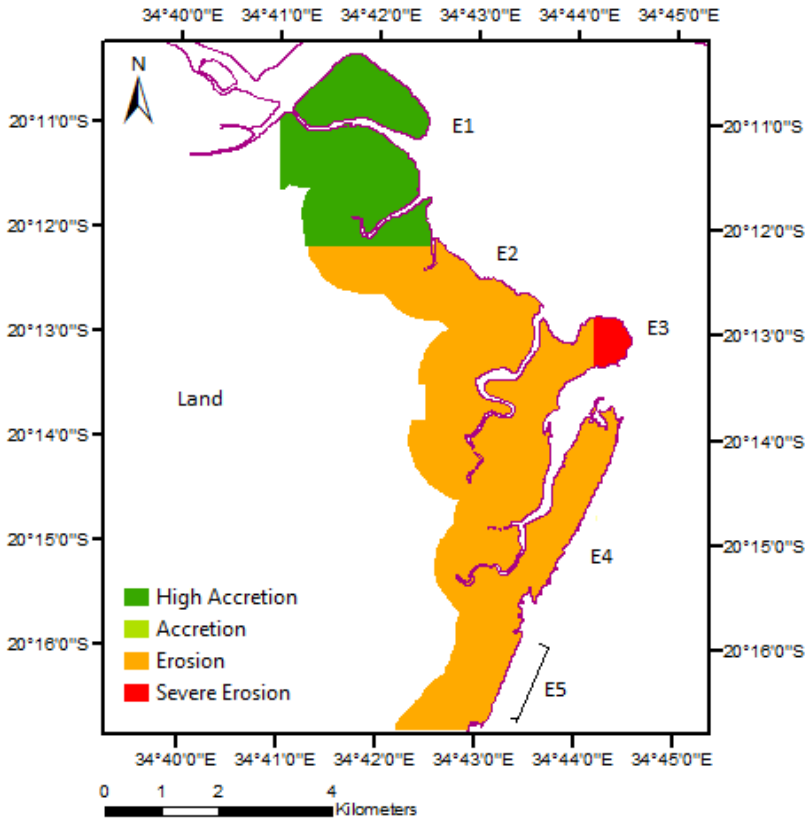

Figure 62: Risk classes for Change Rate, site E.

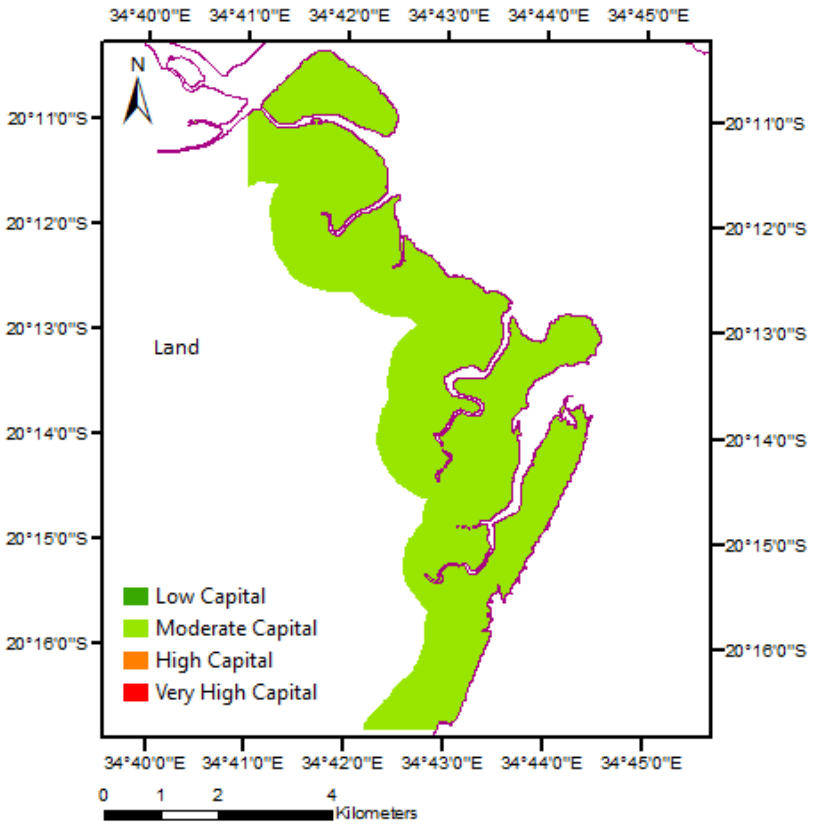

Figure 63: Risk classes for Landuse, site E.

In this site, approximately 53.26km of coastline were classified for every parameter.

High accretion was found in approximately 28.7% of the coastline (E1), erosion class in 67.3% (E2, E4 and E5)and severe erosion in 4% (E3) (Figure 62).

This site belongs entirely to the moderate capital class in terms of landuse, characterized by the existence of mainly mangrove forests within 1km of the coast (Figure 63).

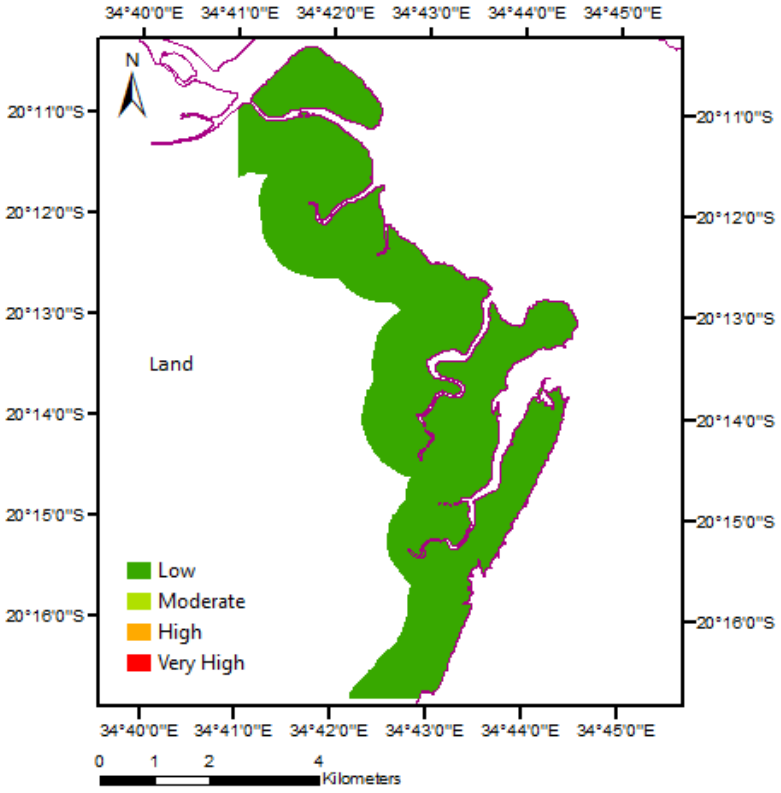

Figure 64: Risk classes for Population density, site E.

Regarding population density, it is entirely within the low density class with less than 500 people per square kilometre (Figure 64). From the data acquired relative to the last 2007 census, it was possible to observe the existence of a village with approximately 3234 people within 1km of the coast in E4. This fact is important since it will have implications in the amount of mangroves harvested for wood and non-wood material, and thus contribute to an increase in the vulnerability of the coast to erosion in this specific region. Further discussion on this point was performed on the discussion section of this thesis.

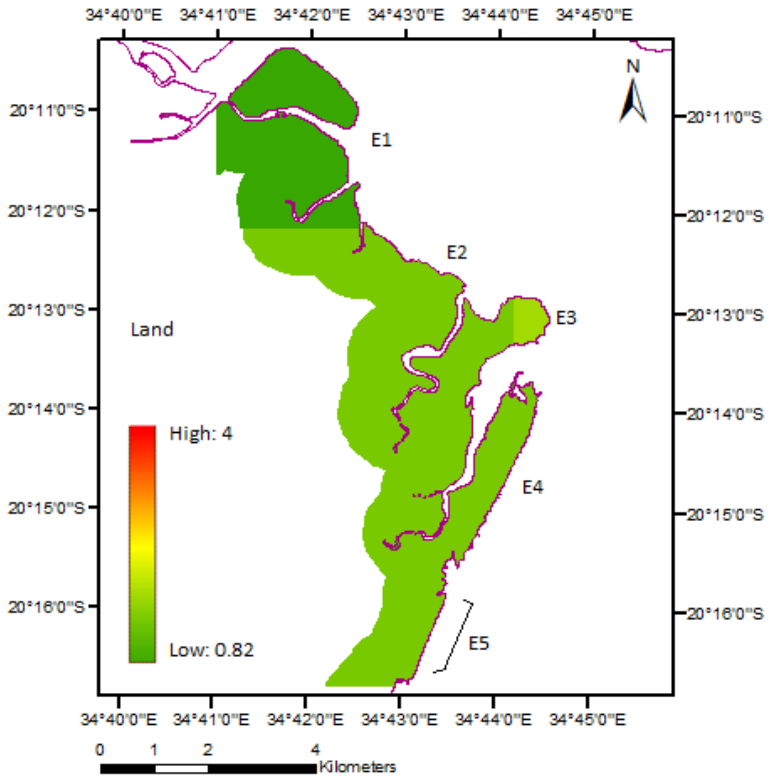

Figure 65: Vulnerability Map, site E.

Computation of the CVI produced the vulnerability map presented in figure 65. In this figure, E1 comprehends the entire part coloured with a darker tone of green, E3 to the lighter tone of green, and the green tone in between the two, to E2, E4 and E5 regions. From this map one can see that approximately 28.7% of the coastline had a vulnerability index of 0.82 (E1), 67.3% a vulnerability of 1.41 (E2, E4 and E5) and 4% 1.63 of vulnerability (E3).

In general, except for site A and B that recorded the highest vulnerability values, in all other sites there was an overall vulnerability bellow 2. Even when a few sites experienced severe erosion or high erosion rates, this vulnerability remained bellow 2. This can be explained by the combination of population density and landuse rankings (generally 1 or 2), which brought the value of CVI to a lower value.

6 Discussion

From the results obtained, SVMs classification method seems to be a good approach for delineating the coastline. For this method, kappa coefficient and overall accuracy revealed to be quite high which translated in a good accuracy of the results obtained. However, it has to be taken into account that the amount of pixels used for the classification is very important since it influences these values. Kappa coefficient and overall accuracy were calculated for the number of pixels used. As such, for this study these values seem to be quite good and this technique very robust. This conclusion was not just based on these values but on visual confirmation of the extracted coastline accuracy.

Accuracy of the delineation was possible to be tested during validation of the results. Errors regarding coastline delineation were, as much as possible, kept to a minimum. That is why, during validation of coastline delineation by the two methods, MNDWI derived coastlines were immediately discarded since they were not delineating the coastline with as much accuracy as SVMs derived ones. This conclusion was reached after careful validation of the results, where one could see that MNDWI derived coastlines were considering in certain regions a considerable amount of intertidal zone as land class, which resulted in overestimation of erosion areas and further results obtained. However, there was also the case of 1989 coastline derived from SVMs being badly delineated in some parts of the coastline. In order to decrease the error in erosion and/or accretion estimation and CVI calculation, areas where this was confirmed to happen were not used. In fact, as mentioned in the results section, this bad delineation of the coastline was only observed in the 1989 derived one, since coastline validation of the rest of the images proved to be quite accurate. It is important to understand that this consideration of intertidal zone in some areas was much worse in MNDWI derived coastlines and instead of just one of them, this happened in almost every coastline extracted. However, for the sites identified where coastline changes were more significant, for every year, coastlines seemed to be very well delimited, except for part of site C, where the problem previously identified was found, carefully described in the results, and in the end discarded to be used in overall change area calculation. All this validation and careful analysis of the results was done in every phase of this thesis in order to decrease the amount of error associated with the estimations and computations performed.

Even though MNDWI derived images were discarded due to not robust coastline delineation, in this study, it does not mean that this index is not suitable to delimit the land/water boundary in other applications. It only means that in this case, and for this region, it was not as suitable and accurate in performing this classification as the SVMs method.

Regarding georeferencing errors, validation and constant visual analysis of the results, to make sure that all images were in accordance with one another and coastlines well delineated, was performed. Interpretation of the images and results obtained led to the conclusion that errors derived from georeferencing are minimal or barely non-existent, possibly less than one pixel (30m), according with visual confirmation. Validation was performed every time the images utilized were processed, such as with

computation of indices or resizing, in order to make sure that the images were still in accordance with each other, in regards to georeferencing, and that no warping had occurred. All these checks and cross checks of data were performed to decrease as much as possible the error associated with coastline delineation and ensure that accurate results would be obtained.

Taking into consideration tide level for coastline delineation, at the time the images studied were taken, it was concluded that high tide was occurring. Tide heights obtained from SHOM were for the region of Beira Port, and they were generalized for the rest of the study area. The central region of Mozambique channel is regarded in the literature for registering tides that can reach and even go over the 6 meters (Palalane et al., 2015; Theron et al., 2012; Moreira, 2005). These findings proved similar to the values obtained via SHOM for the region under study. However, it was concluded that even with height differences of approximately 1 meter from one year to the next (Table 4), these differences would be considered negligible in the delimitation of the coastline and they would not have much influence or overestimate erosion areas obtained. Moreover, the images studied here, were already chosen taking into account this fact in order to decrease or eliminate the error that tide heights could have represented for coastline delimitation.

Regarding change detection analysis, the trends observed were expected. Where recession of the coast related to land movement occurs, it was not surprising that for every year the coastline moves further landward. Where accretion occurs, with no sand movement involved, it was expected that this increase was due to mangrove establishment instead of an increase in land area. In some cases, there seems to be an alternating movement of coastline landward in one year and the following year, seaward, possibly related to sand dynamics, as it was validated through visualization with Google Earth™ images and EMI index, as well with the Landsat source images. No unexpected alternating recession and accretion related with land movement, besides sand, between the years, was found here. Accretion was either due to simple sediment accumulation or mangrove establishment. Losses in land area, were due to a loss in sand, bare soil, in site B, or disappearance or destruction of mangroves. Areas that were not classified with erosion and accretion polygons inside of each site, pertains to the fact that extracted coastlines maintained approximately the same position over the period of study and no relevant changes where detected.

In an overall perspective, site C was where overall changed area recorded was higher, with (-) 9.81ha/km. Site D closely followed with an overall changed area of (-) 8.78ha/km. The remaining sites registered overall changes much lower than in site C and D. These high values for the two sites probably mean that the process to which they are subject to, are much stronger and erosion inducing than for the remaining sites. Accretion area revealed to be higher in site E. Phenomena involved in these changes, of course, depends on the characteristics of each site, and this is why it becomes important to look at each one of them, individually, in order to understand the dynamics and processes involved that may have led to these losses and/or increases in area and to explain the CVI values obtained.

Site A2 (Figure 22) observed sand accumulation was also referred by Theron et al. (2012), for

the period between 1991 and 2004. However, the period of study in this thesis was longer and that is why the area of accumulated sand was higher than the one in the study performed. Increase in sand area in A2 might be due to sediments brought by the highly dynamic river delta observed in the images (Figures 21-24), that ended accumulating in this region (Theron et al., 2012). A1 and A3 however, experienced erosion processes. As observed in the images, retreat and increase in area, was due to sand movement.

Regarding CVI values obtained for this site, one can see that vulnerability varies considerably. Vulnerability was relatively high in A1a (3.46) and A1b (3) and moderate in A1c (1.73). A1c moderate vulnerability was specially due to the population density parameter changing from very high density to high density and landuse, from high to low capital (Figure 49). Vulnerability was very low in A2 and A3, with 0.82 and 1 respectively, due to accretion experienced and low capital and population density observed.

Site B corresponds mostly to the city of Beira. In figure 26, the trend observed in B2 of increased recession is also observed by Theron et al. (2012), between the years of 1991 ad 2004. Increase in sand in B3 can be attributed to the construction of groins and seawalls over the past years as an attempt to decrease erosion in this region (Palalane et al., 2015). These constructions were also clearly observed during validation using high resolution satellite images from Google Earth™.

However, the field of groins which were built from Malcuti, (North of Ponta Gea) to updrift of Ponta Gea headland on the south coast (covering an extension of nearly 7 km), have increased erosion down drift of the last groin, located along Praia Nova coast. This can also help further explain erosion observed in Praia Nova (B2). It has also been reported that in the most extreme cases, intensified erosion, in this region, led to infrastructures collapse, with loss of private and public properties (Palalane et al., 2015).

A new project to upgrade and reinforce the protection of Beira coast, aiming to reduce its vulnerability to climate change, started to be implemented in December 2012. The construction of a new groin 80 meters long built in Ponta Gea, may have contributed to the great increase in sediment verified from 2007 and 2015 in B3 (Figure 26). In the most erosive area of Praia nova, a 350 meter long groin was also built in the wake of the project mentioned which may have contributed to a decrease of coastline recession verified from 2007 to 2015, when compared with previous years. A new seawall was also built in 2013, which may have also contributed to this fact (Figure 66) (Palalane et al., 2015).

Erosion in B1 might be mainly due to continuous action of river water flow velocity causing erosion of the surface, since this region is characterized by bare soil.

Population and landuse highly contribute to the great vulnerability experienced in this site, with maximum vulnerability of 4, being experienced in some of the regions within this site, namely in Praia Nova.

Figure 66: Construction of a new Seawall in February 2013, Praia Nova. Acquired from Palalane et al. (2015).

This region, although considered in terms of landuse, for being greatly urbanized, it also characterized by the existence of mangroves, specially in Praia Nova (Palalane et al., 2015; Chevallier, 2013). High cyclone vulnerability can also contribute to explain the great amount of erosion area lost in this region. In fact, as mentioned before, the destructive cyclone that hit Ponta Gea and Praia Nova in 2010 has also led to great destruction of mangroves, leading to further increase of eroded area. Not only cyclone vulnerability has contributed to the decrease of mangroves in the this region but destruction and overexploitation of this resource have further increased pressure in the coast and led to intensified erosion hazards (Palalane et al., 2015). With the increasing trend of people moving to these coastal cities and their outskirts, mangrove forests will probably continue to decrease since their wood is highly used for construction purposes and very important for the economy of the country and specially in Beira city. This decrease contributes even further to the vulnerability of the coast, specially to erosion inducing factors.

Mean erosion rate along Beira city, considering only site B, was observed to be of 1.2m/year, which was approximately in agreement with the value reported by Maansson (2011) of 1m/year for Beira, although conditions and exact location of this estimations are unknown. Considering site A and B, mean value was around 1.02 m/year, and so, still in agreement.

High population density in this area allied to landuse and change rate experienced, have contributed to the high vulnerability values obtained for this site. A vulnerability of 4 was a combination of the high risk associated to the three parameters used for the calculation. Very high population density can be pointed as the most contributing factor for such high vulnerability in this region. Low capital landuse contributed to a moderate vulnerability value, of 1.73, even though population and erosion risks were

quite high.

Site C was characterized for being very contrasting in terms of erosion, with the highest erosion rate observed in C3b location (Figure 54). Moreover, low population density and moderate capital landuse, dominated mainly by the existence of mangrove forests also characterized this site. Erosion observed in this region was mostly due to destruction and overexploitation of mangroves. This is a serious problem since destruction of mangroves intensifies coastal vulnerability to tide currents and it also decreases a barrier against flooding and cyclones. This explanation is not only applied to this specific site but to all sites studied here.

However, vulnerability in this site was quite low (Figure 57). This was precisely due to the low population density and moderate capital landuse which decreased the vulnerability even though erosion in this region is quite serious. C2 experienced the lowest vulnerability values since this represents in fact an accretion area. Once again, this gain in area is expected to be due to mangrove establishment. No explanation was found for the fact that in this particular area, it seems to be occurring mangrove establishment, while in the rest of the region destruction was occurring. However, it can be inferred that C2 is probably not so affected by processes related to tide currents, from the Mozambique channel, and in that specific region, sediments transported by the river might become accumulated allowing mangroves to establish and develop. However, this is purely an interpretation of the facts known in order to come up with a reasonable explanation for this fact, but no actual references were found to back it up.

In site D, only erosion was observed. CVI computation resulted in an overall value of 1.41, relatively low when compared with the maximum value of 4 (Figure 61). This low value was due to low population found, with much less than 500 people per square kilometre. However, this region being characterized by mainly the existence of Mangroves, erosion in this area was probably mainly related with its destruction and disappearance. This disappearance is of great importance since it will intensify even further pressure over these areas and increase erosion hazard. River processes, such as water flow velocity, may have also contributed to their destruction. However, overexploitation is probably a much credible reason (Chevallier, 2013; Hoguane, 2007). It is important to take note, once again, that previous authors refer to these processes occurring in the entire region of the Sofala Bank and not to this specific site.

In site E, accretion area was quite high (E1), while erosion was more severe in E3, with a change rate of less than -10m/year, which pertains to the severe erosion class (Figure 62). Area gained was most likely due to mangrove establishment since this region is characterized, in terms of land use, by the existence of mangroves within 1km landward from the coast. The reason why only in this region there seems to be an increase in mangroves could be because it was not so exposed to the erosive action of wave and tide currents, when compared with E2 to E5, which allowed their development. This could indeed be the reason since in site C, where accretion in C2 was also thought to be due to mangrove establishment, was also not directly exposed to sea currents and tides, being actually in a river bank. Not suffering direct exposure to these processes may be what allowed mangroves to establish

and grow in these regions. Another reason could have been their plantation. However, only reforestation of this areas (C2 and E1) is not very plausible because these regions have not experienced previous destruction of mangroves, at least for the period of study considered.

Lost area was also probably due to mangrove destruction. This region has barely no population at all, however, overexploitation can still occur contributing to its disappearance. In fact, about 1km landward from E4, there is a village with 3234 people. Need for wood and non-wood products that mangroves provide might be the cause for overexploitation of this resource in this site and so, increased erosion area. Sea water currents erosive action may also have contributed to this. Even though barely no population is threatened with erosion occurring here, it is still alarming the rate at which this mangroves are disappearing and with it the protection of the coast against wave erosive action and natural occurring disasters, such as cyclones.

Site E presented overall low vulnerability specially due to very low population density and moderate capital landuse. This was why, even though E3 experiences severe erosion, its vulnerability index was only 1.63, quite low when compared with the maximum of 4. E2, E4 and E5 experience vulnerabilities of 1.41 (Figure 65).

All sites studied here, were very influenced by tide currents processes, which might have also contributed to the increased erosion observed (Moreira, 2005). Tidal amplitudes that can exceed the 6 meters, observed in Beira, also contributed to increasing effects of erosion along the coast (Palalane et al., 2015; Hoguane, 2007).

Sediment transport from the Zambezi river, north of the region of study, also affects coastline dynamics specially in areas of sand (Palalane et al., 2015). However, and as mentioned by several authors, since the construction of the Cahora-Bassa dam (1974) and the Kariba dam (1969), there was a reduction of water volumes from this river, and with it the amount of sediments transported. These authors believe in the existence of a link between the construction of these dams and increased erosion in the region between the Zambezi and Save river, which includes the entire area of study (Davies et al., 2001; NAPA, 2007; UNEP/Nairobi, 2009).

In the Sofala Bank the destruction of overall mangrove forest has been observed to be mainly due to overexploitation, which can explain, and as mentioned for some of the cases, why a lot of mangrove area seems to be disappearing (Chevallier, 2013; Hoguane, 2007). Even though Mozambique is one of the regions in Africa where mangrove forests are more abundant, the rate of their disappearance along Sofala Bay has been increasing, accounting to 4.9% per year (Sitoe et al., 2014). With increasing urbanization, demand of wood for construction and other basic necessities, like energy and heating, will also increase and with it the area of mangrove forests destroyed, since this type of wood has been extensively used in this region for these purposes (Hoguane, 2007).

It is also important to mention that if some other parameters like sea level rise or cyclone predictions over the area of study had been implemented, for certain vulnerability computation would

have delivered higher values.

Change detection maps obtained, give a clearer view of the actual erosion and/or accretion occurring along the Mozambican coast and approximate values of changed area in hectares associated with these phenomena.

Vulnerability values obtained for these sites, under the data utilized for this study, are considered to be a representation of present and future values, if nothing is done to change it. Taking this into consideration, the vulnerability maps can be used for better understanding of the current vulnerability the coast is subject to. Hopefully, they can be a source for further and more detailed maps developed in the future that will allow better planning and management of the coastal zone.

As a last note, other sites could have been chosen to perform change detection analysis and CVI calculation, however, during careful analysis of the coastlines extracted and the differences between them, these sites were chosen as the ones identified where changes were more relevant. It was also taken into account to choose sites that experienced different situations, in terms of population density and/or landuse. Different considerations were made in order not only to visualize the most affected but also analyse areas where changes were due to various processes and to different situations.

7 Conclusion

Results from this thesis reveal the serious erosion suffered in Mozambique's coastline, more specifically in the area studied here. It was possible to conclude that extensive erosion and coastline retreat are occurring in this region even though CVI calculation revealed low to moderate vulnerability, throughout the sites studied, with exception of regions within site B, that obtained maximum vulnerability, one of them being Praia Nova. These results were entirely dependant on the parameters studied, since they greatly influence the value computed. If other parameters, like sea level rise and cyclone vulnerability data, had been used, the values obtained would have certainly been much higher for all the sites chosen.

In terms of overall change rate, higher values were observed in site C and E (Figures 53 and 61 respectively). However, after computation of the CVI, higher vulnerability values were found in site B, since this region corresponds mostly to the city of Beira, where pressure from high population density is intensified. Sites A and B seem to be the ones most conditioned by population density, while sites C to E, were mainly dominated by mangrove forests, with moderate capital landuse, and very low in population density. This is why for these regions the CVI obtained was quite low.

Remote sensing and GIS technologies were suitable and useful in the study of spatio-temporal dynamics of the coast, related to erosion processes. Regarding techniques used for coastal delineation, it was possible to conclude that SVMs techniques employed here proved to be very accurate in coastline delineation, even though it has not been one of the most extensively classification techniques used for coastline extraction in the scientific community. The DSAS tool, also used by many other authors, has been very helpful for quantifying actual coastline change rate.

Integration of aerial photography with high resolution imagery could improve accuracy of the results, however, in regards to this study, Landsat derived images revealed to be very useful and adequate for the scale of the changes that were observed here. For identification of small scale changes Landsat data might not be the best choice, and images with higher spatial resolution should be employed. However, in the wake of this study, Landsat data proved to be a very efficient tool to extract the coastlines and identify coastline changes.

For the future, high resolution satellite images would be a great tool to analyse with further detail the processes studied here, for which they would probably deliver more detailed results. This study was performed for a small region but it would be convenient to extend it to the entire Mozambican coast in order to have a full scale understanding of the coastal changes this country is experiencing. Although this is the first time such study regarding CVI computation was performed in the area, future studies should be carried in order to have an even better understanding of the processes that contribute to the vulnerability of the coast. In this thesis, with the exception of coastline change rate, the other parameters used were socio economic variables, which have great importance and influence in the processes that occur along the coast. However, including coastal forcing characteristics such as tidal dynamics and sea

level rise predictions, could improve the vulnerability characterization of the coast.

Further studies to characterize risk associated with coastal hazards in Mozambique could be a very useful tool for coastal managers to develop better planning for these regions and mitigate losses due to phenomena that take place in the coast. With climate change being more and more evident as time passes by, this will not only add new hazards to the coast but also intensify the current ones and increase their destructive action. This is why, continuous monitoring of the coast making use of EO and GIS techniques is revealing to be of extreme importance in order to understand the dimensions and rates of change experienced by an ever changing coastline.

References

Addo, K. A. and Kodzo, K. S. (2013). Medium resolution satellite imagery as a tool for monitoring shoreline change . Case study of the Eastern coast of Ghana. *Journal of Coastal Research*, Special Issue, (65):511–516.

Alesheikh, A. A.; Ghorbanali, A., and Nouri, N. (2007). Coastline change detection using remote sensing. *International Journal of Environmental Science and Technology*, 4(1):61–66.

Alhin, K. A. and Niemeyer, I. (2009). Coastal monitoring using remote sensing and geoinformation systems: Estimation of erosion and accretion rates along Gaza coastline. *International Geoscience and Remote Sensing Symposium (IGARSS)*, 4:29–32.

Appeaning Addo, K.; Walkden, M., and Mills, J. P. (2008). Detection, measurement and prediction of shoreline recession in Accra, Ghana. *ISPRS Journal of Photogrammetry and Remote Sensing*, 63(5):543–558.

Barsi, J. A.; Hook, S. J.; Schott, J. R.; Raqueno, N. G., and Markham, B. L. (2007). Landsat-5 Thematic Mapper Thermal Band Calibration Update, 4(4):552–555.

Boak, E. H. and Turner, I. L. (2005). Shoreline Definition and Detection: A Review. *Journal of Coastal Research*, 214:688–703.

Cambers, G.; Hendry, M.; Troost, D. G., and Suzjumov, A. E. (1998). *Coping with beach erosion: with case studies from the Caribbean*. Unesco Publishing Paris.

Chander, G.; Markham, B. L., and Barsi, J. A. (2007). Revised Landsat-5 Thematic Mapper radiometric calibration. *IEEE Geoscience and Remote Sensing Letters*, 4(3):490–494.

Chandrasekar, N.; JoeVivek, V., and Saravanan, S. (2013). Coastal Vulnerability and Shoreline Changes for Southern Tip of India-Remote Sensing and GIS Approach. *Journal of Earth Science & Climatic Change*, 04(04):144.

Chemane, D.; Motta, H., and Achimo, M. (1997). Vulnerability of coastal resources to climate changes in Mozambique: a call for integrated coastal zone management. *Ocean & Coastal Management*, 37(1):63 – 83.

Chevallier, R. (2013). *Balancing Development and Coastal Conservation : Mangroves in Mozambique*.

Cohen, J. E.; Small, C.; Mellinger, A.; Gallup, J., and Sachs, J. (1997). Estimates of coastal populations. *Science*, 278(5341):1209–1213.

Davies, Bryan R; Beilfuss, Richard D., and Thoms, Martin C. (2001). Cahora Bassa retrospective , 1974 – 1997 : effects of flow regulation on the Lower Zambezi River. *Journal of the International Association of Limnology*, (27):2149–2157.

DNET (2010). Dnet Consult Aps, Assessment of Options for Coastal Protection of the Beira Shoreline. *Beira, Mozambique: Swiss Agency for Development and Cooperation*. 36p.

Dolan, R.; Fenster, M. S., and Holme, S. J. (1991). Temporal analysis of shoreline recession and accretion. *Journal of Coastal Research*, pages 723–744.

Donato, T. F. and Klemas, V. V. (2001). Remote Sensing and Modeling Applications for Coastal Resource Management. *Geocarto International*, 16(2):25–32.

ENVI (2016). *ENVI On-line Software Users's Manual, Harris Geospatial Solutions*. `https://www.harrisgeospatial.com/docs/routines-136.html`.

Fletcher, C. H.; Romine, B. M.; Genz, A. S.; Barbee, M. M.; Dyer, M.; Anderson, T. R.; Lim, S. C.; Vitousek, S.; Bochicchio, C., and Richmond, B. M. (2012). *National assessment of shoreline change: Historical shoreline change in the Hawaiian Islands*. US Department of the Interior, US Geological Survey.

Ge, L.; Li, X.; Wu, F., and Turner, I. L. (2013). Coastal erosion mapping through intergration of SAR and Landsat TM imagery. *International Geoscience and Remote Sensing Symposium (IGARSS)*, pages 2266–2269.

Gens, R. (2010). Remote sensing of coastlines: detection, extraction and monitoring. *International Journal of Remote Sensing*, 31(7):1819–1836.

Ghosh, M. K.; Kumar, L., and Roy, C. (2015). Monitoring the coastline change of Hatiya Island in Bangladesh using remote sensing techniques. *ISPRS Journal of Photogrammetry and Remote Sensing*, 101:137–144.

Gibb, J. G. (1978). Rates of coastal erosion and accretion in New Zealand. *New Zealand Journal of Marine and Freshwater Research*, 12(4):429–456.

Gornitz, V. M.; Daniels, R. C.; White, T. W. and Birdwell, K. R. (1993). The Development of a Coastal Risk Assessment Database: Vulnerability to Sea-Level Rise in the U.S. Southeast. *Journal of Coastal Research*, pages 327–338.

Guariglia, A.; Buonamassa, A.; Losurdo, A.; Saladino, R.; Trivigno, M. L.; Zaccagnino, A., and Colangelo, A. (2006). A multisource approach for coastline mapping and identification of shoreline changes. *Annals of Geophysics*, 49(1):295–304.

Guiloviça, C. (2011). Caracterização da Agitação Marítima ao Largo da Baía de Maputo. *Maputo, Mozambique: Eduardo Mondlane University, Licenciatura's Thesis*, 63p.

Himmelstoss, E.A.; Thieler, E.R.; Zichichi, J.L., and Ergul, A. (2009). Digital Shoreline Analysis System (DSAS) version 4.0 — An ArcGIS extension for calculating shoreline change. *U.S. Geological Survey Open-File Report 2008-1278*, 3:79.

Hoguane, A. (2007). Perfil Diagnóstico da Zona Costeira de Moçambique. *Revista da Gestão Costeira Integrada*, 7(1):69–82.

Huang, C.; Song, K.; Kim, S.; Townshend, J. R.; Davis, P.; Masek, J. G., and Goward, S. N. (2008). Use of a dark object concept and support vector machines to automate forest cover change analysis. *Remote Sensing of Environment*, 112(3):970–985.

INE (2016). Data Portal Mozambique. Mozambique. *Instituto Nacional de Estatística*. `http://www.ine.gov.mz/`,accessed on 20/03/2016.

INGC (2009). INGC (Instituto Nacional de Gestão de Calamidades) Climate Change Report: Study on the Impact of Climate Change on Disaster Risk in Mozambique. 34p.

ISDR (2009). Global Assessment Report on Disaster Risk Reduction. United Nations, Geneva, Switzerland.

Jana, A. and Bhattacharya, A. K. (2013). Assessment of Coastal Erosion Vulnerability around Midnapur-Balasore Coast, Eastern India using Integrated Remote Sensing and GIS Techniques. *Journal of the Indian Society of Remote Sensing*, 41(3):675–686.

Kavzoglu, T. and Colkesen, I. (2009). A kernel functions analysis for support vector machines for land cover classification. *International Journal of Applied Earth Observation and Geoinformation*, 11(5):352–359.

Khiry, M. A. (2007). *Spectral mixture analysis for monitoring and mapping desertification processes in semi-arid areas in North Kordofan State, Sudan*. PhD thesis, University of Heidelberg, Germany.

Kuenzer, C.; Ottinger, M.; Liu, G.; Sun, B.; Baumhauer, R., and Dech, S. (2014). Earth observation-based coastal zone monitoring of the Yellow River Delta: Dynamics in China's second largest oil producing region over four decades. *Applied Geography*, 55(2014):92–107.

Kumar, T. S.; Mahendra, R. S.; Nayak, S.; Radhakrishnan, K., and Sahu, K. C. (2010). Coastal Vulnerability Assessment for Orissa State, East Coast of India. *Journal of Coastal Research*, 26(3):523–534.

Langa, J. (2007). Problemas na zona costeira de Moçambique com ênfase para a costa de Maputo. *Revista de Gestão Costeira Integrada*, 7(1):33–44.

Leggett, D. J. and Jones, A. (1996). The application of GIS for flood defence in the anglian region: developing for the future. *International Journal of Geographical Information Science*, 10(1):103–116.

Li, X. and Damen, M. C. (2010). Coastline change detection with satellite remote sensing for environmental management of the Pearl River Estuary, China. *Journal of Marine Systems*, 82:S54–S61.

Liu, H. and Jezek, K. (2004). Automated extraction of coastline from satellite imagery by integrating canny edge detection and locally adaptive thresholding methods. *International Journal of Remote Sensing*, 25(5):937–958.

Liu, X. (2011). The coastal erosion of the abandoned Yellow River Delta in northern Jiangsu province, China: Based on analysis of remote sensing images. *19th International Conference on Geoinformatics*, pages 1–5.

Maansson, F. (2011). Desk Study To Support the Identification of Support Option in the Area of Coastal Defence and Land Reclamation in the City of Beira. Beira, Mozambique: Netherlands Water Partnership, pages 1–34.

Mahapatra, M.; Ramakrishnan, R., and Rajawat, A. S. (2015). Coastal vulnerability assessment of Gujarat coast to sea level rise using GIS techniques: a preliminary study. *Journal of Coastal Conservation*, pages 241–256.

Maktav, D.; Erbek, F. S., and Kabdasli, S. (2002). Monitoring coastal erosion at the Black Sea coasts in Turkey using satellite data: A case study at the Lake Terkos, north-west Istanbul. *International Journal of Remote Sensing*, 23(19):4115–4124.

Martins, D. (2012). Characterization of the wave climate in the Mozambique coast. *Barcelona, Spain: Barcelona University, Master's thesis*, 30p.

McLaughlin, S.; McKenna, J., and Cooper, J. (2002). Socio-economic data in coastal vulnerability indices: constrains and opportunities. *Journal of Coastal Research*, 497(36):487–497.

MICOA (2007). Relatório nacional sobre ambiente marinho e costeiro. Maputo, Moçambique: Ministério para coordenação da acção ambiental–direção nacional de gestão ambiental.

Moreira, M. (2005). A Dinâmica Dos Sistemas Litorais Do Sul De Moçambique Durante Os Últimos 30 Anos. *Finisterra–Revista Portuguesa de Geografia*, 79:121–135.

Mountrakis, G.; Im, J., and Ogole, C. (2011). Support vector machines in remote sensing: A review. *ISPRS Journal of Photogrammetry and Remote Sensing*, 66(3), 247-259.

NAPA (2007). National adaptation programme of action (NAPA), ministry for the co-ordination of environmental affairs, Maputo, Moçambique. Approved by the Council of Ministers at its 32nd Session.

Orive, A.C.; de la Fuente Martín, P.; Ansorena, Í.L., and Guijarro, E.D. (2012). Regeneracion de las playas y rehabilitacion de los canales de desague de Beira (Mozambique). *Revista de Obras Públicas*, (3532):7–22.

Otukei, J. R. and Blaschke, T. (2010). Land cover change assessment using decision trees, support vector machines and maximum likelihood classification algorithms. *International Journal of Applied Earth Observation and Geoinformation*, 12:S27–S31.

Palalane, J., Larson M., Hanson, H., and Juízo, D. (2015). Coastal erosion in Mozambique: Governing processes and remedial measures. *Journal of Coastal Research*, 32(3):700–718.

Pardo-Pascual, J. E.; Almonacid-Caballer, J.; Ruiz, L. A., and Palomar-Vázquez, J. (2012). Automatic extraction of shorelines from Landsat TM and ETM+ multi-temporal images with subpixel precision. *Remote Sensing of Environment*, 123:1–11.

Pendleton, E. A.; Williams, S. J., and Thieler, E. R. (2004). Coastal Vulnerability Assessment of Assateague Island National Seashore (Asis) To Sea-Level Rise. *US Department of the Interior, US Geological Survey*.

Petropoulos, G.; Knorr, W.; Scholze, M.; Boschetti, L., and Karantounias, G. (2010). Combining aster multispectral imagery analysis and support vector machines for rapid and cost-effective post-fire assessment: a case study from the greek wildland fires of 2007. *Natural Hazards and Earth System Sciences*, 10(2):305–317.

Petropoulos, G.; Arvanitis, K. and Sigrimis, N. (2012a). Hyperion hyperspectral imagery analysis combined with machine learning classifiers for land use/cover mapping. *Expert systems with Applications*, 39(3):3800–3809.

Petropoulos, G. P.; Kalivas, D. P.; Griffiths, H. M., and Dimou, P. P. (2015). Remote sensing and GIS analysis for mapping spatio-temporal changes of erosion and deposition of two Mediterranean river deltas: The case of the Axios and Aliakmonas rivers, Greece. *International Journal of Applied Earth Observation and Geoinformation*, 35:217–228.

Petropoulos, G. P.; Partsinevelos, P., and Mitraka, Z. (2012b). Change detection of surface mining activity and reclamation based on a machine learning approach of multi-temporal Landsat TM imagery. *Geocarto International*, 28(4):323–342.

Rao, K. N.; Subraelu, P.; Rao, T. V.; Malini, B. H.; Ratheesh, R.; Bhattacharya, S.; Rajawat, A. S., and Ajai (2009). Sea-level rise and coastal vulnerability: An assessment of Andhra Pradesh coast, India through remote sensing and GIS. *Journal of Coastal Conservation*, 12(4):195–207.

Savvidis, Y. G.; Koutitas C. G., and Krestenitis, Y. N. (2005). Modelling the water mass exchange through navigational channels connecting adjacent coastal basins - application to the Channel of Potidea (North Aegean Sea). *Annals of Geophysics*, (23):231–238.

Sitoe, A. A.; Mandlate, L. J. C., and Guedes, B. S. (2014). Biomass and carbon stocks of Sofala Bay mangrove forests. *Forests*, 5(8):1967–1981.

Theron, A.K; Barwell, L.B; Rossouw, M., and Maherry, A. (2012). Coastal Planning and Adaptation to Mitigate Climate Change Impacts—Responding to Climate Change in Mozambique (Phase II, Theme 2). *Stellenbosch, South Africa: Council for Scientific and Industrial Research, Report prepared for Mozambican National Institute for Disaster Management*, 263p.

Thieler, E. R and Danforth, W. W. (1994). Historical shoreline mapping (I): improving techniques and reducing positioning errors. *Journal of Coastal Research*, 10(3):549–563.

Thieler, E. R. and Danforth, W. W. (1994). Historical shoreline mapping (II): application of the digital shoreline mapping and analysis systems (dsms/dsas) to shoreline change mapping in Puerto Rico. *Journal of Coastal Research*, pages 600–620.

Tirkey, N.; Biradar, R. S., Pikle, M., and Charatkar, S. (2005). A study on Shoreline changes of Mumbai coast using remote sensing and GIS. *Journal of the Indian Society of Remote Sensing*, 33(1):85–91.

UNEP (2001). *GESAMP (IMO/FAO/UNESCO-IOC/WMO/WHO/IAEA/UN/UNEP Joint Group of Experts on the Scientific Aspects of Marine Environmental Protection) and Advisory Committee on Protection of the Sea. Protecting the oceans from land-based activities - Land-based sources and activities affecting the quality and uses of the marine, coastal and associated freshwater environment*, volume 71.

UNEP/Nairobi Convention Secretariat and WIOMSA (2009). *An assessment of hydrological and land use characteristics affecting river-coast interactions in the Western Indian Ocean region, UNEP, Nairobi Kenya*.

USGS (2016a). Frequently asked questions about the Landsat missions. *United States Geoogical Survey (USGS)*. `http://landsat.usgs.gov/band_designations_landsat_satellites.php`,accessed on 22/06/2016.

USGS (2016b). Geometry. *United States Geoogical Survey (USGS)*. `http://landsat.usgs.gov/geometry.php`,accessed on 22/06/2016.

USGS (2016c). Using the USGS Landsat 8 product. *United States Geoogical Survey (USGS)*. `http://landsat.usgs.gov/Landsat8_Using_Product.php`,accessed on 22/06/2016.

Van, T.T. and Binh, T.T. (2008). Shoreline Change Detection to Serve Sustainable Management of Coastal Zone in Cuu Long Estuaries. *International Symposium on Geoinformatics for Spatial Infrastructure Development in Earth and Allied Sciences*, pages 1–6.

Vinayaraj, P.; Johnson, G.; Udhaba Dora, G.; Sajiv Philip, C.; Sanil Kumar, V., and Gowthaman, R. (2011). Quantitative Estimation of Coastal Changes Along Selected Locations of Karnataka, India: A GIS and Remote Sensing Approach. *International Journal of Geosciences*, 02(04):385–393.

Volpi, M.; Petropoulos, G. P., and Kanevski, M. (2013). Flooding extent cartography with Landsat TM imagery and regularized kernel fisher's discriminant analysis. *Computers & Geosciences*, 57:24–31.

Xu, H. (2006). Modification of Normalised Difference Water Index (NDWI) to enhance open water features in remotely sensed imagery. *International Journal of Remote Sensing*, 27(14):3025–3033.

Yang, X. (2011). Parameterizing Support Vector Machines for land cover classification. *Photogrammetric Engineering & Remote Sensing*, 77(1):27–37.